THE SIEVING MECHANISM IN HYDRAULIC FILTRATION

By

ROSS MAXWELL STUNTZ

Bachelor of Science
Oklahoma State University
Stillwater, Oklahoma
1964

Master of Science
Oklahoma State University
Stillwater, Oklahoma
1965

Submitted to the Faculty of the Graduate College
of the Oklahoma State University
in partial fulfillment of the requirements
for the Degree of
DOCTOR OF PHILOSOPHY
July, 1971

THE SIEVING MECHANISM IN

HYDRAULIC FILTRATION

Thesis Approved:

E. L. Fitch
Thesis Adviser

W. M. Liedermann, Jr.

Allen Rowe

R. Leroy Sallee

A. Durham
Dean of the Graduate College

ACKNOWLEDGEMENT

I wish to express my sincere appreciation and thanks to the following people and organizations who have encouraged and supported my doctoral program:

Dr. E. C. Fitch, who served as my major adviser and graduate committee chairman. His advice and counsel have been a unique and rewarding educational experience. Dr. Fitch suggested this thesis research area.

My graduate committee, composed of Dr. J. L. Folks, Dr. A. M. Rowe, and Dr. W. G. Tiederman, Jr., whose guidance and criticisms have been of great help during my doctoral program.

The Basic Fluid Power Research Program and the U. S. Army Mobile Equipment Research and Development Center, Ft. Belvoir, Virginia, whose sponsored research has provided employment during my graduate studies.

My colleagues at the Fluid Power Research Center, especially Mr. L. E. Bensch who read the manuscript and made many helpful suggestions.

My wife, Ann, for her preparation of the manuscript for this thesis.

TABLE OF CONTENTS

Chapter Page

V. (CONTINUED)

LIST OF TABLES

LIST OF FIGURES

Figure Page

CHAPTER I

INTRODUCTION

Over the course of the last three years the author has conducted an intensive study of the unresolved questions which confront researchers in hydraulic filtration mechanics. The general approach, which involves the stochastic analysis of these problems from measurable geometric probability density functions, has become known as "Filtration Physics." A fundamental goal of the initial study was to order the unresolved problems into a logical sequence whose solution would lead to the understanding and possible optimization of the hydraulic filtration process. Ideally, the total investigation will provide the answers to practical questions as well as idealized questions.

In Chapter II the state-of-the-art in hydraulic filtration will be discussed. It will be shown that one of the most fundamental and least resolved problems in hydraulic filtration is the relative importance of mechanical particulate removal by sieving. As a consequence, the objectives of the research presented herein include the modeling of the sieving process in terms of geometrically measurable random variables. In Chapter III formulation of the present investigation will be presented in such a way that the techniques developed can be extended to further aspects of filtration mechanics problems. The general analysis necessary to describe the sieving process is derived in Chapter IV. Solution techniques for the expressions obtained are presented in

Chapter V. Special geometric cases are then treated experimentally in Chapter VI, and analytically in Chapter VII. The resultant comparison demonstrates factors which cause the experimental model to deviate from predicted performance. The total development is presented to demonstrate the applicability of stochastic analysis to the problems inherent to viscous liquid filtration mechanics. Final conclusions and extensions of the present study are presented in Chapters XIII and IX.

CHAPTER II

SIEVING IN HYDRAULIC FILTRATION

Hydraulic Filtration

Hydraulic filtration, in the context of this study, is meant to denote the removal of particulate matter from liquid hydraulic fluids such as those used in automotive, mobile, or aerospace systems. Just as in any field in which success is largely measured by economic considerations, progress has been made at a rate governed by supply and demand. The resulting approach to hydraulic filtration mechanics research has left many fundamental questions unanswered. For instance, the various filter performance rating systems, based upon the largest particle observed after passage (1), the cumulative particulate separation efficiency (2), or gravimetric separation efficiency, all tend to obscure the stochastic nature of the basic problem. That is, neither the influent particulate distribution nor effluent particulate distribution is treated as a function of random variables. Instead, only a representative value (usually the expected value) is considered. This example is typical of the vast majority of parameters by which hydraulic filters are evaluated and compared.

The development of filtration mechanics technology may be characterized as "applications oriented." Relatively new applications, however, are rapidly providing motivation for the solution of some of the problems which had been heretofore circumvented. An example is

the trend toward higher pressure hydraulic systems (3). As system pressures are raised the clearances between moving parts of hydraulic components must be reduced. Consequently, the system fluid cleanliness level must reflect a lower concentration of particles in the new range of component vulnerability. Thus, a new demand is present in the market and new technology may be required to economically design a filter medium possessing at least the minimum required performance.

Another factor which will undoubtedly bring about the demand for systematically designed filter media is the increasing availability of system component contaminant tolerance levels (3). If the minimum particulate cleanliness level at which a component will survive for a specified life is indeed known, the filter which will provide that cleanliness level for a given particulate ingression rate becomes economically desirable. That is, a cost optimal combination of filter element price and cost of replacement may be obtained for the most economical system contamination level. Only through a more complete understanding of the filtration process than has been found in the literature, can filter media be selectively designed to meet specific cleanliness levels.

Relationship to Aerosol Filtration

By comparison with hydraulic filtration, research in aerosol filtration has had a long and rigorous history. The reason may be attributed to users of aerosol filters in bio-medical and chemical process fields who have been able to define their requirements in terms of acceptable particulate probability density functions since the mid 1940's. The current state-of-the-art in aerosol filtration reflects

significant understanding of the mechanisms involved and consitututes ample evidence that rigorous analysis of the filtration process is a reasonable goal. Furthermore, recent aerosol research has demonstrated the feasibility of stochastic analysis based on geometrically measurable random variables, as in the findings of Clarenburg and Van Der Waal (4), and Corte and Lloyd (5).

Many aspects of hydraulic filtration can be treated similarly to those of aerosol filtration. For instance, the medium geometry found in commercially available aerosol filters is geometrically similar to that found in hydraulic filters. That is, the shape of the solid surfaces and void volumes found in each medium are geometrically similar to the other. Also, the velocity profile of a viscous fluid slowly flowing through a small tortuous passage can often be modeled by the same equations for the aerosol or for the hydraulic problem (6).

Unfortunately, complete solutions for the mathematical models of the similar cases mentioned above have not been found by aerosol researchers. Also, there exist other problems which are unique to hydraulic filtration. These problems center around modeling of the way in which particles are captured by the filter medium. It can be conclusively shown that the sieving mechanism is not dominant in aerosol filtration. If the design of aerosol filter media were such that sieving were allowed to predominate, rapid clogging and short life would result. Instead, these filter media are designed so that surface forces will cause small particles to be retained on the sides of comparatively large pores. The relative importance of particle retention by surface forces as opposed to retention by sieving is a question which has not been resolved by hydraulic filtration experts. Increased understanding of

this basic phenomenon is obviously fundamental to the systematic design of filter media. The importance of this problem lends relevance to rigorous study of the sieving mechanism.

Transport and Retention Mechanisms

Any particle capture not due to sieving must be explained in the classic terms of transport and retention mechanisms. These principles have been applied with wide acceptance to aerosol problems. To a lesser degree the same principles have been applied to the filtration of small biological and inorganic particulate matter from water (7), (8).

Transport mechanisms are a categorization of the way in which particle trajectories may be forced to encounter elements of the filter medium. Ives (7) and Chen (9), as well as many other authorities, classify transport mechanisms as gravity, diffusion, inertia and impaction (see Figure 1). These terms will be only briefly discussed here. A more detailed exposition may be found in Reference 6.

Gravity simply describes the settling of particles in a viscous liquid. For most particles in the typical hydraulic filtration size distribution, gravity is not an important transport mechanism.

Diffusion is caused by the interaction of particles rebounding or repelling from other bodies. Normally, diffusion is not important to the transport of particles larger than one micrometer (2, 6).

Impaction describes the case of the streamline which coincides with a particle trajectory that passes within a particle radius of a solid boundary. Since in steady flow there is no deviation of the particle from the streamline, the analysis is reduced to modeling flow patterns around an obstacle.

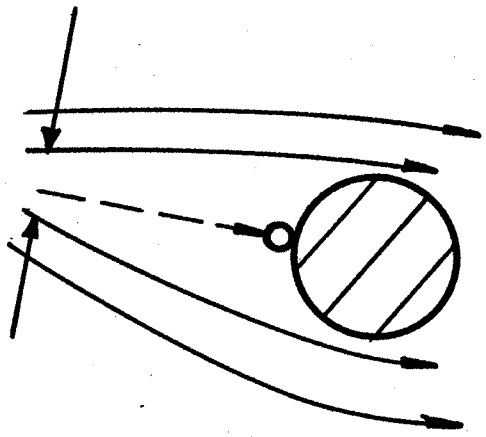

Impaction

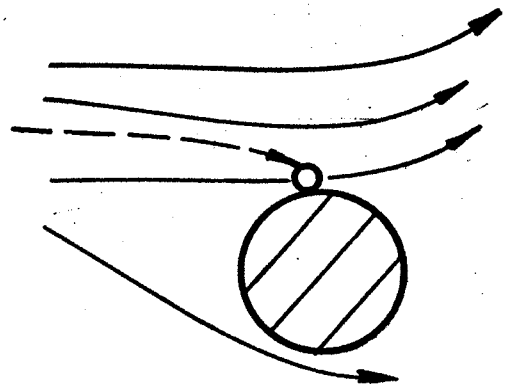

Inertia

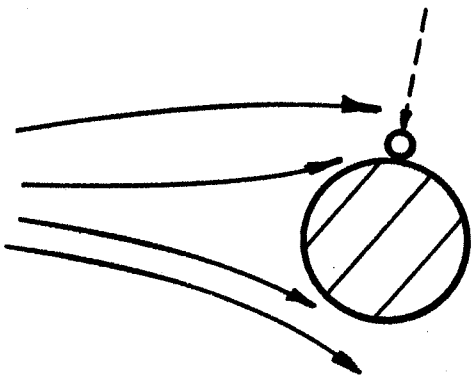

Gravity

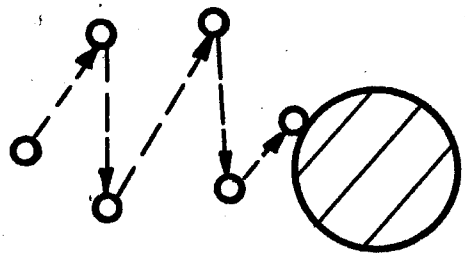

Diffusion

Figure 1. Capture Mechanisms

The inertia mechanism denotes the deviation of a particle from a curved streamline due to the difference in particle and fluid densities Authors sometimes include particle movement due to hydrodynamic forces (or lift) in this category. Accurate modeling of the inertia mode requires modeling of the fluid velocity field surrounding the elements of the filter medium.

Each of the above mentioned transport mechanisms is important to the capture of particles only if there exists a mechanism which retains particles that come into contact with (or at least come very near) the filter medium. That is, if capture is based on the transport mechanisms, the assumption must be made that a particle which approaches a fiber or element of filter medium is forced to remain in a fixed position. The attractive forces which constitute the adsorption process are often called surface forces. These forces are further classified as Van Der Waal's-London forces or electrostatic forces.

In the case of a liquid interface between particle and filter medium the system is known as a secondary system. Secondary systems are difficult to model, although some pertinent literature is becoming available (10). Measurement of the parameters associated with the description of secondary systems is also a formidable obstacle. Further details on surface forces may be found in Reference 6.

The Sieving Mechanism

The apparent alternative to capture of particles by surface forces is capture by mechanical forces. A more common name for the mechanical process is "sieving." Sieving is the capture of a particle by virtue of its geometry at several points of contact with other solid

matter. In a relatively nontortuous, recleanable filter medium, capture by surface forces or sieving appears to adequately categorize all possible retention mechanisms.

For the purposes of this research, only the sieving mode will be modeled. That is, the capture mechanism which is modeled will be mechanical in nature and involve at least one point of contact between the particle in question and the filter medium. There remains the possibility of an unstable sieving mode in which a fluid transient or impact of another particle could dislodge a previously captured particle. In order to realistically analyze the unstable sieving mode, surface forces would have to be calculated. Since this discussion is to deal exclusively with the sieving mode, the analysis will be restricted to particle and pore configurations in which stable sieving is predominant. A particle which has been captured will remain captured and motionless for all subsequent time.

The Relevance of Sieving to Depth Medium Filtration

The disagreement about the quantitative importance of the sieving mechanism in hydraulic filtration is a dramatic illustration of the need for research in fundamental filtration physics. Only when the phenomena involved in particle capture can be adequately modeled will there be real hope of filter medium optimization. A logical first step in the sequence of research needed to bring about the final model is the analysis of the sieving mechanism.

The qualitative existence of the sieving mechanism has been easily demonstrated in the Oklahoma State University Fluid Power Research Center Laboratory. Filtration tests in which particle sizes exceed

pore sizes have demonstrated the existence of the sieving mechanism. Filtration tests in which significant numbers of particles smaller than the smallest pore were captured have provided evidence supporting the existence of active surface forces. The conclusion to be drawn from the qualitative data is that both sieving and capture due to transport mechanisms and surface forces can be important in hydraulic filtration. The relative importance of each phenomenon is dependent upon many parameters which include pore and particle geometry. An accurate model of the sieving process could be used deductively to estimate the magnitude of capture by surface forces.

An important extention of a planar sieving model would be the simulation of depth medium filtration. To implement such a model, it would be necessary to know particle shape and size densities, pore shape and size densities, and the velocity patterns of the liquid phase in the pores. Ideally, these parameters would be known in terms of geometrically measurable random variables. While a completely satisfactory pore size model has not been found in the literature, some promising work has been done (5, 6, 11, 12, 13). In any case numerical pore size data gathered by porosimetry or other techniques could be used to analyze filtration performance in the three dimensional problem. A more complete discussion of the parameter measurement which would be necessary to initialize a sieving analysis can be found in Reference 6.

The previous work of the author and that of other investigators summarized in this chapter has established the need for a fundamental model of the sieving process in hydraulic filtration. In the following chapter the requirement will be stated in the definitive way necessary to attack the problem in a systematic manner.

CHAPTER III

FORMULATION OF THE PROBLEM

Objectives

The primary objective of the present research was to rigorously model the process by which particles suspended in a hydraulic fluid are mechanically captured by a sieve type filter medium. The mechanical capture, or sieving mechanism, is defined as the geometric interference between the particle and filter medium or between the particle, filter medium, and previously captured particle(s), which results in the capture of the particle.

In order to insure the utility of the model, some secondary objectives were defined. First, the model must be derived in terms of geometrically measurable random variables. This restriction insured that the resultant model would lend itself to compensation. Also the basis for rigorous derivation of the process was established.

Second, all variables which are random in nature were treated as such. In much of the literature random variables in filtration problems are represented by an expected value. A third objective was to evaluate solution techniques appropriate to the general model. The most applicable solution technique was applied to the solution of several problems to demonstrate the use of the model.

A further objective was a controlled laboratory study designed to be compatible with the problems previously considered.

As a final objective, a comparison of the experimental and theoretical results was desired. The comparison was needed to demonstrate the validity of the analytical process.

Constraints Used to Narrow the Problem

Certain constraints were applied to the general topic in order to narrow the study to a meaningful scope. With respect to the analytical development the following conditions were imposed:

1. Geometrically regular shapes, such as spheres, ellipsoids and prisms, were used to model pore and particle geometries.

2. Modeling was restricted to the sieving mechanism. That is, only mechanical capture due to geometric properties of the particle and pore was considered. In the case of partially blocked pores, capture was required to involve contact with the filter medium on at least one point.

3. Only steady flow conditions were considered over the gross area of the filter medium.

4. Since the sieving mechanism was to be studied the model of each sieve mesh layer was considered a two dimensional problem.

The following constraints were defined to describe the empirical test conditions:

1. Measurement of all measurable random variables was accomplished by microscopic observation. These variables included pore size, pore shape, particle size and particle shape.

2. The sieve mesh tested was to be devoid of any tortuosity. This restriction had the effect of limiting the geometric capture to a stable and observable sieving process.

3. Measures were taken to reduce the effect of surface forces. Grounding the filter media and use of a conductivity additive were anticipated.

Statement of the Problem

In view of the stated objectives and the constraints just mentioned, the following statement of the problem was formulated:

The principal goal of the research is to rigorously derive a model of the sieving mechanism in hydraulic filtration. The model will describe stable sieving of particulate matter on one or more two dimensional layers of sieve mesh. Solution techniques for the model will be evaluated. A comparison of laboratory and predicted filtration performance will be made.

Previous Investigations

A thorough literature search has shown that previous research in hydraulic filtration has been characterized by the use of expected values to represent what, in reality, are random variables. Since the present research is based on treatment of these parameters as random variables, only the few references, which are in some part relevant to hydraulic sieving, will be discussed. Aerosol research was discussed in the previous chapter since the sieving mechanism is not important in aerosol filtration. The bulk of literature which is most relevant to the problem as it has been defined pertains to the fundamental stochastic process relationship necessary for the analysis and will be mentioned where appropriate throughout the development.

A large volume of literature exists on dry sieving. The dry sieving procedure consists of shaking dry dust through a sieve mesh series. Such sieves are available in standard pore sizes as small as 20 micrometers. The literature is primarily concerned with separation rates and is based on mean values of the random parameters involved. Obviously this literature is of limited relevance to the present study. A good summary of dry sieving literature is given by Herdan (14). Herdan mentions the wet sieving process but states that it is bounded by a 60 micrometer lower separation limit. The wet sieving process does not fit the requirements of the present problem since the contaminant is in a concentrated solution in which particle interactions are very significant. No stochastic analysis of wet or dry sieving was discovered.

Banacki and Bowers (15) have attempted to measure the pore size distribution of a paper filter by filtration of a solution containing a distribution of classified glass beads. No explanation was given to substantiate their equating downstream bead distribution with pore size distribution. Actually, what these authors measured was separation efficiency for the explicit conditions of their test.

Since empirical modeling of the sieving process has been mentioned, it is at least historically appropriate to note that strictly empirical single pass separation efficiency tests have appeared in the literature, e.g., (16). These tests were, in general, run on tortuous filter media.

The first positive step toward understanding the phenomena under study was made by Tucker (17). Tucker conducted tests using Dutch twill woven wire mesh and artificial contaminants. Although the wire

cloth did possess considerable tortuosity some of the results reported appear to be caused by the sieving mechanism. Tucker stated that separation efficiency at a given particle size can be expressed for a single layer as

$$\epsilon(p) = \int_0^p f_H(y)\,dy \tag{3-1}$$

where,

$\epsilon(p)$ = separation efficiency in the interval $p - \delta p/2 < p < p + \frac{\delta p}{2}$, where δp approaches zero as a limit

p = particle size

f_H = probability density function of pore size.

The observation was extended to the case of n wire cloth layers in series whose overall efficiency is:

$$\epsilon_n(p) = 1 - \prod_{i=1}^{n}\left[1 - \int_0^p f_{H_i}(y)\,dy\right] \tag{3-2}$$

The experimental results reported show reasonably good correlation between the pore size and efficiency measurements.

It will be shown in the following chapters that what Tucker observed is actually a special case of the general model for sieve performance.

In the present work, several random variables not considered by Tucker have been treated, including: particle shape, pore shape, particle attitude, and relative angular orientation between particle and pore. Partial pore blockage is also considered for the series cascade of sieve mesh layers. The general nature of the analysis presented herein allows the modeling of filtration due to arbitrary contaminant and pore shapes in terms of geometrically measurable random variables.

Since the experimental portion of the present research was restricted to nontortuous media all capture due to sieving was microscopically observable. Careful control of the particle concentration was possible.

Plan of Attack

Once the problem had been defined and the pertinent work of other investigators reviewed, a plan of attack was formulated. The course of action which was followed will be discussed briefly here to explain the continuity of the research effort.

The first step in the research was to formulate the general model based upon the assumptions implied in the statement of the problem and in terms of the following random variables:

1. Particle size.
2. Particle shape.
3. Pore size.
4. Pore shape.
5. Particle attitude.
6. Angular relationship between projection of particle in plane of mesh and the pore.

The following sub-processes were to be modeled:

1. Partial blockage of a pore by a particle of differing size and shape.
2. Passage of multiple populations of particles through one or more layers of sieve mesh.

It was anticipated that some of the input probability density functions would be known only in numerical form. Also, it was

anticipated that known functional forms of some input probability density functions would be too complicated to allow solution of the integral expressions in the general model in closed form. The following solution techniques were proposed for a feasibility evaluation:

1. Direct numerical integration.
2. Weighted simulation.
3. Monte Carlo simulation.

The general model and the appropriate solution technique were to be demonstrated by application to the problem types described in Table I.

TABLE I

EXAMPLE PROBLEMS TO BE CONSIDERED

Problem	Pore Shape	Particle Shape
A	elliptic	ellipsoidal
B	square	ellipsoidal
C	elliptic	spherical
D	square	spherical
E	A two mesh layer combination with one of the contaminants, which was chosen to be two layers of elliptic pore media and spherical particles.	

Critical steps in the empirical study were foreseen to be:

1. Preparation and evaluation of artificial contaminants.

2. Design of special test apparatus.

3. Performance of tests.

4. Evaluation of results.

The final phase of the investigation was planned to be a comparison of the experimental and analytical portions. The comparison was meant to show the validity of the work and to demonstrate the potential of the techniques developed for the solution of other problems.

CHAPTER IV

GENERAL ANALYSIS

Introduction

Objectives

The objective of this chapter is to rigorously derive a model for the sieving mechanism in hydraulic filtration. It is proposed to treat all truly random variables as such. Input data for the model will include all random variables and functional relationships which describe pore and particle, size, shape, frequency and orientation at the upstream sieve mesh surface. The desired output of the model will consist of particle size distribution downstream of the mesh, separation efficiency for each particle size and the new pore size density function for the sieve mesh after passage of the population of particles. Appropriate extensions of the basic model are desired to describe multiple sieve mesh layers and/or multiple populations of particles.

Sequence of Derivation

The rationale which explains the continuity of the entire derivation is expressed in the following sequence of steps: First, the variables of the problem are defined. Second, expressions for the probability of capture and escape are derived for the most fundamental case in which particle capture is defined by the function,

$$\mathcal{L} \geqslant H, \tag{4-1}$$

where

$\mathcal{L}$ = longest particle dimension

H = longest pore dimension.

Third, separation efficiency is derived for the fundamental case. Fourth, the fundamental model is extended to consider the effects of multiple layers of sieve mesh and/or multiple populations of particles. The fifth step is to extend the model to capture due to more complicated pore and particle shapes. This step involves consideration of particle orientation with respect to the plane of the sieve mesh and particle attitude with respect to a vector perpendicular to the sieve mesh. The final step is to derive the effects due to pores only partially blocked by captured particles.

The output variables will, thus, be expressed as integral functions of the input variables and the functional relationships stated by the assumptions. In general, the output functions will represent probability density functions conditioned to meet the statement of the problem.

Assumptions

The fundamental problem which has been defined may be visualized as filtration of a dilute solution of particulate matter through a sieve mesh. The following assumptions are made to relate the physical problem to the model which is being derived:

1. Sieving is the only filtration mechanism considered. That is, particles are captured only by virtue of particle size and shape, and pore size and shape and by virtue of orientation. Each particle

captured must touch the sieve mesh on at least one point.

2. An infinite number of pores and particles exist. In the experimental problem, where finite numbers must exist, satisfaction of the first assumption is sufficient to preclude a filter cake mode from being formed.

3. The sieve is two dimensional. That is, no significant tortuosity exists in the pore structure of the sieve mesh. The pores are thus characterized by their two dimensional geometry on the upstream side of the sieve mesh.

4. All of the following random variables are mutually independent:

a. particle size.

b. particle shape.

c. pore size.

d. pore shape.

e. angular orientation between pore major axis and the projection of the particle major axis in the plane of the sieve mesh.

f. particle attitude with respect to the plane of the sieve mesh.

5. Particles and pores can be modeled by idealized geometric shapes.

6. Pores are blocked by particles in a concentric manner (particle and pore center are on a common vector perpendicular to the plane of the sieve mesh). Experimental observations have shown that while this assumption is not strictly correct, the expected value of particle and pore relationship is reasonably concentric.

7. New pore openings formed by partial blockage of a sieve mesh pore by one or more particles are the same shape as the original pore.

In some instances, this assumption leads to the formation of equivalent pores which fit the assumption exactly only so far as capture properties are concerned. For an example see series C in Appendix A.

8. No inter-particle reactions take place.

9. Flow velocity profiles of the carrier liquid do not alter the assumptions mentioned above.

Conclusions which affect the character of the general model are discussed chronologically as they are required along with appropriate references and explanation.

Definitions

Consider a population of particles each of whose longest dimension is a random variable, P. The probability density function which relates any value, p, to its frequency of occurrences within the population is defined as, $f_P(p)$. Similarly, the probability density function of a longest pore dimension random variable, H, is, $f_H(h)$. The graphical representation of two particular values of these random variables is shown in Figure 2. In the general case the relationship between the particle position and that of the pore is also a function of random variables which define the spacial orientation of the particle with respect to the pore as well as the shape of both fundamental geometric figures. The relationship which defines capture for the general case is, then,

$$\rho^*(\rho, \varphi, \Phi, \Theta) \geq h^*(h, ch), \qquad (4\text{-}2)$$

where

p* and h* are algebraic functions defining critical dimensions of p and h, respectively.

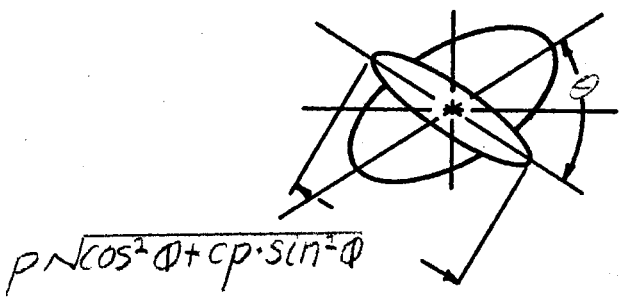

top projection

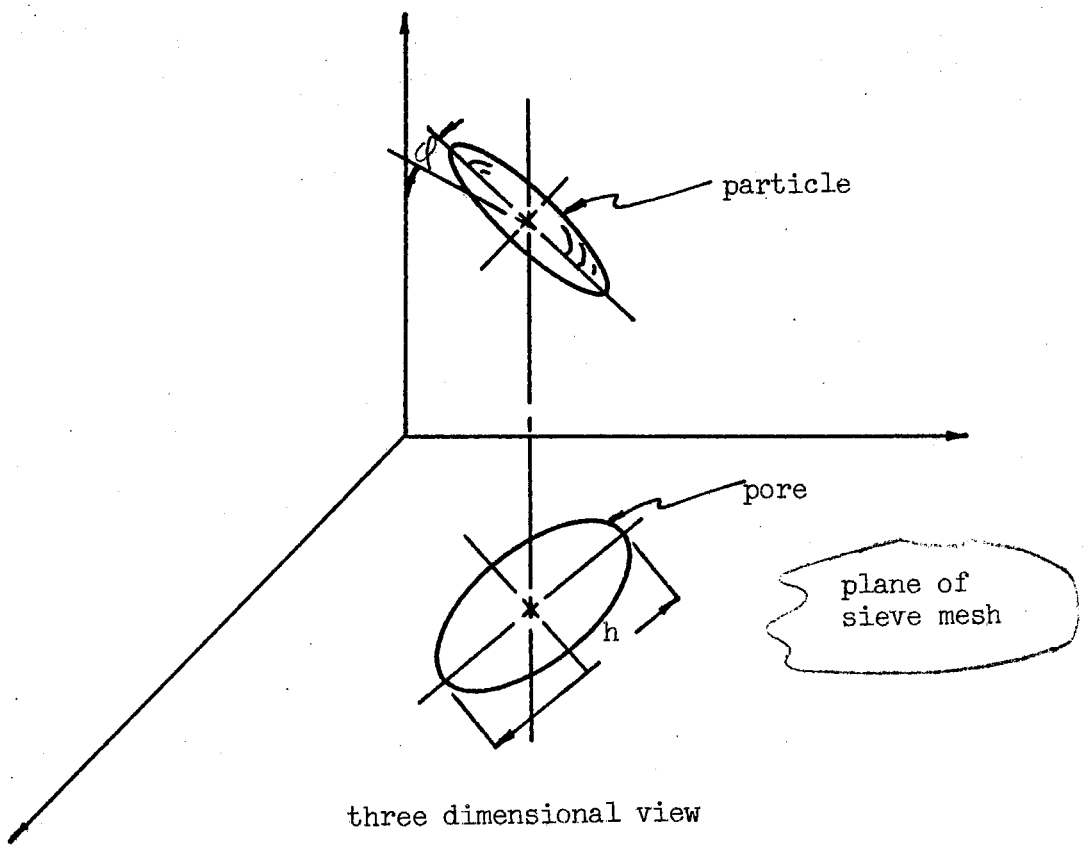

three dimensional view

Figure 2. Nomenclature

cp and ch are variables which determine the shape of the particles and of the pores and are distributed according to $f_{CP}(cp)$ and $f_{CH}(ch)$, respectively.

ϕ = the angular relationship between the major axis of the particle and the plane of the sieve mesh. ϕ is distributed according to $f_{\phi}(\phi)$.

θ = the angular relationship between the major axis of the pore and the projection of the major axis of the particle, in the plane of the sieve mesh. θ is distributed according to $f_{\theta}(\theta)$.

Obviously, Inequality 4-1 is a special case of Inequality 4-2 for which the sizes of the particles and the pores are each completely characterized by a single random variable and the angular relationships vanish. Examples of such a combination are spherical particles confronting round or square pores. More specific examples are discussed in Appendix B. The method of development here will be to derive a set of relationships based on the relationship of Inequality 4-1 and thereafter employ transformations to treat the more general case represented by Inequality 4-2.

By definition, the fraction of p sized particles in a population is defined by the limit:

$$f_L(p) = \lim_{\Delta p \to 0} \frac{Pr\{p - \frac{\Delta p}{2} < L \leq p + \frac{\Delta p}{2}\}}{\Delta p} \qquad (4\text{-}3)$$

Further the integral of Equation 4-3 represents the probability that a randomly selected particle will be of a size less than p, as expressed by:

$$Pr\{L \leq p\} = \int_0^p f_L(y)\, dy. \qquad (4\text{-}4)$$

Of course, exactly analogous expressions to Equations 4-3 and 4-4 for the pore size random variable, H, could be written.

Probabilities of Capture and Escape

For the fundamental case characterized by Inequality 4-1, the probabilities of capture can be derived by consideration of the arbitrary pore and particle density functions shown in Figure 3a. Since the pore size is independent of the particle size, and since capture of a randomly chosen particle is given by integration of the pore and particle density functions over the crosshatched area shown in Figure 3b,

$$Pr\{P \geq H\} = \int_0^\infty \left[\int_y^\infty f_P(x)\,dx\right] f_H(y)\,dy$$
$$= \int_0^\infty \left[\int_0^y f_H(x)\,dx\right] f_P(y)\,dy. \qquad (4\text{-}5)$$

Equation 4-5 is also the expected fraction of all particles which will be retained by the sieve mesh.

Integration of the appropriate density functions over the crosshatched region shown in Figure 3c yields the expected fraction of all captured particles less than any arbitrary size, r. The resultant expression is,

$$Pr\{p < r \mid P \geq H\} = \frac{\int_0^r \left[\int_0^y f_H(x)\,dx\right] f_P(y)\,dy}{\int_0^\infty \left[\int_0^y f_H(x)\,dx\right] f_P(y)\,dy}. \qquad (4\text{-}6)$$

The fraction of captured particles within a certain size interval, say $r - \frac{dr}{2} < P \leq r + \frac{dr}{2}$, is given by

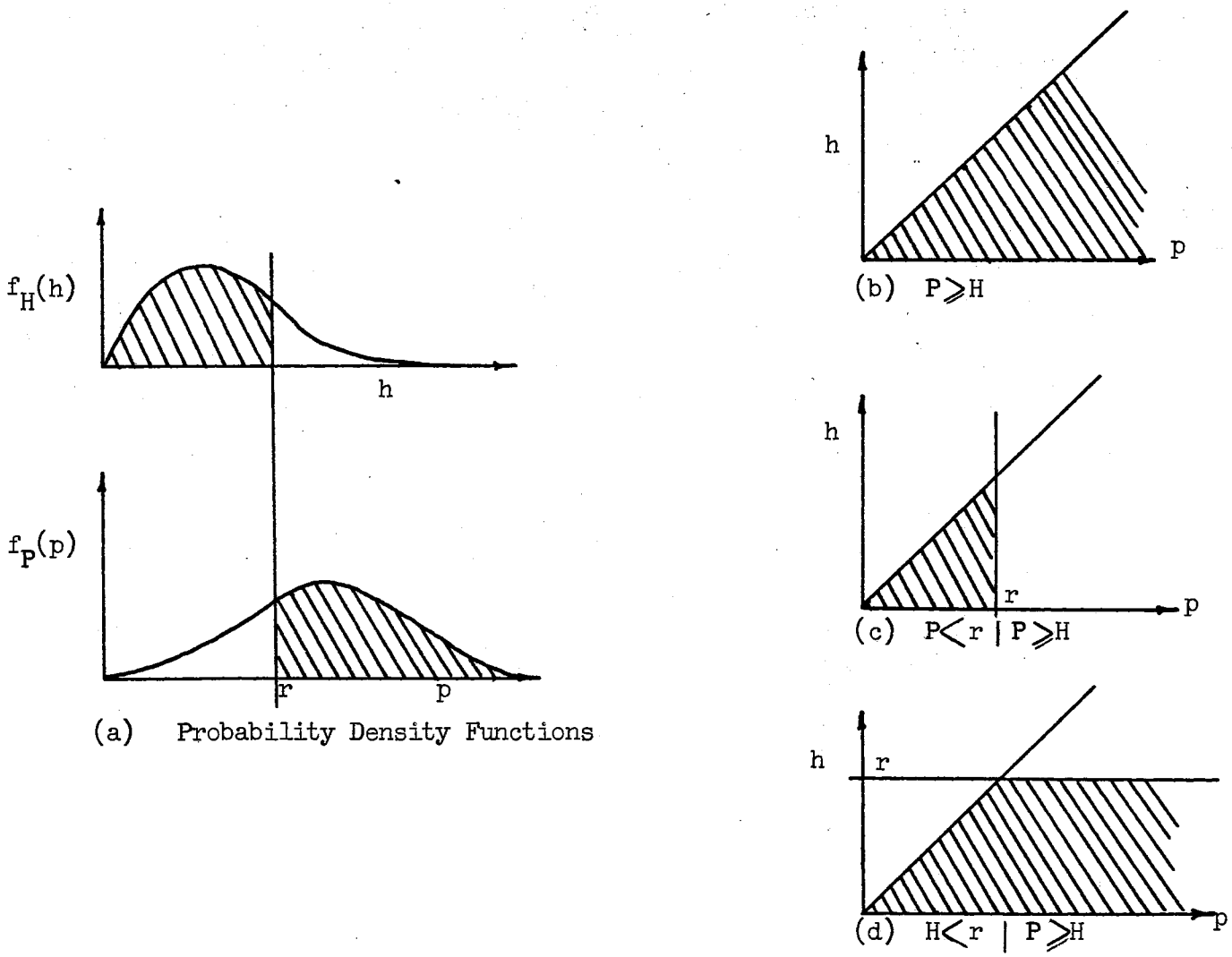

Figure 3. Schematics for Derivation of the Probability of Capture

$$Pr\{r-\tfrac{dr}{2}<P\leq r+\tfrac{dr}{2}\,|\,P\geq H\}=\int_{r-\frac{dr}{2}}^{r+\frac{dr}{2}}\int_{o}^{y} f_H(x)\,dx\, f_P(y)\,dy \Big/ \int_{o}^{\infty}\left[\int_{o}^{y} f_H(x)\,dx\right] f_P(y)\,dy \qquad (4\text{-}7)$$

In a similar way the pore distribution blocked by particles can be used to condition the probability. Thus, the expected fraction of pores less than size r blocked after one passage is:

$$Pr\{H<r\,|\,P\geq H\}=\int_{o}^{r}\left[\int_{y}^{\infty} f_P(x)\,dx\right] f_H(y)\,dy \Big/ \int_{o}^{\infty}\left[\int_{y}^{\infty} f_P(x)\,dx\right] f_H(y)\,dy \qquad (4\text{-}8)$$

The expected fraction of blocked pores in an interval of size dr is:

$$Pr\{r-\tfrac{dr}{2}<H\leq r+\tfrac{dr}{2}\,|\,P\geq H\}= \int_{r-\frac{dr}{2}}^{r+\frac{dr}{2}}\left[\int_{y}^{\infty} f_P(x)\,dx\right] f_H(y)\,dy \Big/ \int_{o}^{\infty}\left[\int_{y}^{\infty} f_P(x)\,dx\right] f_H(y)\,dy \qquad (4\text{-}9)$$

The same rationale is used in conjunction with Figure 4 to describe the probability of escape. That is, each probability is conditioned by the probability $\{P<H\}$. The analogous results are:

$$Pr\{P<H\}=\int_{o}^{\infty}\left[\int_{o}^{y} f_P(x)\,dx\right] f_H(y)\,dy = \int_{o}^{\infty}\left[\int_{y}^{\infty} f_H(x)\,dx\right] f_P(y)\,dy \qquad (4\text{-}10)$$

$$Pr\{P<r\,|\,P<H\}=\int_{o}^{r}\left[\int_{y}^{\infty} f_H(x)\,dx\right] f_P(y)\,dy \Big/ \int_{o}^{\infty}\left[\int_{y}^{\infty} f_H(x)\,dx\right] f_P(y)\,dy \qquad (4\text{-}11)$$

$$Pr\left\{r-\frac{dr}{2}<P\leq r+\frac{dr}{2}\,|\,P<H\right\}=\frac{\int_{r-\frac{dr}{2}}^{r+\frac{dr}{2}}\left[\int_{y}^{\infty}f_H(x)\,dx\right]f_P(y)\,dy}{\int_{0}^{\infty}\left[\int_{y}^{\infty}f_H(x)\,dx\right]f_P(y)\,dy} \tag{4-12}$$

$$Pr\left\{H\leq r\,|\,P<H\right\}=\frac{\int_{0}^{r}\left[\int_{0}^{y}f_P(x)\,dx\right]f_H(y)\,dy}{\int_{0}^{\infty}\left[\int_{0}^{y}f_P(x)\,dx\right]f_H(y)\,dy} \tag{4-13}$$

$$Pr\left\{r-\frac{dr}{2}<H\leq r+\frac{dr}{2}\right\}=\frac{\int_{r-\frac{dr}{2}}^{r+\frac{dr}{2}}\left[\int_{0}^{y}f_P(x)\,dx\right]f_H(y)\,dy}{\int_{0}^{\infty}\left[\int_{0}^{y}f_P(x)\,dx\right]f_H(y)\,dy}. \tag{4-14}$$

Filtrate and Pore Size Densities

The remaining step in the fundamental analysis is to derive the probability density function which describes the pore size distribution and downstream particulate distribution after passage of one population of particles through a layer of sieve mesh. The notation $f_{H(j)}^{(i)}(h)$ will denote the density of open pores of the j th sieve mesh layer after passage of the i th population of particles. Similarly, $f_{P(j)}^{(i)}(p)$ will denote the size density of the i th population of particles after passage through the j th sieve mesh layer.

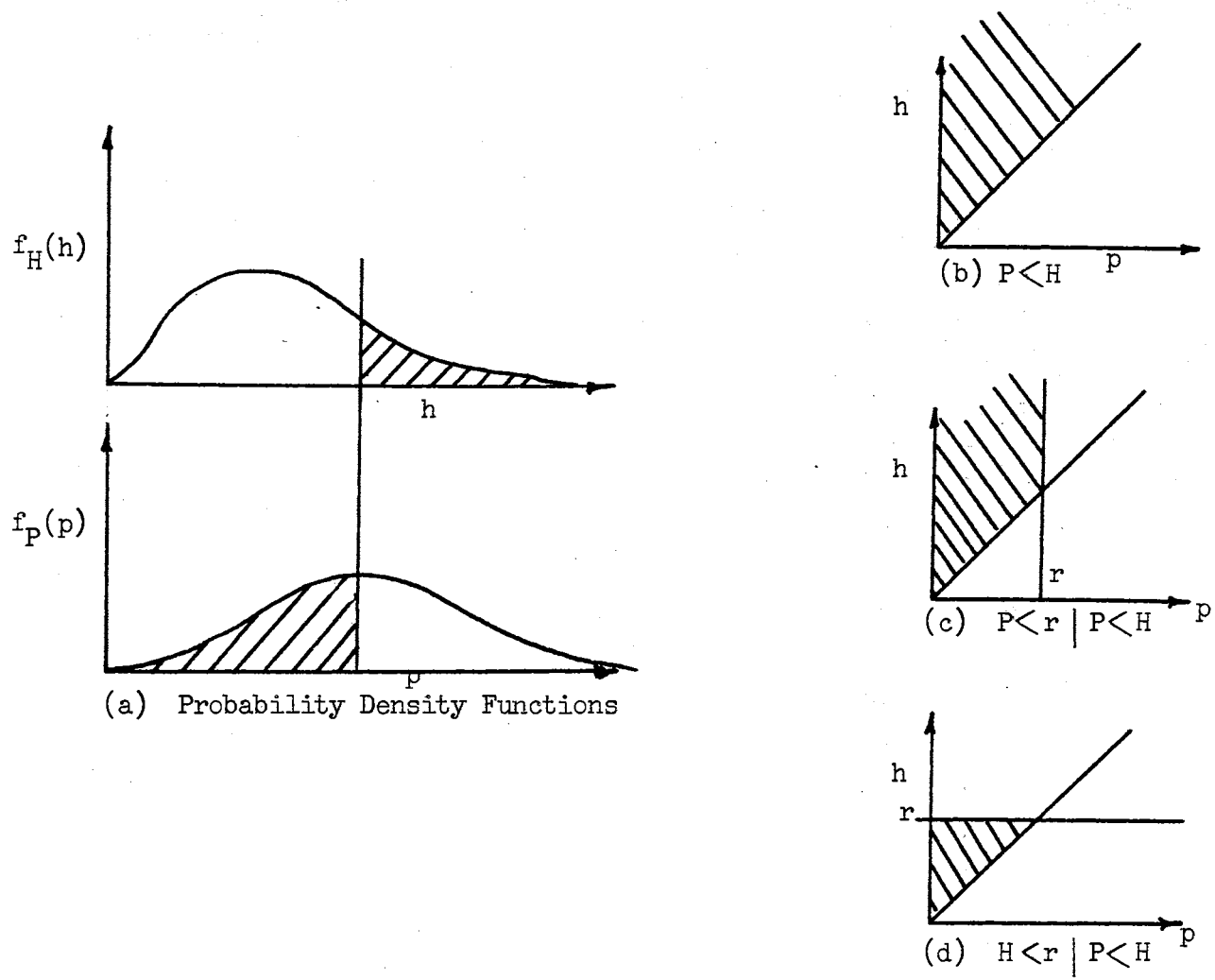

Figure 4. Schematics for Derivation of the Probability of Escape

By definition the distribution function, F, is an integral function of the probability density function, f, and can be related to the associated probability as follows for the particulate density,

$$f^{(1)}_{P_{(1)}}(p \mid P<H) = \frac{d}{dp}\left[F^{(1)}_{P_{(1)}}(p \mid P<H)\right] = \frac{d}{dp}\left[Pr\{P<p \mid P<H\}\right]. \quad (4\text{-}15)$$

With the notation given above and using Equation 4-11, Equation 4-15 becomes,

$$f^{(1)}_{P_{(1)}}(p \mid P^*<H^*) = \frac{f^{(1)}_{P(0)}(p)\int_p^\infty f^{(0)}_{H_{(1)}}(x)\,dx}{\int_0^\infty\left[\int_y^\infty f^{(0)}_{H_{(1)}}(x)dx\right] f^{(1)}_{P_{(0)}}(y)\,dy}, \quad (4\text{-}16)$$

which is the particulate density of the filtrate after passage of one population of particles through one sieve mesh layer. Hereafter the subscripts and superscripts of the probability density functions representing initial conditions will be suppressed. The notation $P^*<H^*$ will be used to denote the critical condition for capture on the appropriate population of particles at the appropriate sieving source.

Similarly, the pore size density of a single layer after passage of a population of particles can be expressed as follows:

$$f^{(1)}_{H_{(1)}}(h \mid P^*<H^*) = \frac{d}{dh}\left[F^{(1)}_{H_{(1)}}(h \mid P<H)\right]$$

$$= \frac{d}{dh}\left[Pr\{H<h \mid P<H\}\right] \quad (4\text{-}17)$$

$$= \frac{f_H(h)\int_0^h f_P(x)\,dx}{\int_0^\infty\left[\int_0^y f_P(x)dx\right] f_H(y)\,dy}.$$

Separation Efficiency

The fraction of p sized particles downstream is

$$\text{Particles Downstream} = Pr\{L<H\}\, f^{(1)}_{L_{(1)}}(p \mid L<H). \qquad (4\text{-}18)$$

Thus, the separation efficiency for a single layer may be defined,

$$\epsilon^{(1)}_{(1)}(p) = 1 - \left[Pr\{L<H\}\, f^{(1)}_{L_{(1)}}(p \mid L<H)\right] / f_L(p). \qquad (4\text{-}19)$$

As a matter of clarity, the equivalent frequency analysis expression would be given by,

$$\epsilon(p) = \frac{\text{No. p size particles upstream - No. p size particles downstream}}{\text{No. p size particles upstream}} \qquad (4\text{-}20)$$

For any general condition of capture, the efficiency can be expressed,

$$\epsilon^{(1)}_{(1)}(p) = 1 - \left[Pr(escape)\, f^{(1)}_{L_{(1)}}(p/escape)\right] / f_L(p). \qquad (4\text{-}21)$$

For the fundamental case under discussion, use of Equations 4-16 and 4-19 yields the special case,

$$\epsilon^{(1)}_{(1)}(p) = 1 - \int_p^\infty f_H(y)\, dy = \int_o^p f_H(y)\, dy. \qquad (4\text{-}22)$$

which demonstrates that the condition observed by Tucker (16) is a special case of the general expression.

A hypothetical example is now presented to clarify the preceding exposition. Consider spherical particles which oppose cylindrical pores with the following densities

$$f_H(h) = 1/3, \qquad 0 < h \leq 3,$$

and,

$$f_P(p) = 1/3 , \quad 0 < p \leq 3.$$

The resultant pore and particle size densities, probability of capture and separation efficiencies can be calculated as follows:

$$f^{(1)}_{P(1)}(p \mid P < H) = \frac{2}{9}(3-p) \tag{4-16}$$

$$f^{(1)}_{H(1)}(h \mid P < H) = \frac{2}{9} h \tag{4-17}$$

$$Pr\{P < H\} = 1/2 \tag{4-10}$$

$$\epsilon(p) = p/3. \tag{4-22}$$

The reader will, no doubt, perceive that problems of even limited complexity will generate integral expressions that will be difficult or impossible to solve in closed form. Solution techniques will be discussed in Chapter V.

Multiple Sieve Mesh Layer Analysis

It is of interest to extend the single layer analysis to include passage of a population of particles through n sieve layers in series. Later we will discuss m populations of particles passing through one sieve layer and m populations of particles passing through n sieve layers in series. Since the single layer case has been derived, the objective of this section is to find an algebraic identity which will reduce the effort of performing the single layer calculation n times. It is obvious that if the initial pore size distributions are not identical, the simplification may not be obtained. Thus, consider a population of particles with density function, $f_P(p)$, passing through n

sieve meshes with densities, $f^{(0)}_{H_{(1)}}(h) = f^{(0)}_{H_{(2)}}(h) = \ldots = f^{(0)}_{H_{(n)}}(h) = f_H(h)$.

A simple iterative process based on Equation 4-16 yields the desired expression as follows:

$$f^{(1)}_{P_{(2)}}(p \mid P^* < H^*) = \frac{f^{(1)}_{P_{(1)}}(p) \int_p^\infty f_H(x)\,dx}{\int_0^\infty \int_y^\infty f_H(x)\,dx\, f^{(1)}_{P_{(1)}}(y)\,dy}.$$

$$= \frac{f_P(p) \int_p^\infty f_H(x)dx \int_p^\infty f_H(x)dx}{\int_0^\infty \int_y^\infty f_H(x)\,dx\, f_P(y) \int_y^\infty f_H(x)\,dx\,dy}$$

$$= \frac{f_P(p) \left[\int_p^\infty f_H(x)dx\right]^2}{\int_0^\infty \left[\int_y^\infty f_H(x)\,dx\right]^2 f_P(y)\,dy},$$

$$f^{(1)}_{P_{(3)}}(p \mid P^* < H^*) = \frac{f^{(1)}_{P_{(2)}}(p) \int_p^\infty f_H(x)dx}{\int_0^\infty \int_y^\infty f_H(x)\,dx\, f^{(1)}_{P_{(2)}}(y)dy}$$

$$= \frac{f_P(p) \left[\int_p^\infty f_H(x)dx\right]^3}{\int_0^\infty \left[\int_y^\infty f_H(x)\,dx\right]^3 f_P(y)\,dy}.$$

The process is repeated until the expression for the n th layer is obtained, or,

$$f^{(1)}_{P_{(n)}}(p \mid P^* < H^*) = \frac{f_P(p)\left[\int_p^\infty f_H(x)\,dx\right]^n}{\int_o^\infty \left[\int_y^\infty f_H(x)\,dx\right]^n f_P(y)\,dy}. \qquad (4\text{-}23)$$

The density function of unblocked pores in the n th layer after passage of the first population of particles is found by combination of Equations 4-23 and 4-17 to be,

$$f^{(1)}_{H_{(n)}}(h \mid P^* < H^*) = \frac{f_H(h)\int_o^h f^{(1)}_{P_{(n-1)}}(x)\,dx}{\int_o^\infty \left[\int_y^\infty f_H(x)\,dx\right] f^{(1)}_{P_{(n-1)}}(y)\,dy} \qquad (4\text{-}24)$$

$$= \frac{f_H(h)\int_o^h f_P(x)\left[\int_x^\infty f_H(y)\,dy\right]^{n-1} dx}{\int_o^\infty \left[\int_y^\infty f_H(x)\,dx\right]^n f_P(y)\,dy}.$$

The combination of Equation 4-10 and Equation 4-23 for the population after the n-1 th layer, represents the probability that a randomly chosen particle in the population remaining between the n-1 th and n th sieve layer will escape capture, or,

$$Pr^{(1)}_{(n)}\{P^* < H^*\} = \frac{\int_o^\infty f_P(y)\left[\int_y^\infty f_H(x)\,dx\right]^n dy}{\int_o^\infty f_P(y)\left[\int_y^\infty f_H(x)\,dx\right]^{n-1} dy}. \qquad (4\text{-}25)$$

The probability that a randomly chosen particle from the original population will escape capture is expressed by the product,

$$Pr^{T(1)}_{(n)}\{P^* < H^*\} = \prod_{i=1}^{n}\left[Pr^{(1)}_{(i)}\{P^* < H^*\}\right].$$

Use of the above expression and Equation 4-25 with appropriate cancellations gives,

$$Pr_{(n)}^{T(1)}(P^*<H^*) = \int_0^\infty f_P(y)\left[\int_y^\infty f_H(x)\,dx\right]^n dy. \qquad (4\text{-}26)$$

Combining Equations 4-18, 4-26, and 4-23 yields the series separation efficiency for n layers, or,

$$\epsilon_{(n)}^{T(1)}(p) = 1-\left[\int_p^\infty f_H(y)\,dy\right]^n. \qquad (4\text{-}27)$$

Now consider the previous example as applied to the multiple layer problem. If a population of particles is passed through three (n = 3) sieve layers in series the resultant pore size density, particle size density, probability of capture and separation efficiency are respectively, calculated by the appropriate equations as follows:

$$f_{P_{(3)}}^{(1)}(p\,|\,P^*<H^*) = \frac{4}{3^4}(3-p)^3 \qquad (4\text{-}23)$$

$$f_{H_{(3)}}^{(1)}(h\,|\,P^*<H^*) = \frac{4}{3^5}\left[3^3-(3-h)^3\right] \qquad (4\text{-}24)$$

$$Pr_{(3)}^{(1)}(P^*<H^*) = 3/4 \qquad (4\text{-}25)$$

$$Pr_{(3)}^{T(1)}\{P^*<H^*\} = 1/4 \qquad (4\text{-}26)$$

$$\epsilon_{(n)}^{T(1)}(p) = 1-\left(\frac{3-p}{3}\right)^3. \qquad (4\text{-}27)$$

Multiple Populations of Particles Analysis

A similar development can be established for the case of m identical populations of particles which are sequentially passed through a single sieve mesh. The iterative process is based on Equation 4-17 and is summarized below:

$$f_{H_{(1)}}^{(2)}(h \mid P^* < H^*) = \frac{f_{H_{(1)}}^{(1)}(h) \int_0^h f_P(x)\,dx}{\int_0^\infty \left[\int_0^y f_P(x)\,dx\right] f_{H_{(1)}}^{(1)}(y)\,dy}$$

$$= \frac{f_H(h)\left[\int_0^h f_P(x)\,dx\right]^2}{\int_0^\infty f_H(y)\left[\int_0^y f_P(x)\,dx\right]^2 dy},$$

so that,

$$f_{H_{(1)}}^{(m)}(h \mid P^* < H^*) = \frac{f_{H_{(1)}}^{(m-1)}(h) \int_0^h f_P(x)\,dx}{\int_0^\infty \left[\int_0^y f_P(x)\,dx\right] f_{H_{(1)}}^{(m-1)}(y)\,dy} \qquad (4\text{-}28)$$

$$= \frac{f_H(h)\left[\int_0^h f_P(y)\,dy\right]^m}{\int_0^\infty f_H(y)\left[\int_0^y f_P(x)\,dx\right]^m dy}.$$

Combination of Equations 4-16 and 4-28 yields the expression for the particle size density due to passage of the m th population of particles through the single layer, or,

$$f_{P_{(1)}}^{(m)}(p \mid P^* < H^*) = \frac{f_P(p)\left[\int_p^\infty f_{H_{(1)}}^{(m-1)}(y)\,dy\right]}{\int_0^\infty \int_0^y f_P(x)\,dx\, f_{H_{(1)}}^{(m-1)}(y)\,dy}$$

$$f^{(m)}_{P(1)}(p \mid P^* < H^*) = f_P(p) \frac{\int_p^\infty \left[\int_0^y f_P(x)\,dx\right]^{m-1} f_H(y)\,dy}{\int_0^\infty \left[\int_0^y f_P(x)\,dx\right]^{m} f_H(y)\,dy}. \qquad (4\text{-}29)$$

The probability of a particle randomly selected from the m th population escaping capture can be found from Equations 4-10 and 4-28 to be,

$$Pr^{(m)}_{(1)}(P^* < H^*) = \int_0^\infty \left[\int_0^y f_P(x)\,dx\right] f^{(m-1)}_{H(1)}(y)\,dy$$

$$= \frac{\int_0^\infty f_H(y)\left[\int_0^y f_P(x)\,dx\right]^m dy}{\int_0^\infty f_H(y)\left[\int_0^y f_P(x)\,dx\right]^{m-1} dy}. \qquad (4\text{-}30)$$

The probability that a particle randomly selected from a randomly selected population will escape is found by the summation,

$$Pr^{T(m)}_{(1)}(P^* < H^*) = \sum_{i=1}^{m} \frac{Pr^{(i)}_{(1)}(P^* < H^*)}{m}$$

$$= \frac{1}{m}\sum_{i=1}^{m} \frac{\int_0^\infty f_H(y)\left[\int_0^y f_P(x)\,dx\right]^i dy}{\int_0^\infty f_H(y)\left[\int_0^y f_P(x)\,dx\right]^{i-1} dy}. \qquad (4\text{-}31)$$

The total efficiency can be found from the summation,

$$\epsilon^{T(m)}_{(1)}(p) = 1 - \sum_{i=1}^{m} \frac{f^{(i)}_{P(1)}(p \mid P^* < H^*) Pr^{(i)}_{(1)}(P^* < H^*)}{m\, f_P(p)}$$

$$\epsilon_{(1)}^{T(m)}(p) = 1 - \frac{1}{m}\sum_{i=1}^{m} \frac{\int_p^{\infty}\left[\int_0^y f_L(x)\,dx\right]^{i-1} f_H(y)\,dy}{\int_0^{\infty} f_H(y)\left[\int_0^y f_L(x)\,dx\right]^{i-1} dy} \qquad (4\text{-}32)$$

It should be noted that the limiting case of Equations 4-30 and 4-31 as m becomes large may violate the assumption which prohibits capture by means other than sieving. The expression for overall efficiency for multiple populations of particles is essentially a stepwise calculation and, thus, is only reported in the form of Equation 4-32.

Application of the conditions of the previous example can be used to demonstrate the calculation of particle and pore densities due to passage of three populations of particles (m = 3) through a single sieve mesh. The results are:

$$f_{L(1)}^{(3)}(p \mid L^* < H^*) = \frac{4}{3^5}\left(3^3 - p^3\right) \qquad (4\text{-}29)$$

$$f_{H(1)}^{(3)}(h \mid L^* < H^*) = \frac{4}{3^4}\,h^3 \qquad (4\text{-}28)$$

$$Pr_{(1)}^{(3)}(L^* < H^*) = 3/4 \qquad (4\text{-}30)$$

$$\epsilon_{(1)}^{T(3)}(p) = 1 - \frac{1}{3}\sum_{i=1}^{3}\left[\frac{(3^i - p^i)}{3^i}\right] \qquad (4\text{-}32)$$

$$Pr_{(1)}^{T(3)}(P^* < H^*) = 23/36 . \qquad (4\text{-}31)$$

Equations 4-23 through 4-30 are expressed in terms of the initial pore and particle density functions. They, therefore, offer a worthwhile computational tool. No apparent algebraic manipulation exists to compute the conditions after passage of m populations of particles through n layer of sieve mesh. The problem is one which must be solved in a stepwise manner. A technique for mechanization of the problem will be considered in the next chapter.

Particle Capture

Even in a study restricted to idealized particle and pore geometries, the criterion for particle capture is generally more complicated than that of Equation 4-1. Figure 2 graphically depicts the random variables upon which capture depends. The most general condition for escape can be written in terms of critical pore and particle random variables P* and H*, and is,

$$P^*(P, CP, \Phi, \Theta) < H^*(H, CH) \qquad (4\text{-}33)$$

where, the random variables correspond to those defined on pages 22 and 24. If the geometric relationships implied by Inequality 4-33 are known and the random variables are independent, then the expressions which were previously derived can be extended to reflect the more complicated geometric capture.

From geometric relationships the probabilities,

$$Pr\{\mathcal{P}<p \mid \mathcal{P}^*<H^*\}$$

and

$$Pr\{H<h \mid \mathcal{P}^*<H^*\}$$

are derived as integral expressions. Then the desired conditional probability densities after filtration can be calculated as follows:

$$f^{(1)}_{\mathcal{P}_{(1)}}(p \mid \mathcal{P}^*<H^*) = \frac{d}{dp} Pr\{\mathcal{P}<p \mid \mathcal{P}^*<H^*\} \tag{4-34}$$

and,

$$f^{(1)}_{H_{(1)}}(h \mid \mathcal{P}^*<H^*) = \frac{d}{dh} Pr\{H<h \mid \mathcal{P}^*<H^*\}. \tag{4-35}$$

Examples will now be considered to demonstrate the use of Equations 4-34 and 4-35. Some useful geometric relationships are derived in Appendix A. Only the results are employed here.

Consider spherical particles approaching elliptical pores as shown in Figure 5c. If the major and minor axes of the pores are related by a constant, k_1, the proper criterion for escape is,

$$\mathcal{P}<k_1 H. \tag{4-36}$$

The operations corresponding to Equation 4-34 and Inequality 4-36 are,

$$f^{(1)}_{\mathcal{P}_{(1)}}(p \mid \mathcal{P}<k_1 H) = \frac{d}{dp} \frac{\int_0^p \int_{y/k_1}^\infty f_H(x)dx\, f_{\mathcal{P}}(y)dy}{\int_0^\infty \int_{y/k_1}^\infty f_H(x)dx\, f_{\mathcal{P}}(y)dy} \tag{4-37}$$

$$= \frac{f_{\mathcal{P}}(p) \int_{p/k_1}^\infty f_H(x)\,dx}{\int_0^\infty \int_{y/k_1}^\infty f_H(x)dx\, f_{\mathcal{P}}(y)dy},$$

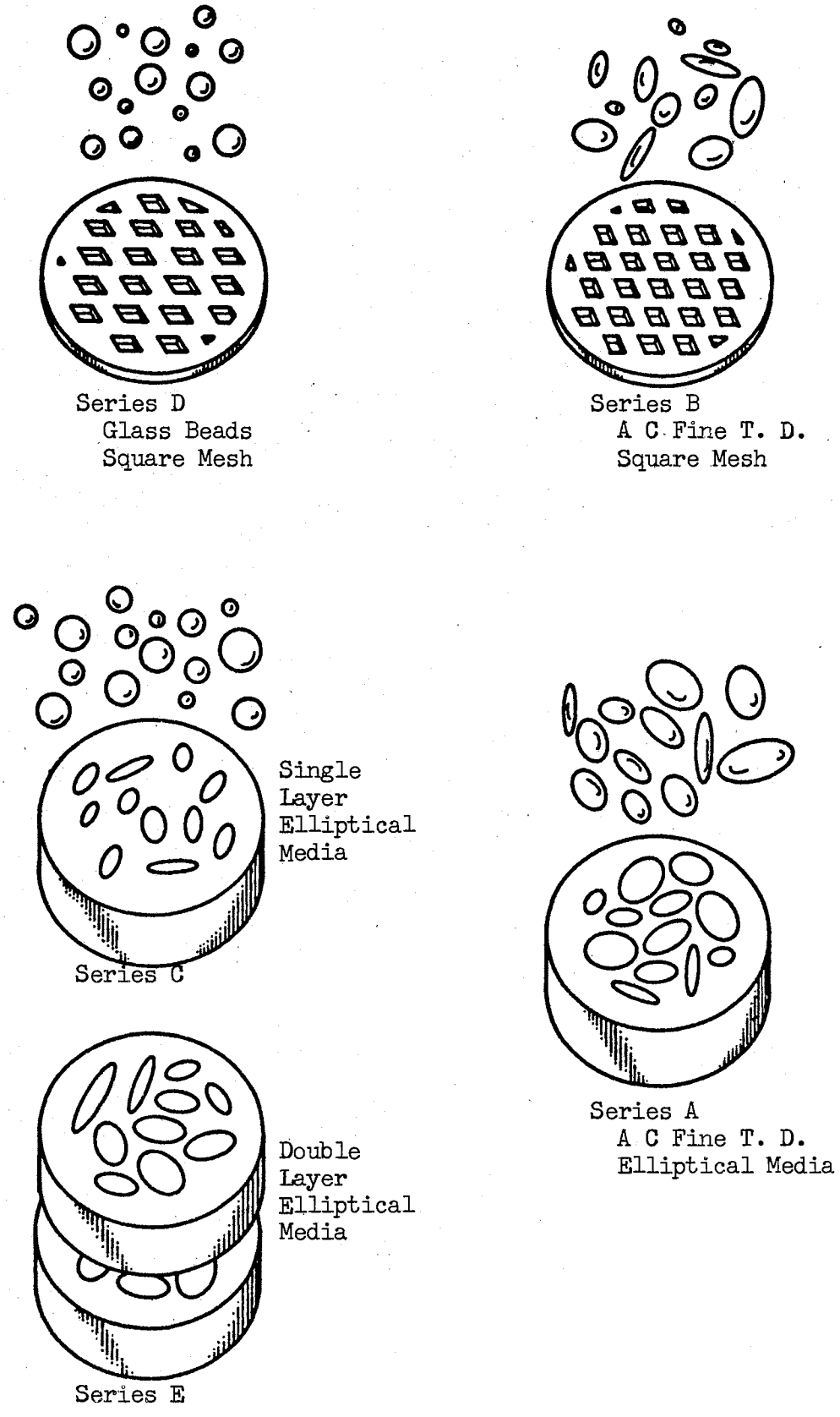

Figure 5. Filtration Geometries

and

$$f_{H_{(1)}}^{(1)}(h \mid P<k_1 H) = \frac{f_H(h)\int_0^{k_1 h} f_P(x)\,dx}{\int_0^{\infty}\int_0^{k_1 y} f_P(x)\,dx\, f_H(y)\,dy}. \qquad (4\text{-}38)$$

The region of integration is shown in Figure 6.

The, by now familiar, example can be solved for $k_1 = \frac{1}{2}$ to yield,

$$f_{P_{(1)}}^{(1)}(p \mid P<H/2) = \frac{4}{9}(3-2p), \quad p_{max} = 3/2 \qquad (4\text{-}37)$$

$$f_{H_{(1)}}^{(1)}(h \mid P<H/2) = \frac{2}{9}h, \qquad h_{max} = 3 \qquad (4\text{-}38)$$

Now suppose the critical dimension of the particle had been an arbitrary function of p such that the criterion for escape was,

$$P < g(H). \qquad (4\text{-}39)$$

By referring to Figure 6b, the solution for the downstream particulate density can be seen to be,

$$f_{P_{(1)}}^{(1)}(p \mid P<g(H)) = \frac{f_P(p)\int_{g^{-1}(p)}^{\infty} f_H(x)\,dx}{\int_0^{\infty}\int_{g^{-1}(y)}^{\infty} f_H(x)\,dx\, f_P(y)\,dy}. \qquad (4\text{-}40)$$

Similarly the remaining pore size distribution is,

$$f_{H_{(1)}}^{(1)}(h \mid P<g(H)) = \frac{f_H(h)\int_0^{g(h)} f_P(x)\,dx}{\int_0^{\infty}\int_0^{g(y)} f_P(x)\,dx\, f_H(y)\,dy}. \qquad (4\text{-}41)$$

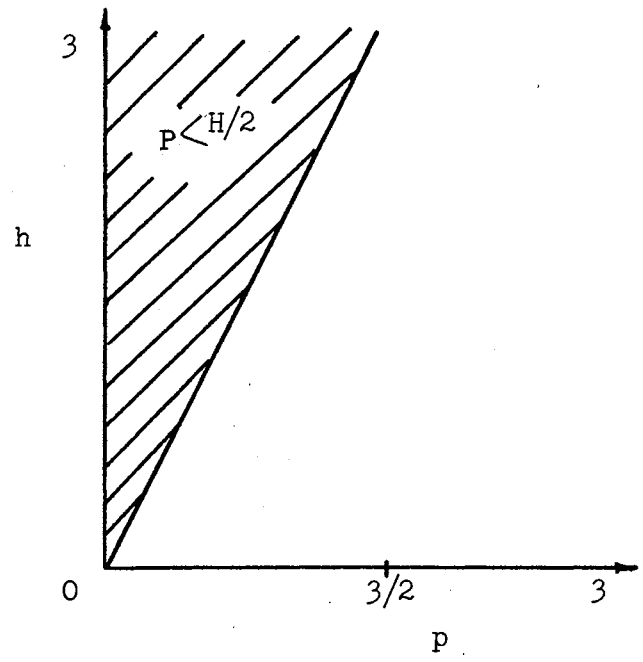

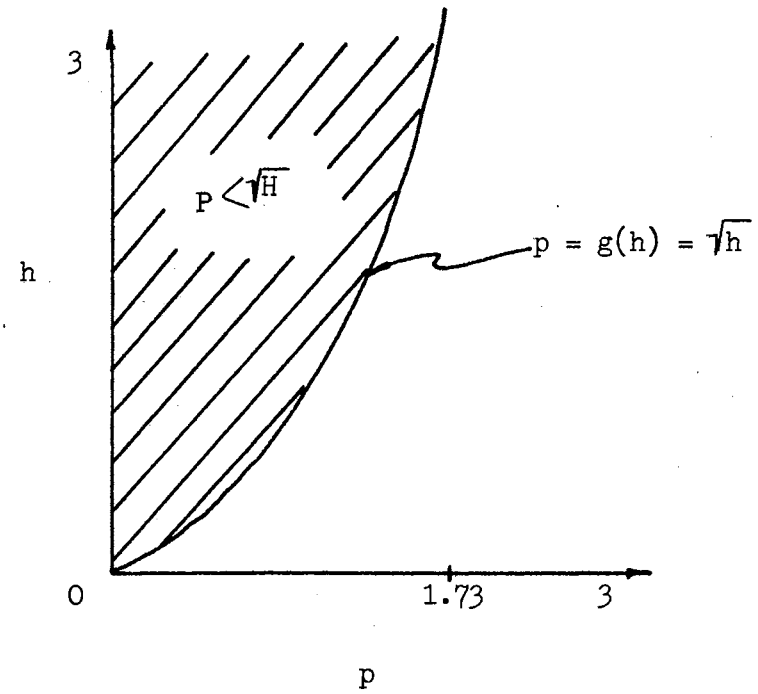

Figure 6. Regions of Integration

Once again the former example is employed, this time with $g(H) = \sqrt{H}$. The result is,

$$f^{(1)}_{P_{(1)}}(p \mid P<\sqrt{H}) = \frac{3-p^2}{2\sqrt{3}}, \quad p_{max}=\sqrt{3}, \qquad (4\text{-}40)$$

$$f^{(1)}_{H_{(1)}}(h \mid P<\sqrt{H}) = \frac{\sqrt{h}}{2\sqrt{3}}, \quad h_{max}=3. \qquad (4\text{-}41)$$

Another possibility is that the criterion of capture can be affected by more than one random variable. Suppose, for instance, that the shape factor, CH, of the ellipsoidal pores shown in Figure 5c is itself a random variable with density function $f_{CH}(ch)$. To find the desired results of filtration, first define a new random variable by use of the function,

$$h^* = ch \cdot h,$$

The density function, $f_{H^*}(h^*)$, may be found by a widely known transformation (See Breipohl [18] on page 151). First, define

$$u = h,$$

then,

$$f_{U,H^*}(u, h^*) = f_{H,CH}(h(u), ch(u, h^*))\,|J| \qquad (4\text{-}42)$$

where

$$J = \begin{vmatrix} \frac{\partial h(u)}{\partial u} & \frac{\partial h(u)}{\partial h^*} \\ \frac{\partial ch(u,h^*)}{\partial u} & \frac{\partial ch(u,h^*)}{\partial h^*} \end{vmatrix} = \frac{\partial ch(u,h^*)}{\partial h^*}.$$

Since CH has previously been assumed to be independent of H, the joint

density Equation 4-42 is known in terms of marginal densities, and the random variable, U, can be removed as follows,

$$f_{H^*}(h^*) = \int_0^\infty f_H(h(u)) f_{CH}(u, h^*) \left| \frac{\partial ch(u, h^*)}{\partial h^*} \right| du. \quad (4\text{-}43)$$

The problem of the downstream particle size distribution is, at this point, analogous to the fundamental problem whose solution is Equation 4-16, so that

$$f^{(1)}_{P_{(1)}}(p \mid P < H^*) = \frac{f_P(p) \int_p^\infty f_{H^*}(x)\, dx}{\int_0^\infty \int_y^\infty f_{H^*}(x) dx\, f_P(y)\, dy}. \quad (4\text{-}44)$$

The remaining pore size distribution is analogous to Equation 4-17. The calculation yields,

$$f^{(1)}_{H^*_{(1)}}(h^* \mid P < H^*) = \frac{f_{H^*}(h^*) \int_0^{h^*} f_P(x)\, dx}{\int_0^\infty \int_0^y f_P(x)\, dx\, f_{H^*}(y)\, dy}. \quad (4\text{-}45)$$

The remaining pore size density in terms of the measured dimension, h, is obscured since CH, and H are no longer independent after filtration. That is to say, the pores with small values of h and/or ch tend to be selectively blocked. However, the h* variable is more meaningful physically than the h variable for further capture analysis.

For example, consider the density on ch given by,

$$f_{CH}(ch) = 1.44/ch, \quad .5 < ch \leq 1.$$

The density is shown in Figure 7 along with the mapping from the (h, ch)

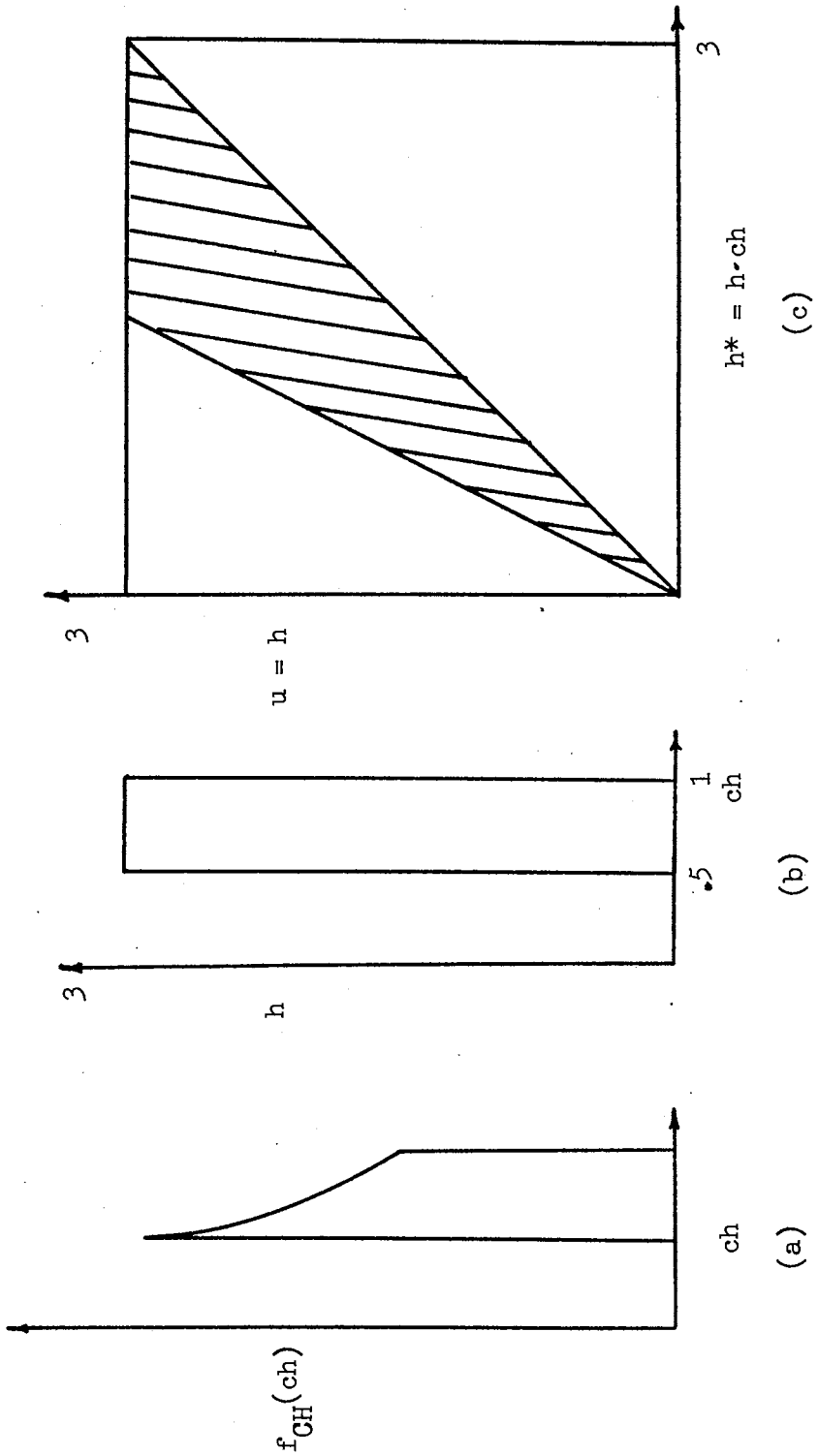

Figure 7. Random Pore Shape Example

plane to the (u, h*) plane necessary to perform the integration described by Equation 4-43. The new critical dimension density must be expressed over two intervals as follows:

$$f_{H^*}(h^*) = \frac{1.44}{3}\int_{h^*}^{2h^*} \frac{u}{h^*}\left|\frac{\partial h^*/u}{\partial h^*}\right| du = \frac{1.44}{3}, \quad 0 < h^* \leqslant \frac{3}{2},$$

and,

$$f_{H^*}(h^*) = \frac{1.44}{3}\int_{h^*}^{3} \frac{1}{h^*}\, du = \frac{1.44}{3}\left(\frac{3}{h^*} - 1\right), \quad \frac{3}{2} < h^* \leqslant 3.$$

The remaining application of Equations 4-44 and 4-45 is straightforward.

Capture Due to Angular Relationships

A still more general condition for particle capture involves a particle of shape such that its capture is, at least some times, a function of its orientation. Simple examples are shown in Figures 5a and 8. The corresponding criterion for escape is,

$$P^*(P, \measuredangle P, \Theta) < H^*(H, \measuredangle H).$$

As an example of this sort of problem, consider an ellipsoidal particle in the plane of the sieve mesh as it impinges concentrically upon a square pore. the particle will escape, if

(a) $P < H$

or

(b) $P \cdot \measuredangle P < H \leqslant P$

$$\Theta_{min}(p, h) < \Theta < \Theta_{max}(p, h),$$

where

Θ_{min}, Θ_{max} are the minimum and maximum angular displacements which will allow capture. Here let

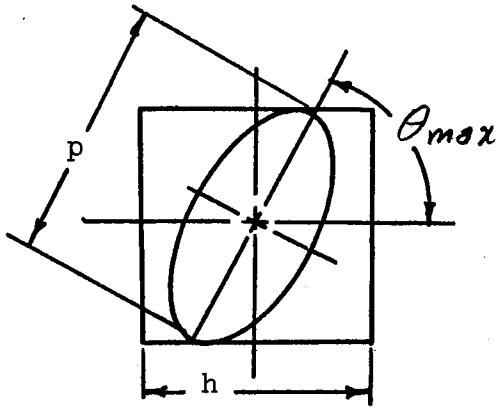

Figure 8. Square Pore and Ellipsoidal Particle

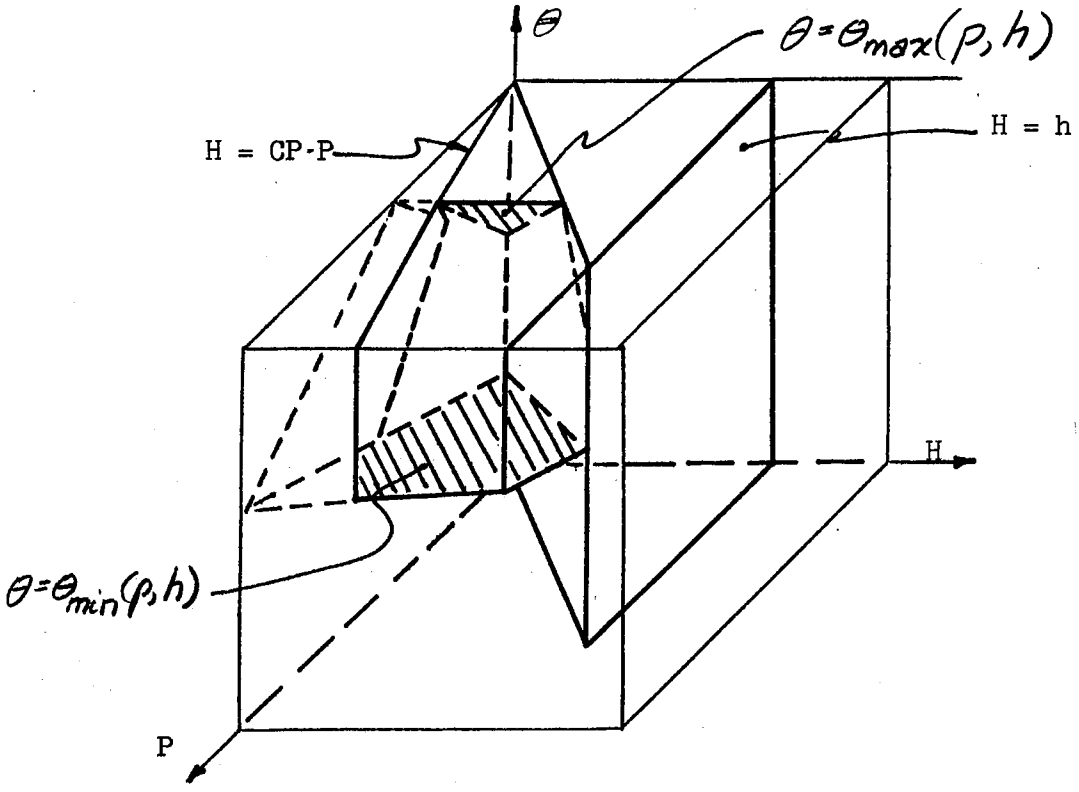

Figure 9. Integral Volume for Escape

cp = constant.

Examples of the functions θ_{min} and θ_{max} are presented for ellipsoidal particles with square and elliptical pores in Appendix A. In the case of concentric elliptical pores and elliptical particles the closed form solutions for θ_{min} and θ_{max} does not exist and must be found numerically. An algorithm to evaluate these quantities is presented in Appendix B.

Since H, P, and θ are independent, the probability used to find the pore size distribution after filtration can be written as

$$Pr\{H<h \mid P<H \bigcup \subset P \cdot P<H \leq P,\ \theta_{min}<\theta<\theta_{max}\}.$$

The required operations may also be carried out in two steps and weighted as

$$Pr\{H<h \mid escape\} = [Pr\{H<h \mid P<H\}\ Pr\{P<H\} + Pr\{H<h \mid Q\}\ Pr\{Q\}] / [Pr\{P<H\} + Pr\{Q\}] \quad (4\text{-}46)$$

$$= \frac{Pr\{H<h,\ P<H\} + Pr\{H<h,\ Q\}}{Pr\{P<H\} + Pr\{Q\}},$$

where

$$Q = \{\subset P \cdot P<H \leq P,\ \theta_{min}<\theta<\theta_{max}\},$$

Thus the desired density function is

$$f_{H(1)}^{(1)}(h \mid escape) = \frac{d}{dh} \frac{Pr\{H<h,\ P<H\} + \frac{d}{dh} Pr\{H<h,\ Q\}}{Pr\{P<H\} + Pr\{Q\}} \quad (4\text{-}47)$$

which can be expressed in general terms, as,

$$f_{H(1)}^{(1)}(h/escape) = \left[f_H(h) \int_0^h f_p(x)\,dx + \right.$$

$$\left. f_H(h) \int_h^{h/\epsilon p} \int_{\theta_{min}(x,h)}^{\theta_{max}(x,h)} f_\theta(z)\,dz\, f_p(x)\,dx \right] / \qquad (4\text{-}48)$$

$$\left[\int_0^\infty \int_0^y f_p(x)\,dx\, f_H(y)\,dy + \int_0^\infty \int_y^{y/\epsilon p} \int_{\theta_{min}(x,y)}^{\theta_{max}(x,y)} f_\theta(z)\,dz\, f_p(x)\,dx\, f_H(y)\,dy \right].$$

In the same manner the analogous expression for the downstream particle size distribution is derived with the result,

$$f_{p(1)}^{(1)}(p/escape) = \left[f_p(p) \int_p^\infty f_H(x)\,dx + \right.$$

$$\left. f_p(p) \int_{\epsilon p \cdot p}^{p} \int_{\theta_{min}(x,p)}^{\theta_{max}(x,p)} f_\theta(z)\,dz\, f_H(x)\,dx \right] / \qquad (4\text{-}49)$$

$$\left[\int_0^\infty \int_y^\infty f_H(x)\,dx\, f_p(y)\,dy + \int_0^\infty \int_{\epsilon p \cdot y}^{y} \int_{\theta_{min}(x,y)}^{\theta_{max}(x,y)} f_\theta(z)\,dz\, f_H(x)\,dx\, f_p y\,dy \right].$$

It is quite obvious from the form of Equations 4-48 and 4-49 that even the most simple density functions and algebraic functions can lead to intractable integral expressions. Solution techniques are discussed in the next chapter.

Particle Attitude

Since particles approaching a sieve mesh are free to assume any orientation in three dimensional space, it is necessary to model the projection of the particle as seen by an observer looking out of a sieve mesh pore. Once a probability density function has been developed for particle size and shape in a controlled spatial orientation, the next step is to determine the probability density function for the size and shape of particle projection in the plane of the sieve mesh. It will be assumed that the particles are uniform solids of rotation or regular flat-sided solids. Thus, the results of transport of a single particle through the viscous medium can be the basis of the required transformation in the stochastic problem. The resulting integral expression can be solved only in closed form for the most simple cases. A numerical technique is outlined in Appendix B for evaluating the expression.

The Deterministic Problem

It is of fundamental interest to model the hydrodynamic forces due to translation of a solid of rotation through a viscous liquid. The general problem must consider relative motion between the particle and the fluid at infinity. Examination of the body forces on small (nominally 25μ) particles in hydraulic oil establishes a terminal velocity yielding a Reynolds number well within the range of creeping flow. The equations of motion in this case can be written without the inertia terms.

Batchelor (19) on page 238, and Happle and Brenner (20) on page 220, refer to Lamb's (21) development for the problem of settling of

solids of revolution. It should be noted, however, that Lamb's solutions for the ellipsoid of revolution settling slowly in a viscous fluid applies only to the cases in which a major axis of the ellipsoid is aligned parallel to its velocity. Happle and Brenner give some useful extensions of Lamb's expressions.

A particularly important concept developed by Happle and Brenner on page 199, is that bodies of revolution possessing fore and aft symmetry and uniform density do not generate a hydrodynamic couple due to slow translation through a viscous medium. Therefore, an ellipsoid will not tumble as it settles in a viscous fluid. The ellipsoid will tend to settle on a nonvertical trajectory with the same orientation throughout its translation. Herdan (14) concludes that compact particles of irregular or angular shape will retain their initial orientation while translating in the creeping mode. Herdan also states that nonspherical particles with three mutually perpendicular planes of symmetry will fall without any preferred orientation. The conclusion which should be drawn for the idealized problem which has been defined is that particle orientation is non-preferential. Therefore, it is appropriate to characterize the probability density function on particle orientation as uniform between 0 and $\pi/2$.

Modification of the Particle Probability Density Function

The general problem has been established to find the probability density function of the projection of the particle, $f_S(s)$, from the probability density function on the particle characteristic dimension, $f_P(p)$ and the algebraic relation relating projection to length, or,

$$s = s(p, \phi) \qquad (4\text{-}50)$$

where ϕ = orientation perpendicular to sieve plane, and

$$f_{\phi}(\phi) = \frac{2}{\pi}, \quad 0<\phi<\pi/2. \tag{4-51}$$

The problem is solved by the application of a well known transformation and the fact that the marginal densities $f_p(p)$, and $f_{\phi}(\phi)$, are independent. In general the transformation is:

$$f_{S,U}(s,u) = f_{P,\phi}(p,\phi)|J| \tag{4-52}$$

$$= f_P(p(s,u)) f_{\phi}(\phi(u))|J|, \tag{4-53}$$

where,

S is defined in Equation 4-50

$$u = \phi,$$

and, therefore,

$$|J| = \left|\frac{\partial p(s,u)}{\partial s}\right|. \tag{4-54}$$

To find the marginal density we need only to integrate Equation 4-53 between the limits established by mapping the boundaries of the p, ϕ plane into the s, u plane, or

$$f_S(s) = \int_{u(s,p_{min})}^{u(s,p_{max})} f_P(p(s,u)) f_{\phi}(\phi(u))|J|\,du. \tag{4-55}$$

For example, if p is the diameter of a hemisphere with

$$f_P(p) = 1/3, \quad 0<p<3, \tag{4-56}$$

then,

$$S = \frac{P}{2}(1 + \cos\Phi).$$

Equation 4-55 becomes:

$$f_S(S) = \frac{4}{3\pi}\int_0^{\pi/2} \frac{1}{1+\cos u}\,du = \frac{4}{3\pi}, \quad 0 < S \leq 3/2 \qquad (4\text{-}57)$$

and

$$f_S(S) = \frac{4}{3\pi}\int_0^{\cos^{-1}\left(\frac{2S}{3}-1\right)} \frac{1}{1+\cos u}\,du = \frac{4}{3\pi}\tan\frac{S}{2}, \quad 3/2 < S \leq 3. \qquad (4\text{-}58)$$

Integration of Equations 4-57 and 4-58 over their respective ranges of S demonstrates that $f_S(s)$ is indeed a density function. A numerical technique for solution of Equation 4-55 is presented in Appendix B.

Partial Blockage

Capture of a particle by a pore whose shape is not identical to that of the particle projection will result in the formation of a finite number of pores smaller than the original pore. It has been previously assumed that the shape of the new pore can be modeled as geometrically similar to that of the original pore so long as the critical size variable for capture, h*, is accurately described. In general, the new pore size is an algebraic function of the formerly mentioned random variables, so that,

$$h_{new} = g_2(p, h, \theta, \Phi, cp, ch).$$

For the purposes of the following exposition, the case in which the new pore size is a function of the former pore size and particle

size, as well as the case involving the angular displacement, θ, will be discussed. In the first case the new size relationship can be expressed,

$$h_{new} = g_3(p, h).$$

If k_3 new pores are formed by one blockage the total pore size distribution remaining after filtration of one population of particles is,

$$f_{\hat{H}}(\hat{h}) = \left[f_H(\hat{h} \mid P^* < H^*) \Pr\{P^* < H^*\} + k_3 f_{H_{new}}(\hat{h} \mid P^* \geq H^*) \Pr\{P^* \geq H^*\} \right] / \left[\Pr\{P^* < H^*\} + k_3 \Pr\{P^* \geq H^*\} \right] \qquad (4\text{-}59)$$

All of the terms of Equation 4-59 have been previously derived with the exception of $f_{H_{new}}(\hat{h} \mid P^* \geq H^*)$. That term can be obtained, in general, by defining,

$$u = h$$

so that

$$f_{H_{new}, U}(h_{new}, u \mid P^* \geq H^*) = \frac{f_P(p(h_{new}, u)) f_H(h(u)) |J|}{\Pr\{P^* \geq H^*\}}$$

where

$$J = \begin{vmatrix} \dfrac{\partial p(h_{new}, u)}{\partial h_{new}} & \dfrac{\partial p(h_{new}, u)}{\partial u} \\ \dfrac{\partial h(u)}{\partial h_{new}} & \dfrac{\partial h(u)}{\partial u} \end{vmatrix} = \frac{\partial p(h_{new}, u)}{\partial h_{new}},$$

$$g_2^{-1} = p(h_{new}, u),$$

and,

$$f_{H_{new}}(h_{new}|L^* \geq H^*) = \frac{\int_0^\infty f_L(p(h_{new},u)) f_H(h(u)) \left| \frac{\partial p(h_{new},u)}{\partial h_{new}} \right| du}{Pr\{L^* \geq H^*\}}.$$

As an example if

$$Pr\{L^* < H^*\} = Pr\{L < H\}$$

then Equation 4-59 becomes,

$$f_{\hat{H}}(\hat{h}) = \frac{f_H(\hat{h}) \int_0^{\hat{h}} f_L(x)\,dx + k_3 \int_0^\infty f_L(p(\hat{h},u)) f_H(h(u))\,du}{k_3 + (1-k_3)\int_0^\infty \int_y^\infty f_H(x)\,dx\, f_L(y)\,dy}. \quad (4\text{-}60)$$

The modification of Equation 4-59 required for consideration of an angular dependency upon capture is as follows, since,

$$h_{new} = g_3(h, p, \theta)$$

and defining

$$u = h$$

and

$$v = \theta$$

it can be shown that

$$J = \frac{\partial p(h_{new}, u, v)}{\partial h_{new}}$$

where

$$g_3^{-1} = p(h_{new}, u, v).$$

Comments on the General Model

In this chapter expressions have been developed for the particulate densities and pore size densities resulting from filtration of liquid born particles through flat sieve mesh layers. Multiple sieve meshes in series and multiple population of particles problems have been analyzed also. The derivations are in terms of the geometrically measurable random variables: pore size, pore shape, particle size, particle shape, particle attitude and the angular displacement between the particle and the pore major axes. Necessary algebraic relationships were also introduced to describe particle capture and partial blockage of pores. A few hypothetical examples have been included, and a number more considered by the author

Examination of at least ten other example problems has led the author to two notable conclusions concerning the utility of the general model. First, equation forms presented above are the most convenient for problem solution. Further manipulation of the general integral expressions will tend to make the calculation of integration limits for a particular problem more difficult. The problem represented by Figure 9 is an example.

Second, only the most simple functional forms will admit closed form solutions for the integral expressions. Therefore, whatever quantitative results are to be obtained for practical problems will have to be based on numerical solutions. Numerical techniques are discussed in the next chapter.

CHAPTER V

SOLUTION TECHNIQUES

Introduction

The general expressions for the probability density functions of pores and particles remaining after sieving have been derived. Of even more specific interest is the expression for separation efficiency which has also been developed. These expressions can be described as nested integral functions of the original marginal probability density functions. It is immediately evident that difficulties will be encountered in integration of these expressions for realistic probability density function.

The elementary doubly nested integral density functions which are integrable in closed form include: uniform, linear, exponential and identical half normal. Those integral density functions which are not integrable in closed form include: Gamma, Beta, log normal, normal and non-identical half normal. Thus, it can be immediately concluded that since lognormal particulate densities are common, a closed form solution cannot be obtained in the general case. It is then necessary to evaluate the means of solution which will admit complicated functions.

The ideal solution method would be straightforward, accurate, economical, and accept data in numerical rather than functional form. Taylor series expansions were attempted without notable success. The remaining methods of solution can be categorized as direct numerical

integration, Monte Carlo simulation and weighted simulation. These methods are discussed in more detail in the remainder of this chapter.

Numerical Integration

No doubt, the most straightforward method of solution for the general forms:

$$I\ II = \int_0^{P_{max}} \int_{H_1(x)}^{H_2(x)} f_H(z)\,dz\, f_P(x)\,dx \qquad (5\text{-}1)$$

$$I\ III = \int_0^{P_{max}} \int_{H_1(x)}^{H_2(x)} \int_{\theta_{min}(x,z)}^{\theta_{max}(x,z)} f_\theta(y)\,dy\, f_H(z)\,dz\, f_P(x)\,dx, \qquad (5\text{-}2)$$

is numerical integration. Provision must be made for calculation of the limiting values at appropriate points in the solution. A general scheme for calling a numerical integration subroutine appropriate to the solution of the expressions marked I II and I III is given in Flow Charts, Figures 10 and 11 respectively. The flow charts and their corresponding digital computer user oriented algorithms are general. However, the algorithm is left sufficiently flexible to allow the user to arrange the order of integration to facilitate computation by taking advantage of known functional relationships. Note that to solve a given problem the algorithm may have to be applied several times.

The general numerical integration technique is easily programmed to accept data in numerical form. With the probability density functions given in numerical form the transformations necessary to describe partial blockage (see Equation 4-55 for example) add complexity to the problem. Linear transformations do not affect the

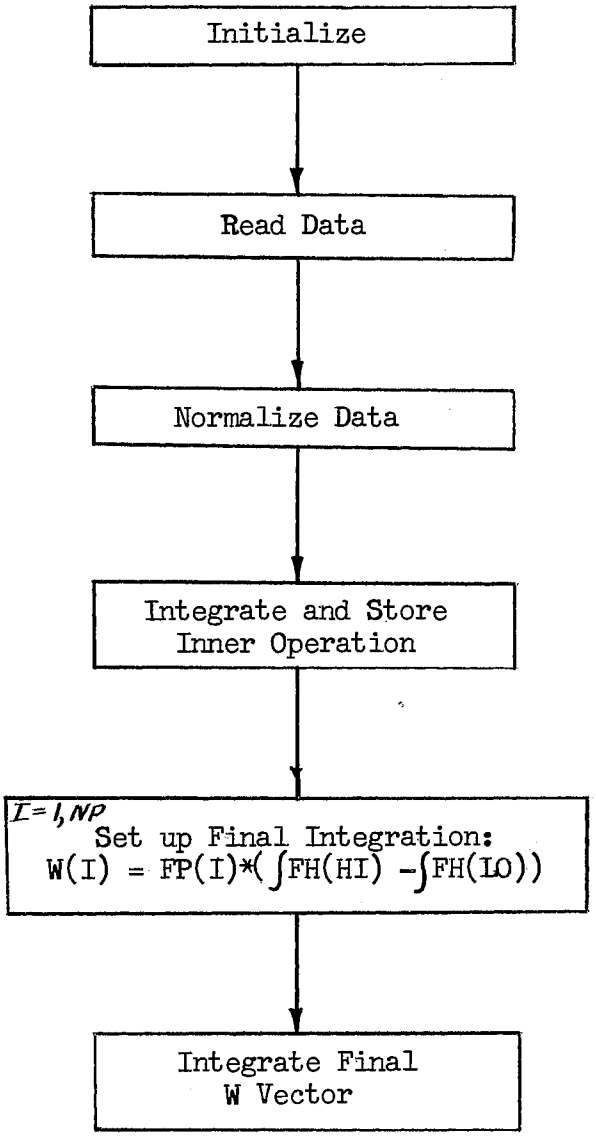

Figure 10. Flow Chart for Doubly Nested Probability Integral

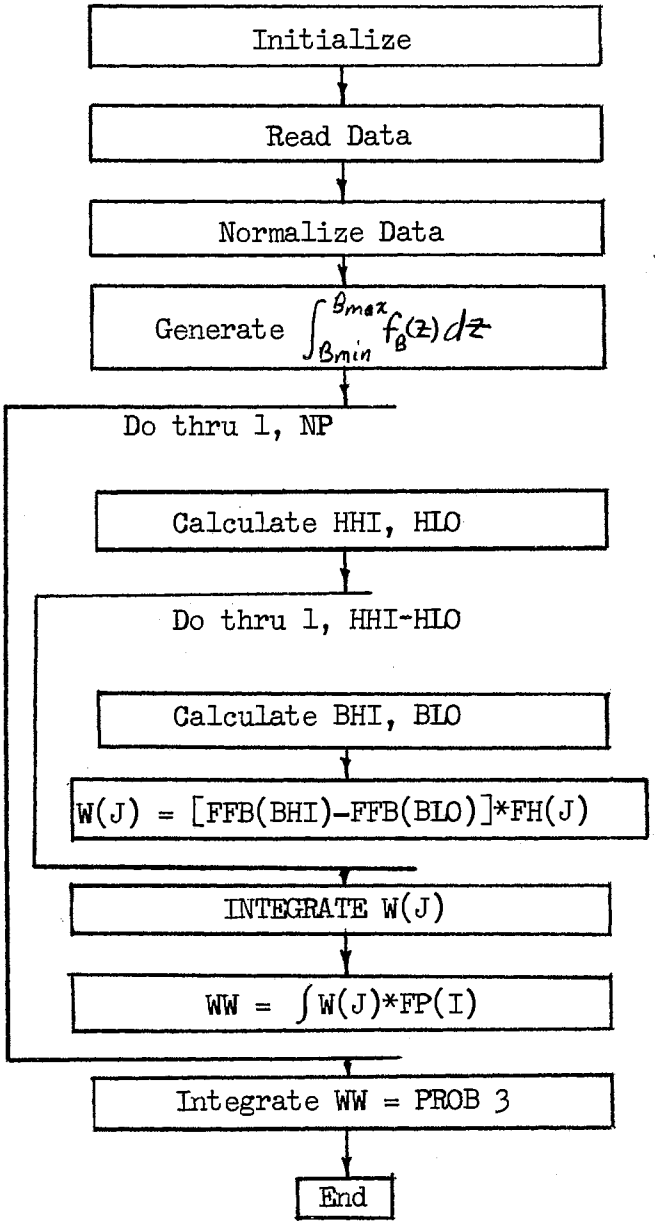

Figure 11. Flow Chart for Triply Nested Probability Integral

size of the independent variable intervals. Non-linear transformations do affect the size of the independent variable intervals. Thus a smoothing routine may be required. The smoothing process is a potential source of significant error since the original histogram data is not unique between data points.

Accuracy in the numerical integration is determined by the size of the increments on the independent variable and order of the integration fitting routine. The size of the increment is practically determined by the data available. A third order fit such as Simpson's Rule (see References 22 and 23) is considered adequate.

As an example the integral of the form of Equation 5-1 was evaluated as,

$$I\ II = \int_0^5 \int_0^x \tfrac{1}{5}\, dz\ \tfrac{1}{5}\, dx = \tfrac{1}{2}. \qquad (5\text{-}3)$$

The numerical solution was solved without significant error since Simpson's 1/3 Rule is exact for up to third order functions.

A similar integral expression whose exact solution is,

$$I\ II = \int_0^{1.41} \int_0^x \tfrac{1}{3}\, dz\ x\, dx = .314, \qquad (5\text{-}4)$$

was solved to demonstrate the error generated due to overlapping intervals. In this case, reduction of the step size in the inner independent variable by a factor of four decreased the error by a factor of five.

A triply nested example was solved according to the algorithm shown in Figure 11. The expression which has the exact solution,

$$I_{III} = \int_0^5 \int_0^{x} \int_{\pi/8}^{3\pi/8} \frac{\pi}{2} \, dz \, \tfrac{1}{5} \, dx \, \tfrac{1}{5} \, dy = \tfrac{1}{4}. \qquad (5\text{-}5)$$

was solved without significant error.

Thus, in the manner shown, any of the expressions generated in the previous chapters may be evaluated. The major sources of difficulty lie in the complexity of the limit functions and in nonlinear transformations which may be required. The problem may be made easier by modeling the numerical probability density function in functional form. However, that modeling is another potential source of error.

Monte Carlo Simulation

The integral relationships solved in the previous section effectively provided a stochastic model of particle capture and pore blockage. These relationships can be estimated by performing the deterministic problem with a large number of randomly selected samples. The general Monte Carlo method is discussed in many references (18, 24). The Monte Carlo simulation is perhaps the most straightforward method which can be applied since it circumvents most of the algebra and calculus associated with the analytical solution of the problem. The characteristic disadvantage of the method is that a large amount of effort may be required to obtain enough random samples to insure the desired accuracy in reconstruction of the data.

The necessary steps in performance of the Monte Carlo simulation are:

1. Select random variables from original distributions.
2. For each set perform deterministic capture and blockage

operations.

3. With the results build new pore and particle densities.

4. Test to see if sufficient samples have been taken.

5. If more samples are required repeat steps one through four.

Implementation of these steps is shown in Figure 12 as a digital computer algorithm.

An additional advantage of the Monte Carlo simulation is that the use of numerical data without a functional approximation is convenient. A suitable uniform random number generator is required. The SSP (23) generator called RANDU has been used thus far. It is assumed that the accuracy of the result will be reasonably as good as the reconstruction of the input probability density functions. The increments on the output function can be made as small as needed.

Hahn and Shapiro (24) point out that estimation of the error band associated with a Monte Carlo generated expected value is the same as estimating the error band for the expected value of the p_b parameter of a binomial distribution. That is, if the investigator specifies an initial estimate of p_b, p_b', it is possible to use binomial tables (25) to calculate the number of samples required to insure that the estimate proportion $\hat{p}_b$ does not deviate more than $\pm E$ from p_b' for a specified confidence level. The calculation is of interest since it is a convenient means of estimating the number of samplings required to reconstruct the input probability density functions within a given error band.

For example, suppose that we wish to use a probability density function, $f_X(x) = .2$ as an input function for a Monte Carlo simulation where $0 \leq x \leq 5$. We must select random samples by some process so that the resulting distribution is uniformly distributed within a specified

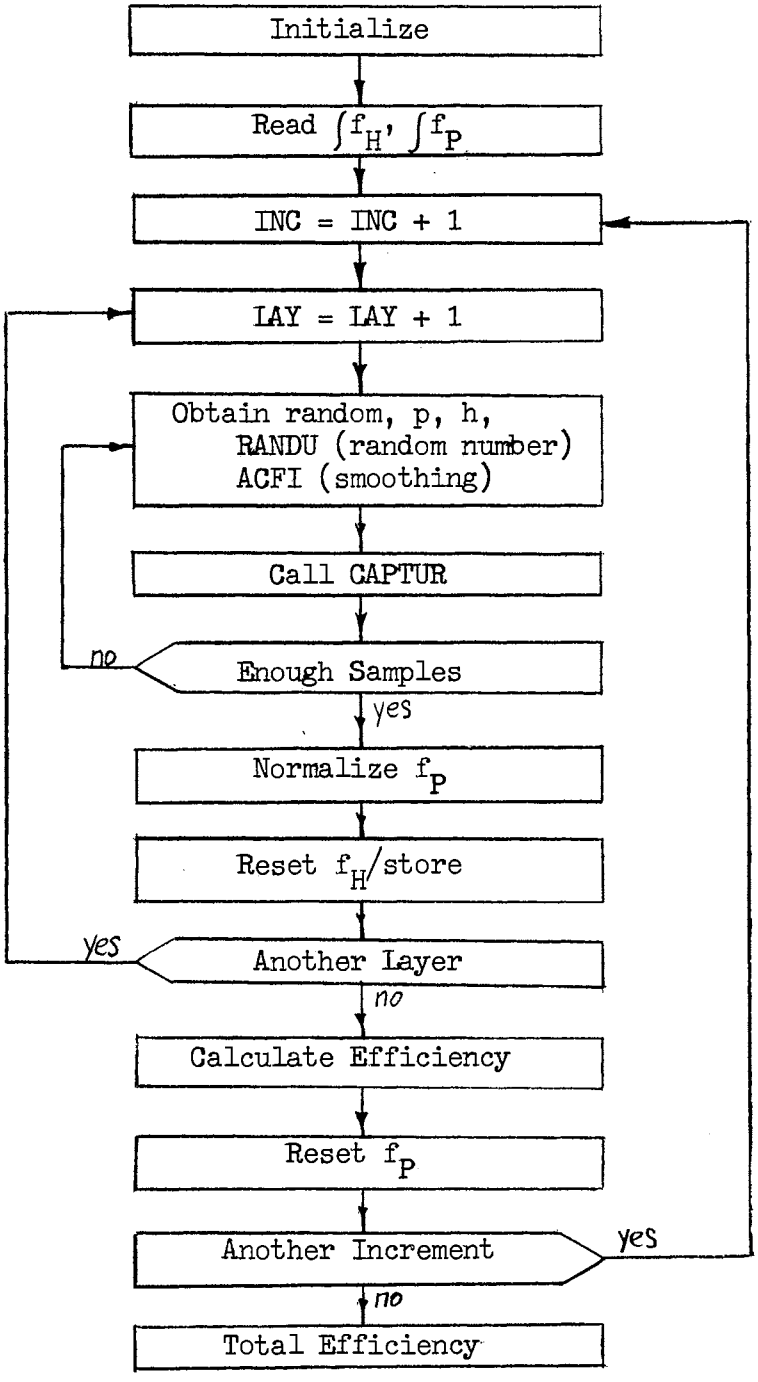

Figure 12. Flow Chart for Monte Carlo Solution

error bound. If an error of ±10 percent is chosen, the number of values on the x axis within any interval of unit length, n_1, must satisfy the expression:

$$.18 < \frac{n_1}{n_t} < .22$$

where n_t is the total number of samples. The number of samples, n_t, necessary to satisfy the condition can be investigated with binomial tables as explained above. For a 95 percent confidence level, the data in Table II was obtained:

TABLE II

MONTE CARLO SAMPLE SIZE EXAMPLE PROBLEM

Number Samples	p'	p_{Hi}	p_{Lo}	PERCENT ERROR
1000	200	225	175	± 12.5
400	80	98	64	±21.3
200	40	52	30	± 27.5

Thus, over 1000 samples will be required. Here the percent error is based on the expected value, p'. Application of the Monte Carlo algorithm shown in Figure 12 for a hypothetical example problem verified the magnitude of the error predicted in Table II.

Weighted Simulation

The second alternative to numerical integration of the general model is similar to the Monte Carlo simulation. In exhaustive weighting, however, instead of reconstructing the input data from randomly selected samples, each possible combination of the independent variables is weighted according to its joint probability of occurrence. The method is straightforward, but is inherently no more accurate than square law integration. For well behaved problems, a smoothing routine might be used to create smaller independent variable increments and thereby improve accuracy. However, counter examples could be constructed which would be less accurate due to the smoothing process.

The following steps are necessary for the weighted simulation:

1. For the first combination of independent variables, determine capture and partial blockage.

2. With the results build the new pore and particle densities weighted by the joint probability of the combination occurring.

3. Iterate through all possible combinations of the independent variables performing steps one and two for each.

Implementation of these steps is detailed in Appendix B as a digital computer algorithm.

The use of probability density functions in numerical data form is convenient with the weighted simulation method. Example problems were solved to demonstrate the accuracy of the method.

Method Comparison

Any of the three methods discussed is theoretically capable of solving the entire multi-layer and/or multi-population problem.

Comparison must be made on the basis of accuracy and economy. The two criteria are dependent on each other since, in general, smaller step size intervals improve the accuracy on each method. Resolution of the output is limited to that of the input for the numerical integration and the weighted simulation. There is no limit on the output function resolution of the Monte Carlo method. Inaccuracies are generated in the Monte Carlo method due to reconstruction of the input functions.

In practical solution schemes the weighted simulation procedure is analogous in accuracy to the square law integration. The numerical integration procedure is exact for up to n th order functions, depending upon the numerical integration scheme used. Providing that a very large number of samples are taken, the Monte Carlo process is as accurate as the smoothing subprogram which operates on the integral of the input probability density functions.

In terms of economy of operation we need to consider the effort required to achieve a certain accuracy. The comparison is complicated by the differences incurred in solution of particular problems. That is, multi-layer problems vs. single layer problems, and numerical data vs. functional form problems could lead us to different conclusions for particular cases. With that condition in mind, we can still make some generalizations in comparing the three methods of solution.

The effort (number of operations) involved in all three methods increases geometrically (as a product) with multiple sieve layers or populations of particles. The weighted simulation technique also increases the number of operations geometrically for each independent variable, while the Monte Carlo technique increases the number of operations additively for each independent variable. Explicitly,

the number of operations are:

$$\text{Number Monte Carlo Operations} = n \cdot m \cdot N_S \cdot N_{IV}$$

where n = Number layers (5-6)

m = Number populations of particles

N_S = Number samples for each passage

N_{IV} = Number independent variables
$= N_P + N_H + N_{CH} + N_{CP} + N_\theta + N_\phi$,

and,

$$\text{Number weighted simulation operations} = n \cdot m \cdot N_P \cdot N_H \cdot N_\theta \cdot N_\phi \cdot N_{CH} \cdot N_{CP}$$

where, N_P = Number intervals on particle density,

N_H = Number intervals on pore density,

N_ϕ = Number intervals on particle attitude density, (5-7)

N_θ = Number intervals on angular density,

N_{CP} = Number intervals on particle shape factor density,

N_{CH} = Number intervals on pore shape factor density.

In general each operation of the Monte Carlo method is computationally about five times slower than those of the weighted simulation method.

Comparison of these methods with the numerical integration method is complicated by the differences in usage in the case of functional relationships and numerical relationships. For the single layer case, the method is efficient, but the effort used in determining the resultant forms and implementing them in subsequent calculations would be significant.

Conclusion

The result of application of the three methods to a simple idealized problem for which an exact solution exists has lead to the following observations:

1. For problems with reasonably simple (closed form) limit functions, the exhaustive weighting simulation is much more economical to operate than the Monte Carlo simulation. The Monte Carlo simulation has the potential of greater accuracy but only at an exponentially increasing number of samples.

2. The most accurate and most economical method is the numerical integration method so long as a transformation of independent variables does not have to be made.

From these observations the following conclusions are drawn about problems not solvable in closed form:

1. Separation efficiency should be calculated by the numerical integration method for the single layer/single population problem.

2. Most problems which involve an independent variable transformation should be solved by the weighted simulation method (includes single layer pore size distribution and therefore most multiple layer/population problems).

3. There remains the possibility of a problem whose solution requires the trial and error solution of a limiting function of such complexity that the Monte Carlo simulation, due to its additive property (Equation 5-6), will be more efficient.

CHAPTER VI

EXPERIMENTAL

The experimental analysis was an essential part of the present study. Satisfactory data was not found to describe the sieving mechanism in hydraulic filtration throughout the long literature search. Only in a microscopically observable experiment could the sieving mechanism be studied in its entirety. The clean room and filtration laboratory of the Oklahoma State University Basic Fluid Power Research Program provided an ideal facility for the testing.

Objectives

Two main objectives were associated with the experimental investigation. First, it was desired to compare the results of an experimental model with results predicted from geometrically measurable random variables by the weighted simulation technique. In this way, the summation of effects which detract from agreement of analytical and empirical models could be observed. The data also served as a desired response for the demonstration of parameter identification techniques. That is, either random variables or deterministic parameters could be adjusted to force the simulated results to more closely fit the experimental results.

The second objective was to generate microscopically observable hydraulic sieving data. The literature appears devoid of such

information. Most hydraulic filtration problems are concerned with tortuous media. Even Dutch twill wire cloth has sufficient tortuosity that many of the captured particles are hidden from microscopic observation of the medium's upstream surface. The nontortuous sieve mesh chosen for the study provided easy microscopic observation of the captures which had taken place on its surface. In so far as was possible, the experiments were designed to promote the sieving mechanism and retard other separation mechanisms.

Experimental Method

The experimental procedure consisted basically of filtration of a dilute aqueous suspension of specially prepared contaminant through a flat sieve mesh. The filtration was performed slowly but at a velocity faster than the calculated sedimentation of the largest particle. The apparatus used was specifically designed for the experiment and is shown in Figure 13. A vacuum pump was attached to the flask to control the rate of filtration. The filtration was categorized as single pass. Microscopic observation of fluid samples upstream and downstream of the sieve mesh provided the basic quantitative particle count data from which separation efficiency was calculated. In addition, microscopic observation of the sieve mesh yielded an essentially qualitative evaluation of the capture process. Particles trapped by partial blockage mechanisms were observable in this way. The upstream contaminant concentration was adjusted after several trials so that sieving would predominate on the medium surface. All of the filtrate was collected downstream so that sampling error was absolutely minimized. The complete test procedure is detailed in Appendix C.

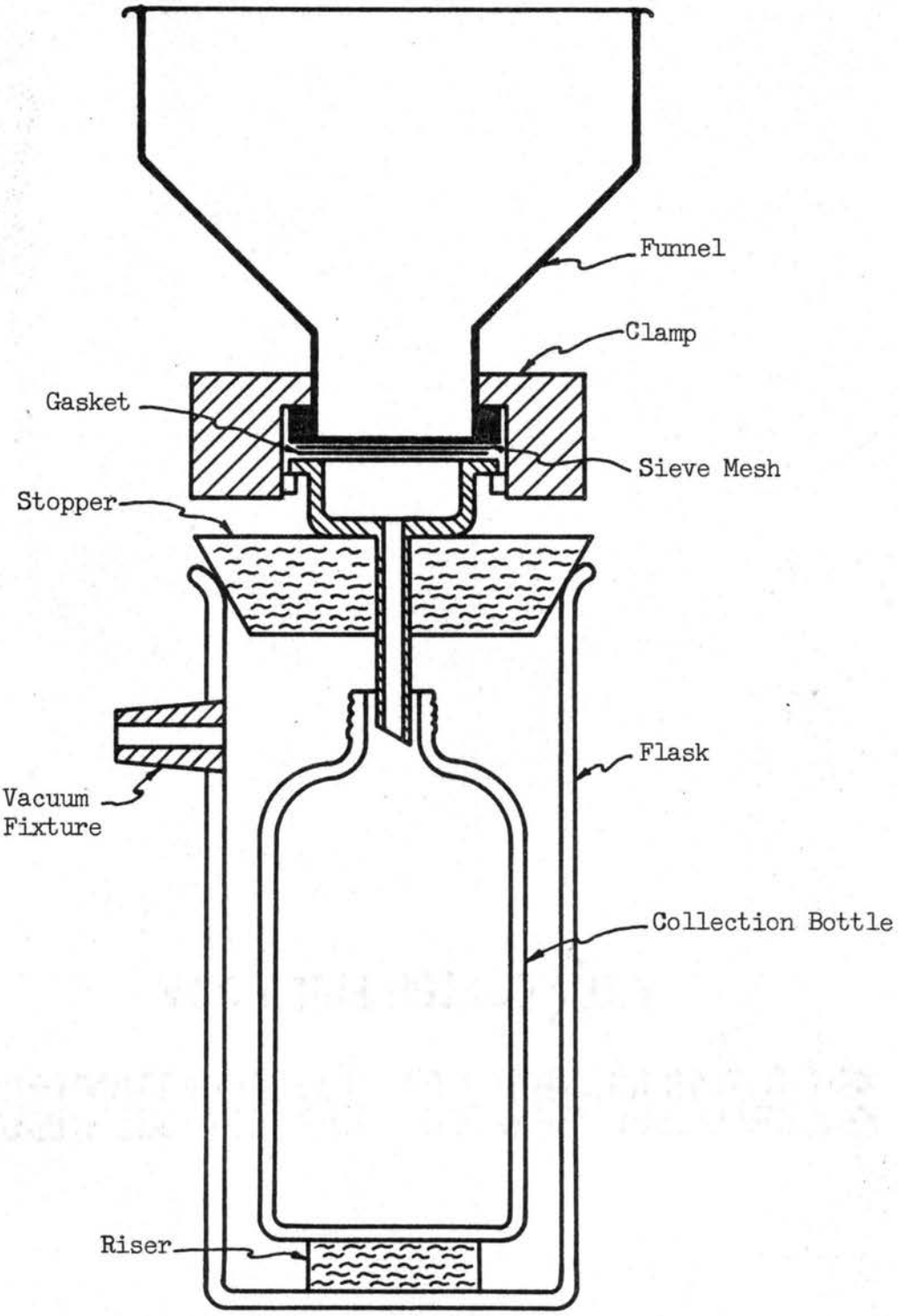

Figure 13. Filtration Apparatus - Section View

Dispersion of particles was accomplished by subjecting the particulate suspension to ultrasonic waves. Thirty seconds duration was used for natural contaminants and five minutes was used for glass beads. All suspensions were shaken in a commercial paint shaker for ten minutes immediately before testing

Aqueous solutions were used instead of petroleum based solutions to facilitate microscopic counting of the particles. Various additives were evaluated to minimize the effect of surface forces. One percent TAMOL - SN (a dispersant agent to prevent flocculation) was used in all of the tests conducted.

Results of the Experimentation

The experiments performed are listed in Table I and shown graphically in Figure 5. Square aperature sieve mesh pores were measured optically and the results listed in Table III. The electro-formed square aperature mesh is nominally .001 inches thick. The sieve mesh with elliptical pores is described in Table IV. The pores are very straight although the nominal thickness of the mesh is .011 inches.

TABLE III

PORE SIZE DISTRIBUTION FOR SQUARE PORE SIEVE

Pore Size (side), Micrometers	Pore Density
16.5	.044
17.5	.286
18.5	.330
19.5	.330
20.5	.011

TABLE IV

PORE SIZE DISTRIBUTION FOR ELLIPTICAL PORE SIEVE

Pore Size (major axis), Micrometers	Pore Density
7.0	.062
9.0	.118
11.0	.203
13.0	.078
15.0	.037

Two contaminants were selected on the basis of size, shape, availability, homogeneity, and dispersion properties. The naturally occurring contaminant used was A C Fine Test Dust. The distribution of particles five micrometers and larger (longest dimension) was prepared. Particles smaller than five micrometers were removed with a Roller classifier since they have a greater tendency to agglomerate. The dust in the range of interest is mainly crushed quartz. The size distribution of the largest dimension for A C Fine Test Dust is presented with the results of tests A and B.

The artificial contaminant used was glass beads. These beads are very nearly spherical. Two different size distributions were prepared for use with the two sieve meshes. The size distributions used are listed with the results of tests C, D, and E.

The results obtained from test series A through E are presented in Tables V through IX, respectively. A note on the statistical procedures used to evaluate the data is given in the next section.

TABLE V

RESULTS OF TEST SERIES A - ELLIPSOIDAL PARTICLES AND ONE LAYER ELLIPTICAL PORE SIEVE MESH

Particle Size, Micrometers	Particles / ml. Upstream	Particles / ml. Downstream	Separation Efficiency	Avg. Separation Efficiency 2 tests
12.5	443.00	69.70	.843	.846
17.5	148.70	12.25	.918	.930
22.5	61.15	3.25	.946	.962
27.5	28.75	1.00	.965	.982
32.5	14.89	.75	.950	.975
37.5	8.29	.25	.981	.990
42.5	4.89	0.	1.	1.
47.5	3.01	0.	1.	1.
52.5	1.94	0.	1.	1.

TABLE VI

RESULTS OF TEST SERIES B - ELLIPSOIDAL PARTICLES AND ONE LAYER SQUARE PORE SIEVE MESH

Particle Size, Micrometers	Particles / ml. Upstream	Particles / ml. Downstream	Separation Efficiency	Avg. Separation Efficiency 2 tests
12.5	443.00	550.00	0.	0.
17.5	148.70	201.00	0.	0.
22.5	61.15	56.92	.069	.044
27.5	28.75	11.15	.612	.615
32.5	14.89	5.39	.638	.617
37.5	8.29	0.38	.817	.781
42.5	4.89	0.	1.	1.
47.5	3.01	0.	1.	1.
52.5	1.94	0.	1.	1.

TABLE VII

RESULTS OF TEST SERIES C - SPHERICAL PARTICLES AND ONE LAYER OF ELLIPTICAL PORE SIEVE MESH

Particle Size, Micrometers	Particles / ml. Upstream	Particles / ml. Downstream	Separation Efficiency	Avg. Separation Efficiency 2 tests
7.0	26.92	9.40	.613	.650
9.0	23.48	2.10	.910	.848
11.0	14.92	.10	.993	.989
13.0	16.00	0.	1.	.997
15.0	6.12	0.	1.	.995
17.0	.92	0.	1.	1.

TABLE VIII

RESULTS OF TEST SERIES D - SPHERICAL PARTICLES AND ONE LAYER OF SQUARE PORE SIEVE MESH

Particle Size, Micrometers	Particles / ml. Upstream	Particles / ml. Downstream	Separation Efficiency	Avg. Separation Efficiency 2 tests
11.	2.6	2.90	0.	0.
13.	6.4	6.23	.027	.014
15.	26.9	25.15	.065	.033
17.	61.5	38.25	.378	.301
19.	78.2	22.50	.712	.627
21.	82.1	6.23	.924	.925
23.	56.4	.25	.996	.996
25.	29.5	0.	1.	1.
27.	14.1	0.	1.	1.
29.	9.0	0.	1.	1.
31.	5.1	0.	1.	1.
33.	2.6	0.	1.	1.
35.	1.2	0.	1.	1.
37.	2.6	0.	1.	1.
39.	2.6	0.	1.	1.

TABLE IX

RESULTS OF SERIES E - SPHERICAL PARTICLES AND TWO LAYERS OF ELLIPTIC PORE SIEVE MESH IN SERIES

Particle Size, Micrometers	Particles/ ml. Upstream	Particles/ ml. Downstream	Separation Efficiency
7.0	26.5	8.400	.683
9.0	23.8	1.600	.933
11.0	15.3	.025	.998
13.0	14.5	0.	1.
15.0	5.0	0.	1.
17.0	1.7	0.	1.

Evaluation Techniques

Each test series, with the exception of series E, consisted of at least two identically performed tests to demonstrate repeatability. The repeatability of series E was verified by series C. Upstream and downstream samples were filtered through .45 micrometer black membrane filters for microscopic particle counting. Most aspects of the particle counting were carried out in accordance with Aerospace Recommended Practice 598A (25). However, the number of counts required for validity was checked in accordance with the method suggested by Fairs (26). Fairs' criterion for microscopic sample size is shown in Figure 14. Thus, the data given in Tables V-IX are arithmetic averages of the counts recorded for several areas of the membrane filter.

Sizing of particles was done with a Cooke Model 1.6X image splitter. A 10X occular and a 40X objective were used in conjunction

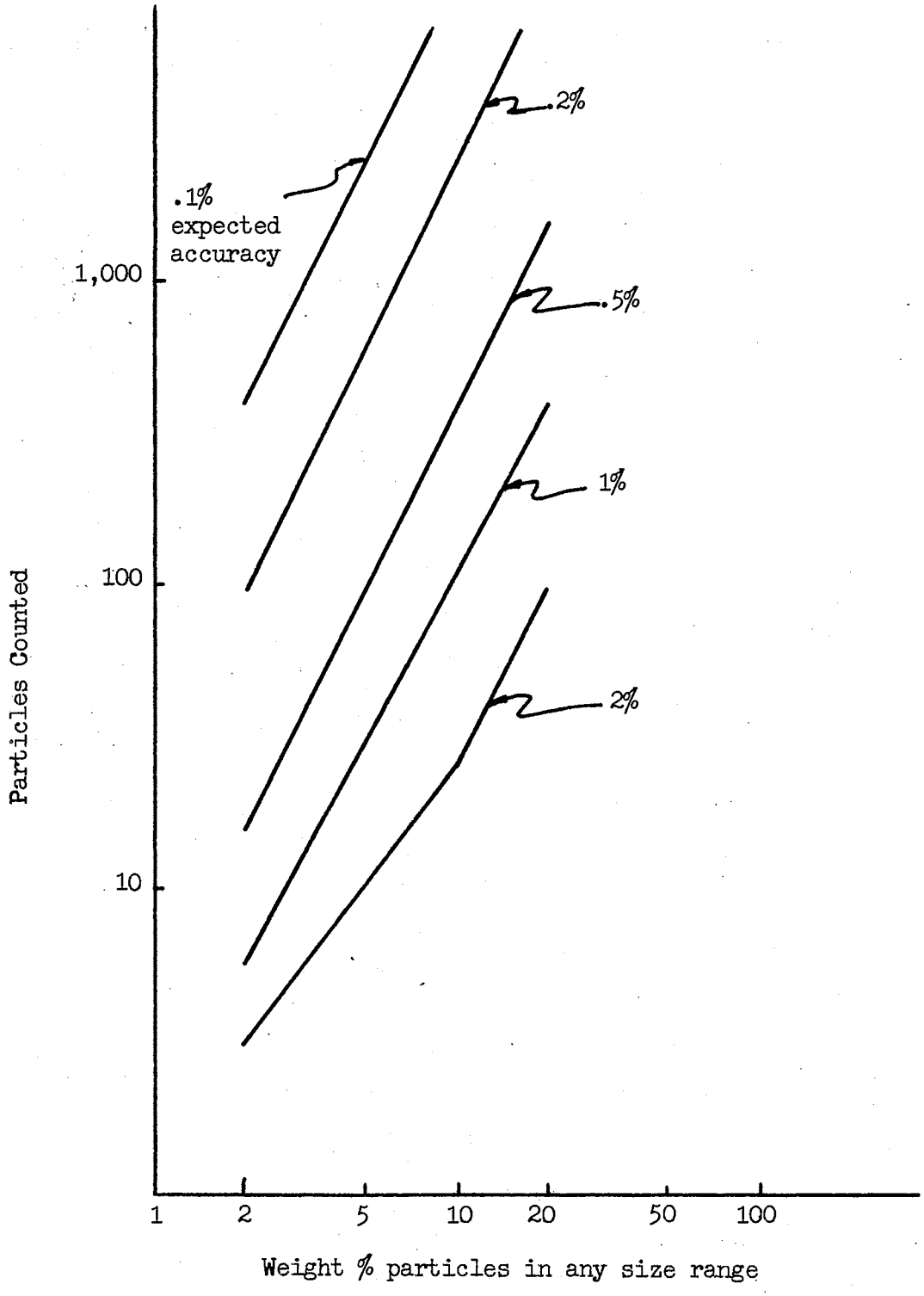

Figure 14. Microscopic Particle Counting Accuracy After Fairs (27)

with the image splitter. Calibration was accomplished with a diffraction grating under the same (oblique) lighting conditions used for particle illumination. The objective had a nominal aperature of n.a. = 0.65. Thus, for light of mean wave length, $\lambda \approx .5\mu$, the minimum resolution is given (28), by,

$$R = \frac{.62\lambda}{n.a.} \approx .5\mu .$$

Other factors including shadows and inaccuracies in the image splitter linkages make a lower limit of $5.\mu$ more acceptable. The smallest particle which was measured had a diameter of 6μ.

If the assumption is made that particle counts deviate normally from a mean value, a confidence interval can be calculated by the interval estimation technique which is covered in many elementary statistics books (e.g., Miller and Freund (29) on page 148). The ninety percent confidence intervals on the mean particle counts shown in Figure 15 were calculated for six optical counts, from three tests in series A. Thus, the author is ninety percent confident that for each size particle the interval contains the mean particle count.

It is the opinion of the author that the data presented in this chapter is sufficiently repeatable and within the expected limits that it will support reasonably drawn conclusions. In the next chapter the results will be discussed and compared with those of the analytical model.

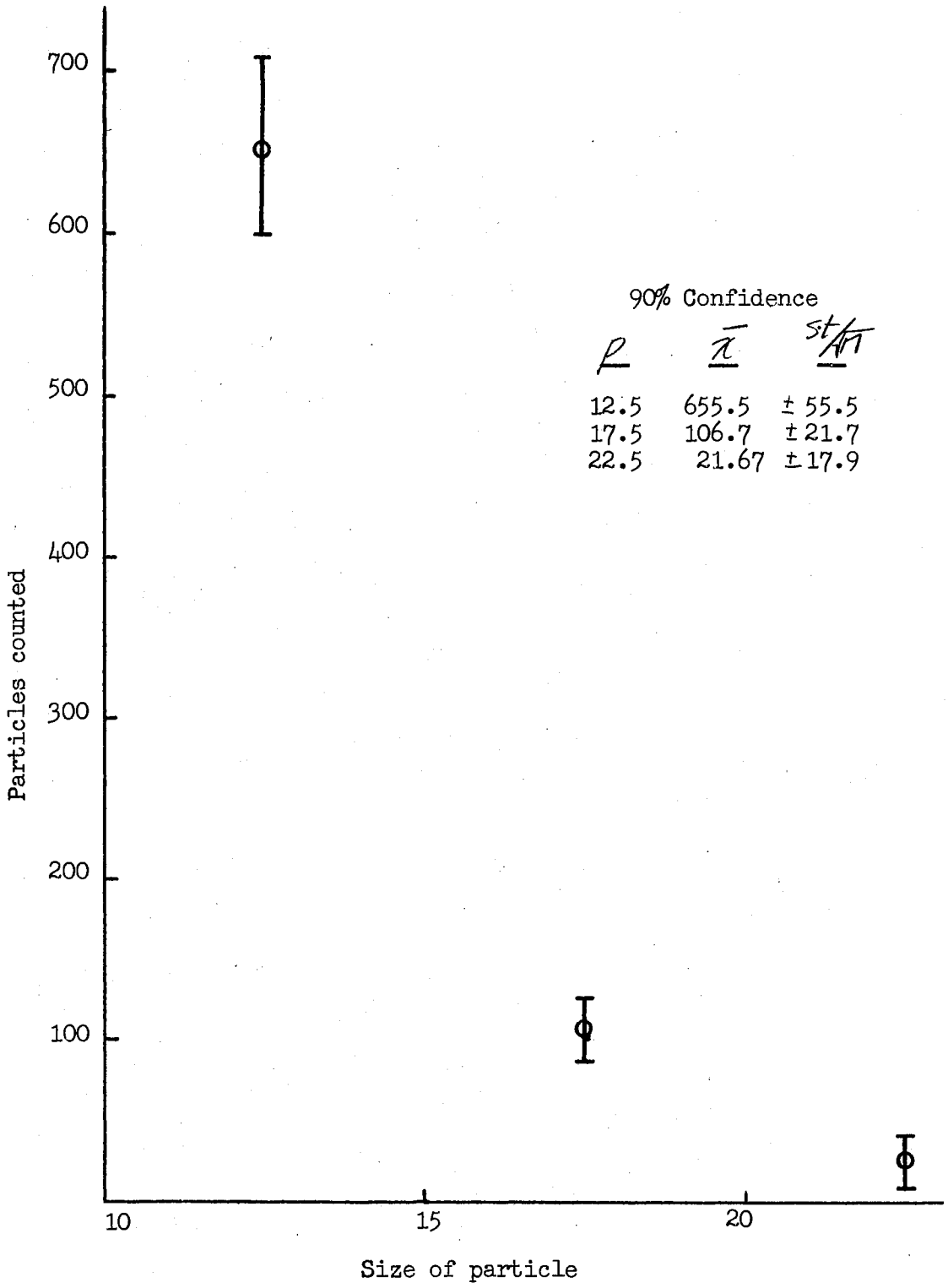

Figure 15. 90% Confidence Interval for Downstream Optical Counts - Series A

CHAPTER VI

DISCUSSION OF RESULTS

In this chapter the analytical techniques developed in Chapter V are used to simulate actual hydraulic sieving problems. The weighted simulation technique is used to obtain quantitative results in all of the problems considered. A comparison of simulated results with the experimental results obtained in Chapter VI is presented to demonstrate the ways in which actual hydraulic filtration differs from the necessarily idealized sieving model. The analytical model is idealized by the use of regular geometric shapes and considers capture only by sieving. In the discussion which follows, separation efficiency and downstream particulate density, both as functions of particle size, are treated as output functions of the sieving process.

One of the main purposes of this chapter is to compare analytical and experimental results. Deviation of experimental output functions from those predicted analytically is due to measurement error and violation of the assumptions upon which the theoretical model is based. Since the analytical model is geometric in nature, it is an accurate representation of the sieving process. If, however, input density functions are inexact representations of physically occurring populations, then predicted output functions will deviate from exactly measured physical downstream conditions. Those downstream conditions are also subject to measurement error.

If processes other than sieving are responsible for particle capture, experimental and analytical results would be expected to differ. Capture of particles by surface forces is an example of such a process. Other violations of the assumptions upon which the analysis is based are potential sources of inaccuracy. Since it is impossible to geometrically model the exact shape of each particle of a naturally occurring contaminant, such as A C Fine Test Dust, a characteristic geometric shape has been assumed.

The comparisons made between experimental and analytical results in this chapter are made on the premise that the simulated results correctly represent the sieving process for the numerical input data furnished. Where appropriate, comments are made to reduce the number of factors responsible for disagreement of analytical and experimental results. Those comments, which are qualitative in nature, arise from the author's association with contamination control measurement and, therefore, are, to an extent, subjective.

The technique by which the output of a mathematical model is forced to approximate a desired data set by adjusting the values of the free parameters is known as parameter identification. If measured values of the free parameters are available, then deviation of the identified values from the measured values must be caused by error in the measurements or infidelity of the geometric shape model. The parameter identification technique is demonstrated in this chapter.

Use of the Weighted Simulation Method

All of the numerical simulations presented in this chapter were obtained using the weighted simulation method. In addition, a direct

numerical integration was performed for part of series D. The simulation was required since the data, or models which would fit the data, did not admit closed form solution of the equations derived in Chapter IV. The weighted simulation technique was chosen over the Monte Carlo simulation and the direct numerical integration based on the comparison of the methods made in Chapter V. Details of the numerical algorithm which was used are given in Appendix B.

As has been mentioned previously, the accuracy of the weighted simulation technique is roughly that of square law integration. Therefore, problem accuracy is enhanced by reducing the size of the intervals on the input density function such as $f_P(p)$ and $f_H(h)$. The practical limitation here is the size discrimination of the measuring techniques used to obtain the input densities. An image splitting eye piece was used to discriminate intervals as small as one micrometer. In the range below two micrometers the instrument is sensitive to operator technique.

Throughout the five example problems under discussion the input density functions are:

1. pore size, $f_H(h)$.
2. particle size, $f_P(p)$.
3. pore shape factor, $f_{CH}(ch)$.
4. particle shape factor, $f_{CP}(cp)$.
5. pore-particle angular relationship, $f_\theta(\theta)$.
6. particle attitude, $f_\phi(\phi)$.

In special cases the random variables CH, and CP, are represented by their expected values. In all cases in which particle capture is dependent on ϕ or θ, the following density functions are assumed:

$$f_\theta(\theta) = 2/\pi, \qquad 0 < \theta \leq \pi/2,$$

and,

$$f_{\phi}(\phi) = 2/\pi, \quad 0 < \phi \leq \pi/2.$$

The justification for this distribution of $f_{\phi}(\phi)$ was given in Chapter IV.

Algebraic relationships required to describe capture limits and/or partial pore blockage are detailed in Appendix A. Only the results are used in this chapter. Output density functions of the solution are: downstream particulate density, $f_{P_{(i)}}^{(j)}(p)$, total separation efficiency, $\epsilon_{(i)}^{(j)T}(p)$, and pore size density after passage of contaminant $f_{H_{(i)}}^{(j)}(h)$.

Comparison of Analytical and Empirical Results

The problems chosen for simulation were meant to represent, as closely as possible, the empirical studies which were conducted. Glass beads were modeled as spheres. A C Fine Test Dust particles were modeled as ellipsoids of revolution. The random variable, P, represented the major axis of the ellipsoid and the minor axis was represented by P·CP. Major and minor axes of the elliptic pores were designated H and CH·H, respectively. The combination of variables which made up each test series is given in Table I and graphically portrayed in Figure 5. Some general observations will be included at the end of this chapter.

Series D

The contaminant modeled in series D is spherical and the pores are modeled as squares. Obviously, particle attitude and angle do not affect the simulation. The partial blockage expression describing the new pore size, h_{new}, after blockage of a h size pore by a p size

particle is

$$h_{new} = \left(\sqrt{p^2+h^2} - p\right)/2\sqrt{2}.$$

In this particular case the criterion for capture is of the fundamental nature and the separation efficiency can be calculated by using Equation 4-22. A simulation was also performed. The results of these calculations are displayed in Figures 16 and 17, and are listed in Table X. Note that the separation efficiencies obtained by direct numerical integration agree well with those obtained by the simulation technique. This result is only to be expected since both algorithms are numerical processes with the same input data and comparable order of accuracy.

Since the criterion for capture is geometrically rigorous, and the idealized particle and pore geometries are good representations of actual geometries, the discrepancy in efficiency between experimental and analytical data at p = 17μ, must be attributed to measurement error. Such error could be found in measurement of the input density functions, the results of the empirical tests, and/or the step size of the input density functions which is limited by the intervals of the input density functions. A zero shift of one micrometer on the input pore size frequency data improved separation efficiency data at p = 17μ, but destroyed the previously good agreement for downstream particulate density at p = 19μ.

Series C

A distribution of spherical particles (not the same distribution as for series D) was modeled in series C. The sieve mesh pores are modeled as ellipses with major axes equal to the random variable, H,

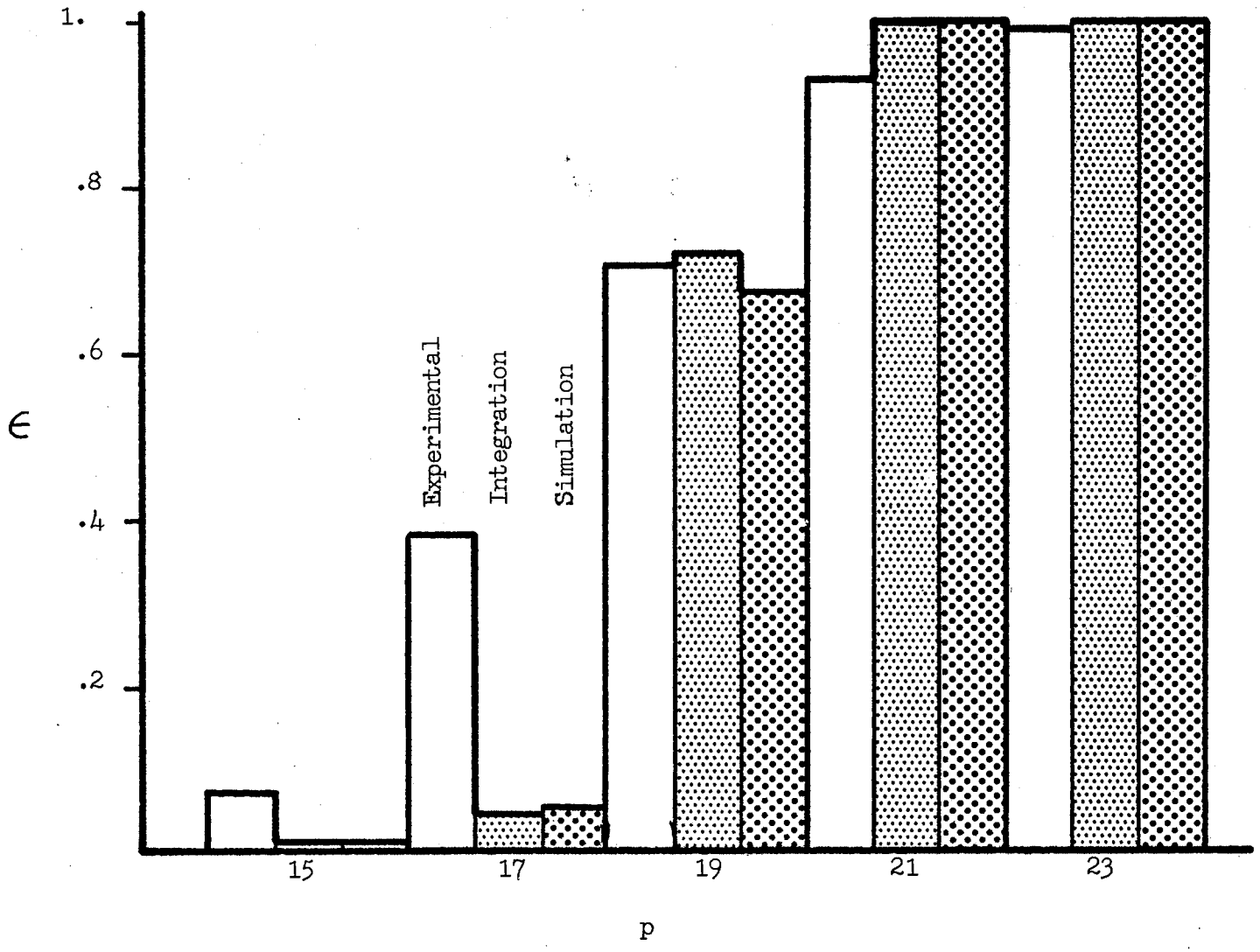

Figure 16. Separation Efficiency vs. Particle Size - Series D

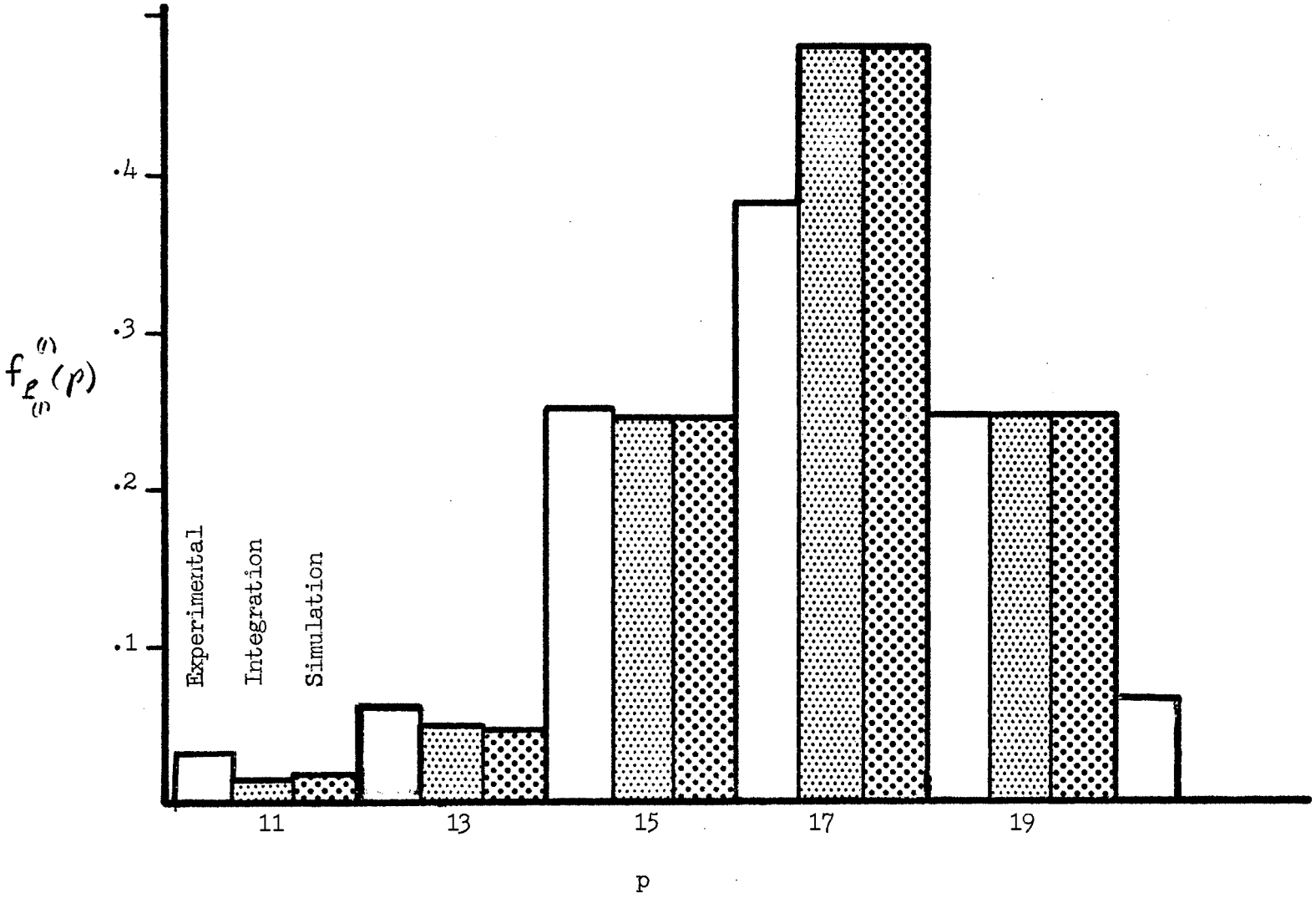

Figure 17. Downstream Particulate Density - Series D

TABLE X

SERIES D NUMERICAL RESULTS

Particle Size, Micrometers	Downstream Particle Density			Separation Efficiency		
	Experimental	Integrated	Simulated	Experimental	Integrated	Simulated
11.	.029	.019	.020	0.	0.	0.
13.	.062	.054	.050	.027	0.	0.
15.	.251	.222	.221	.165	0.	0.
17.	.382	.486	.484	.378	.040	.044
19.	.225	.222	.220	.712	.720	.660
21.	.060	0.	0.	.924	1.	1.
23.	0.	0.	0.	.996	1.	1.

and minor axes equal to CH·H, where CH is also a random variable. Again, no angular relationship is required to describe particle capture. The partial blockage relationship is,

$$h_{new} = (h-p)/2ch.$$

Two pores are formed for each blockage. Note that the pores so described are not the actual shapes formed but are ellipses with smallest dimension equal to the smallest dimension formed.

The distribution which was microscopically measured to represent $f_{CH}(ch)$ is designated Distribution 2 and is shown in Figure 18b. Results of the weighted simulation using Distribution 2 to represent $f_{CH}(ch)$ are compared with experimental data in Figure 19. Predicted separation efficiencies are generally lower than those which were experimentally measured.

Measurement errors, such as those discussed for series D, could have been present. Another potential source of discrepancy, which was not possible in series D, is the removal of particles by surface forces on the long aspect ratio (eight times the aspect ratio of the square pores) walls of the elliptic capillaries. The square pores in series D did not have sufficient wall area for surface forces to be effective. The particle size at which the deviation between experimental and analytical results is most obvious is in the midrange of the sizes for which Herzig (8) predicts surface forces and volume forces are of the same order of magnitude. It was also observed that after the surface of the medium was completely cleaned, beads could be collected in the downstream collector by filtration of clean water at about ten times test flow rate. It is theorized that the increased viscous shear on

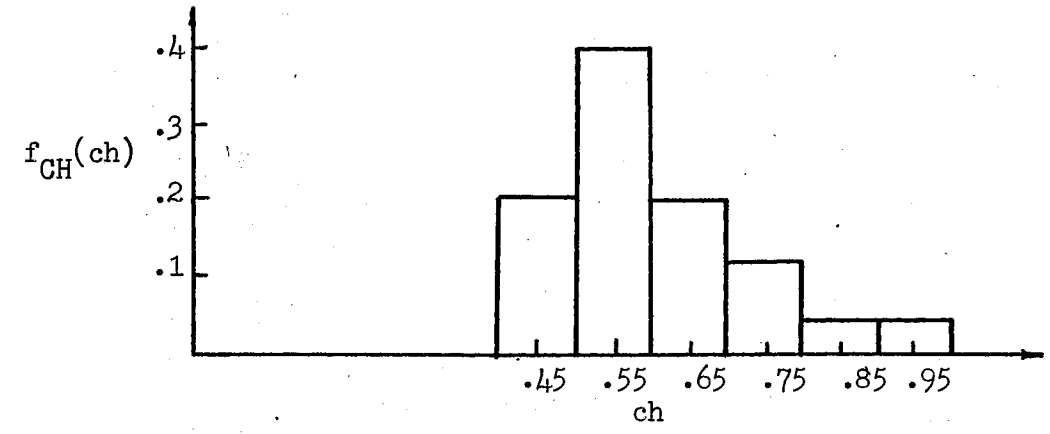

(a) Distribution 1, CH

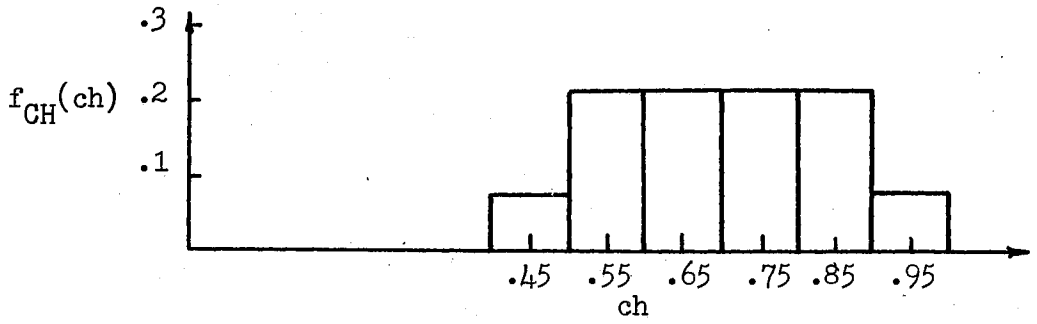

(b) Distribution 2, CH

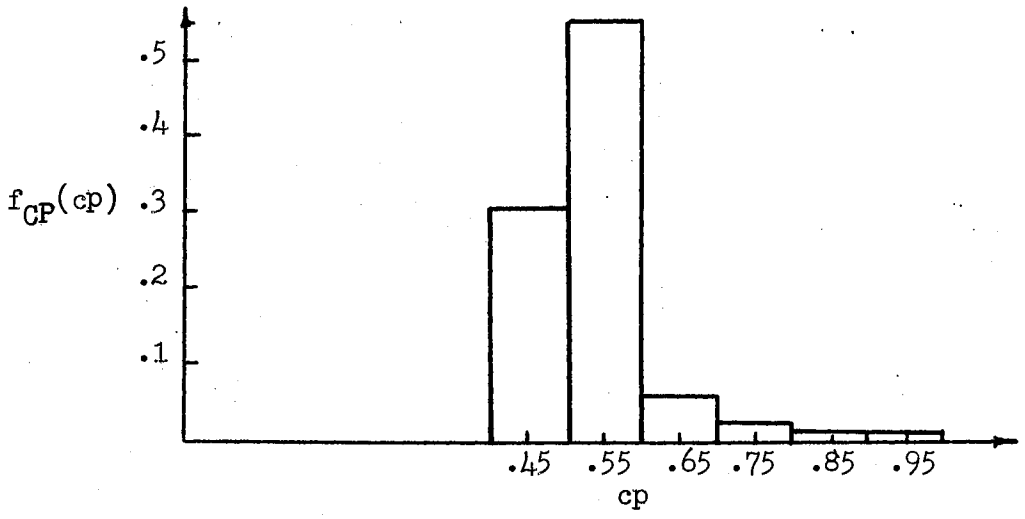

(c) Distribution 6, CP

Figure 18. Input Distributions

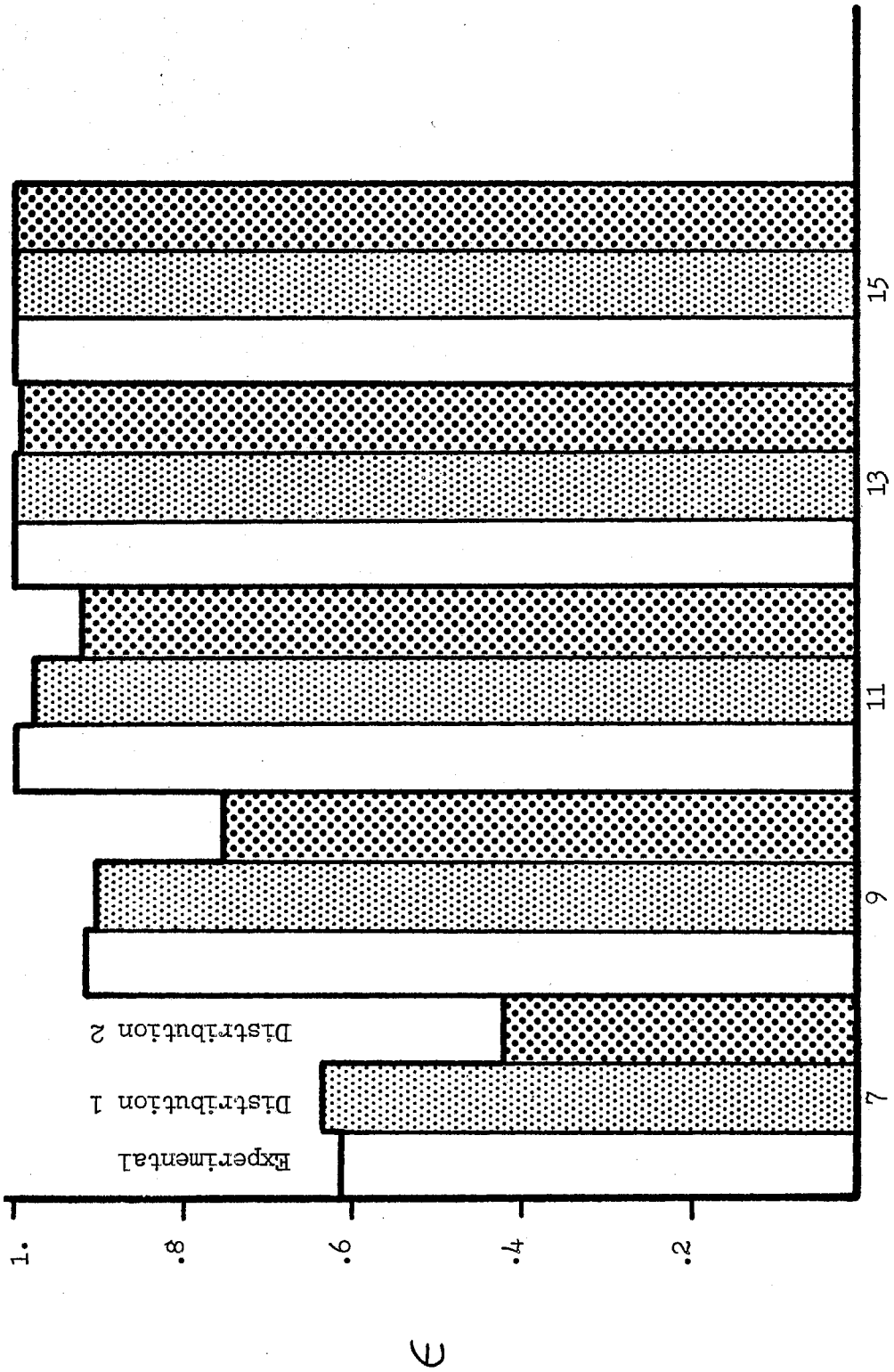

Figure 19. Separation Efficiency vs. Particle Size - Series C

the particles at the higher velocity overcame the surface forces which had retained them.

An identification procedure was performed to determine a density on CH which would force the simulated data to more closely approximate the experimental data. Distribution 1, in Figure 18a, meets this requirement. However, it is the opinion of the author that Distribution 2 is a reasonably accurate representation of $f_{CH}(ch)$. The difference between experimental and analytical results is, with that assumption, due to measurement error and surface forces not described in the sieving model. In all likelihood, the effect of surface forces accounts for the larger part of the deviation since the deviation occurs over a wide range of sizes and is more pronounced at the smaller end of the range.

A comparison of experimental and analytical downstream particulate density functions is given in Figure 20 and Table XI.

Series E

Series E was modeled exactly as was series C except that two layers of identical sieve mesh in series were employed. The comparison of empirical and experimental separation efficiency is shown in Figure 21 and Table XII. Note that the simulation which uses $f_{CH}(ch)$ = Distribution 2 (see Figure 18b), closely fits the experimental data for this problem, while $f_{CH}(ch)$ = Distribution 1 (see Figure 18a) yields a uniformly high value of efficiency. The values of the simulation are, thus, more sensitive to the double sieve layer than are those of the experimental model.

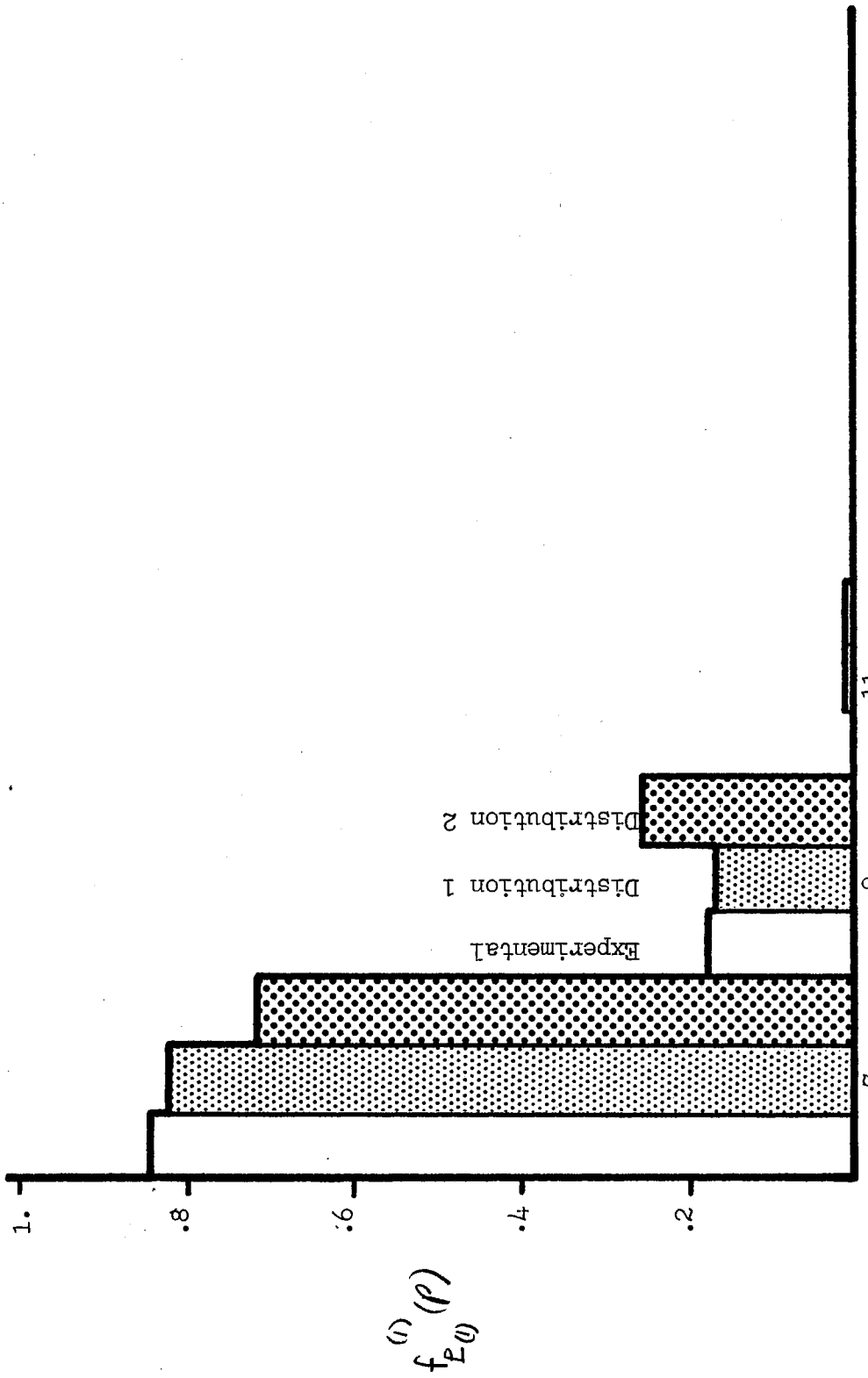

Figure 20. Downstream Particulate Density vs. Particle Size - Series C

TABLE XI

SERIES C NUMERICAL RESULTS

Particle Size, Micrometers	Downstream Particle Density			Separation Efficiency		
	Experimental	Distrib. 1 = $f_{CH}(ch)$	Distrib. 2 = $f_{CH}(ch)$	Experimental	Distrib. 1 = $f_{CH}(ch)$	Distrib. 2 = $f_{CH}(ch)$
7.	.810	.786	.681	.613	.631	.426
9.	.181	.177	.260	.910	.905	.749
11.	.008	.033	.056	.993	.972	.915
13.	0.	.004	.004	1.00	.997	.994
15.	0.	0.	0.	1.	1.	1.

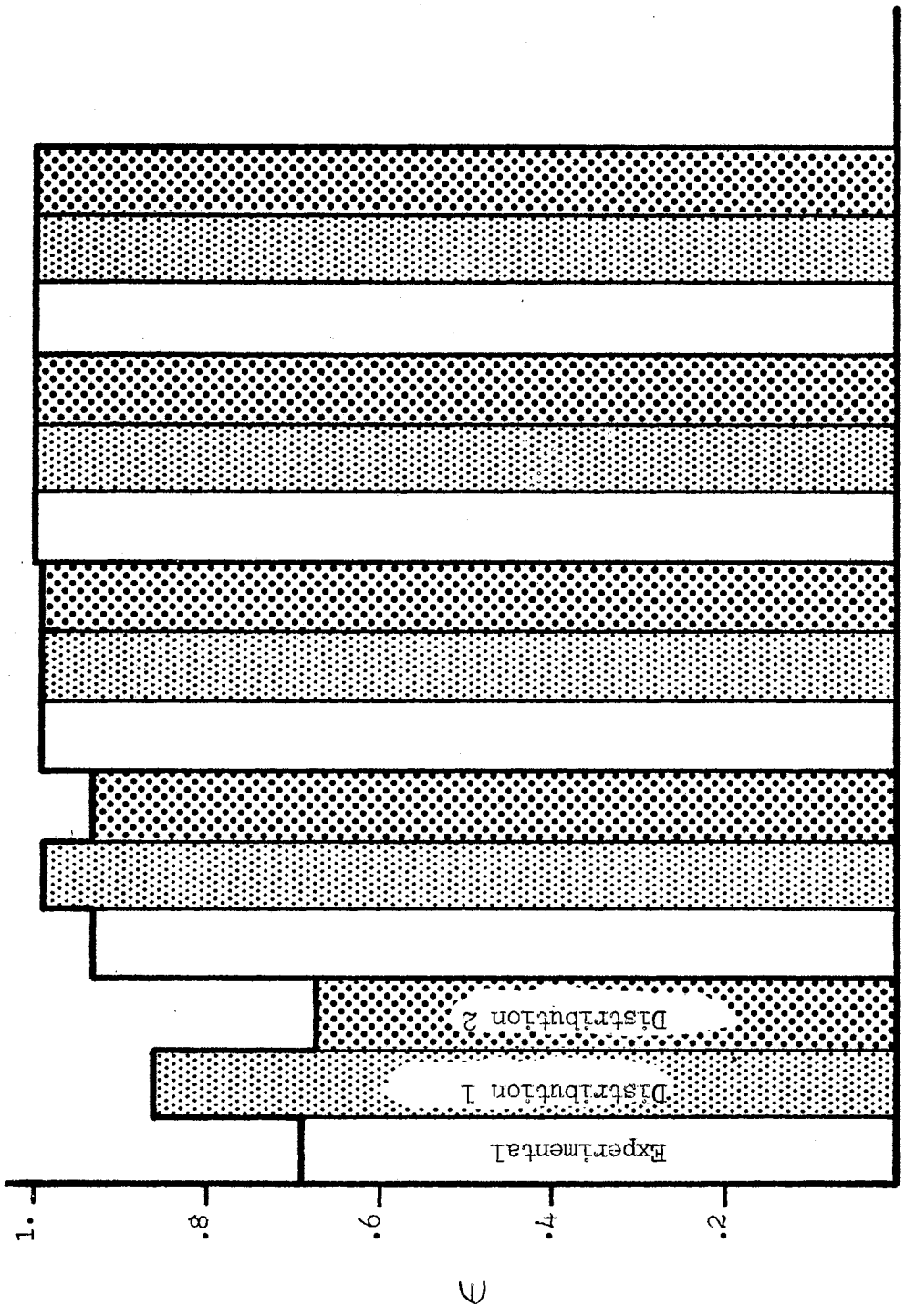

Figure 21. Separation Efficiency vs. Particle Size - Series E

TABLE XII

SERIES E NUMERICAL RESULTS

Particle Size, Micrometers	Downstream Particulate Density			Separation Efficiency		
	Experimental	Distrib. 1 = $f_{CH}(ch)$	Distrib. 2 = $f_{CH}(ch)$	Experimental	Distrib. 1 = $f_{CH}(ch)$	Distrib. 2 = $f_{CH}(ch)$
7.	.84	.942	.845	.683	.863	.670
9.	.16	.054	.145	.933	.990	.937
11.	.003	.003	.011	.998	.999	.993
13.	0.	0.	0.	1.	1.	1.
15.	0.	0.	0.	1.	1.	1.

The explanation for this phenomenon is that, in the experimental model, the gross separation efficiency of the first layer is on the order of 87% (see series C). The remaining particulate distribution as seen by the second sieve layer is, therefore, of a much lower concentration. The main significance of this dilution is that particle capture by surface effects is much less dramatic in the second layer. Also, the assumption that an infinite distribution of particles exists may be altered.

Downstream particulate density is graphically displayed in Figure 22.

Series B

The model for series B consisted of square pores of side, H, and particles described as ellipsoids of revolution with major axis P and minor axis CP·P. In this case particle vs. pore angular relationship, θ, and particle attitude, ϕ, were considered in particle capture and partial blockage calculations. The projected particle length in the plane of the sieve is,

$$P^* = P\sqrt{\cos^2\phi + C_P^2 \sin^2\phi}$$

The condition for escape is

$$P^* < H$$

or

$$P \cdot C_P < H < P^*, \qquad \theta_{min} < \theta < \theta_{max}$$

where

$$\theta_{max} = \tan^{-1}\left[(C_P^2 P^2 - H^2)/(H^2 - P^{*2})\right]^{1/2}$$

$$\theta_{min} = \pi/2 - \theta_{max} .$$

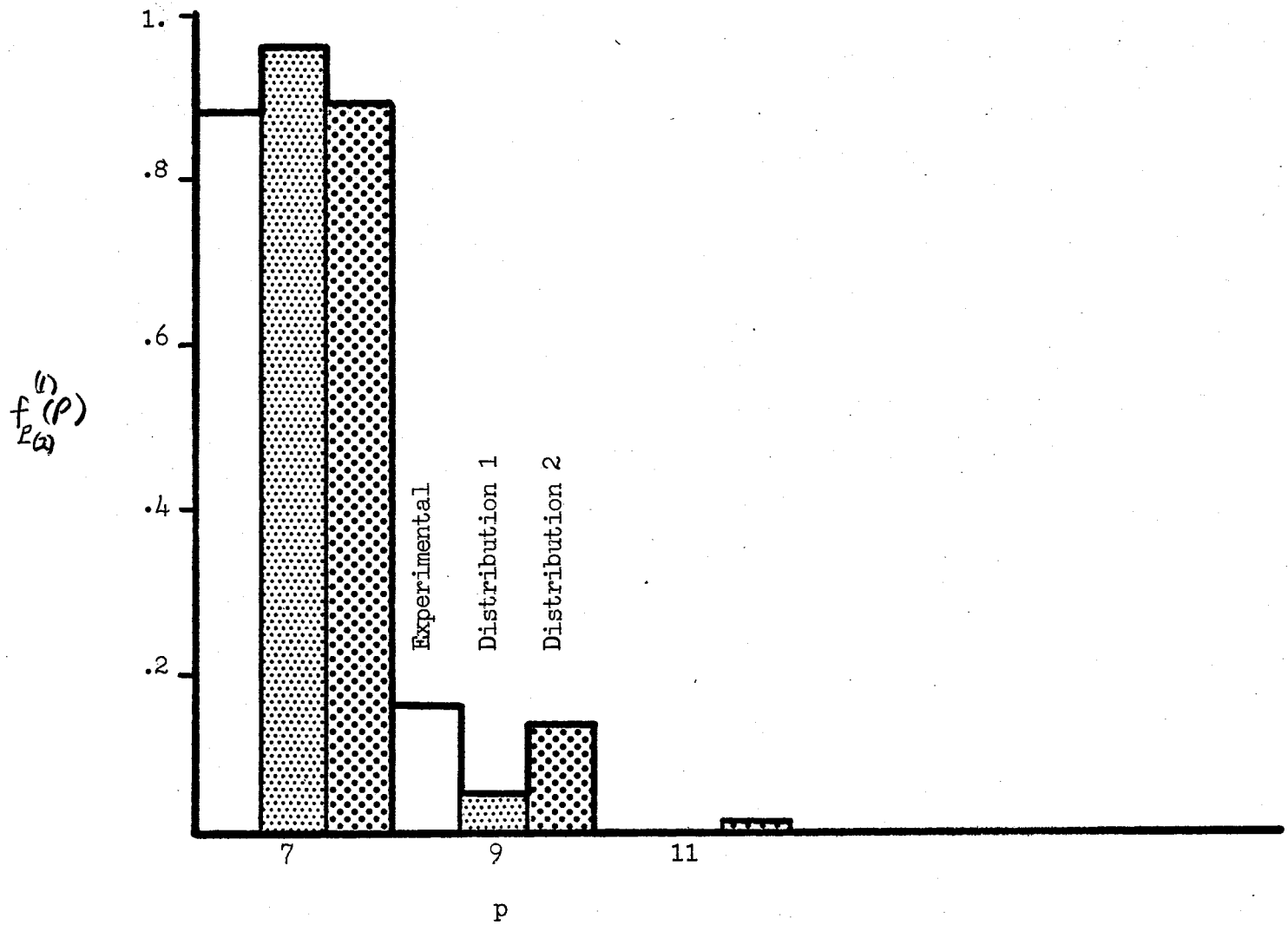

Figure 22. Downstream Particulate Density vs. Particle Size - Series E

The partial blockage condition is

$$h_{new} = (\sqrt{2}\,h - cp \cdot p)/2,$$

and two new pores are formed of this size.

The comparison between experimental and analytical results is given in Figures 23 and 24 and in Table XIII. An optimization routine, GOLD 1, (see Reference 30) was used to fit the simulated results to the experimental data by identification of the best expected value for cp. The result was,

$$cp_{opt} = \frac{\text{minor axis}}{\text{major axis}} = .439.$$

$f_{CP}(cp)$ was also simulated as the distribution shown in Figure 18c. As with series D, a possible cause of the discrepancy in separation efficiency at p = 17.5μ, is measurement error. In this series the particle geometric shape is less faithful to the idealized model than was that of series D.

Series A

Series A was the most complicated model of the examples attempted. In this case the pores were elliptic and the particles were modeled as ellipsoids of revolution. Thus, the projection of the particles could be calculated as in series B. The pores formed by partial blockage were modeled,

$$h_{new} = \left(\frac{h}{2} - cp \cdot p \left[\frac{1 + \tan^2\theta}{cp^2 + \tan^2\theta} \right]^{1/2} \right) / ch.$$

Two new pores were formed for each blockage. The critical angles for capture, θ_{max}, θ_{min}, could not be found in closed form. The solution of a non-linear set of algebraic equations was required. A Newton -

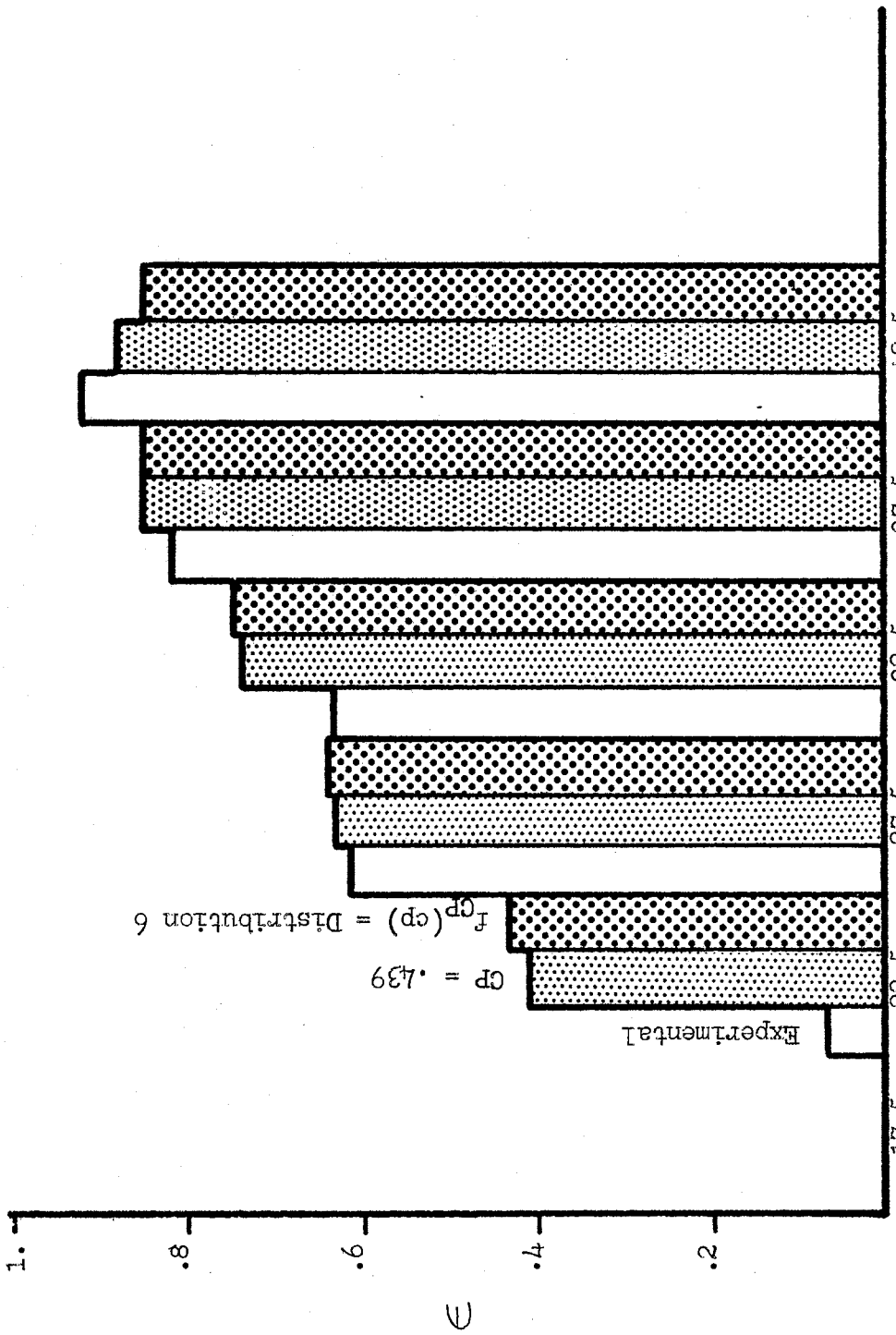

Figure 23. Separation Efficiency vs. Particle Size - Series B

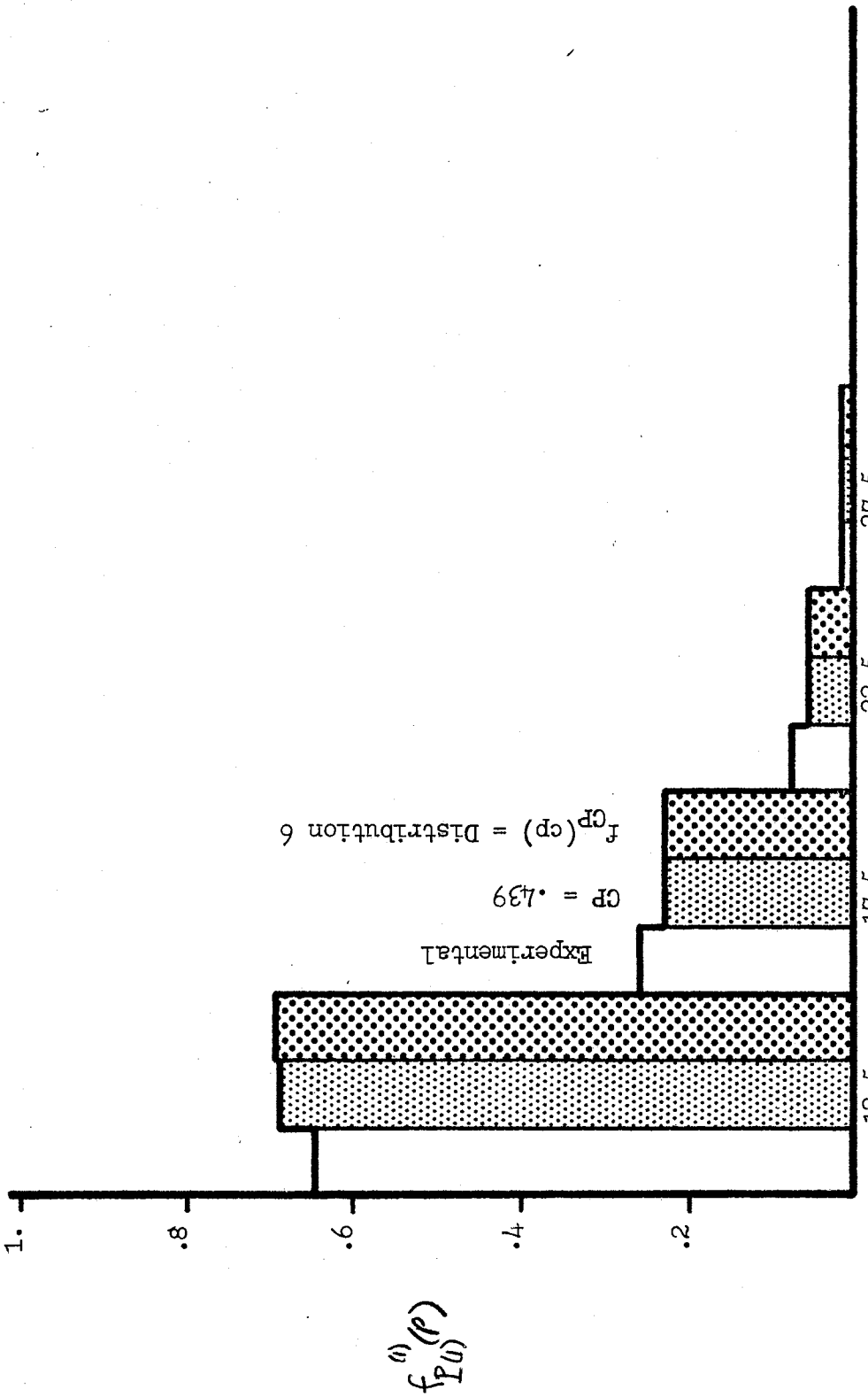

Figure 24. Downstream Particulate Density vs. Particle Size - Series B

TABLE XIII

SERIES B NUMERICAL RESULTS

Particle Size, Micrometers	Downstream Particle Density			Separation Efficiency		
	Experimental	CP = .439	Distrib. 6 = $f_{CP}(cp)$	Experimental	CP = .439	Distrib. 6 = $f_{CP}(cp)$
12.5	.644	.690	.692	0.	0.	0.
17.5	.257	.229	.230	0.	.010	.011
22.5	.076	.056	.054	.069	.411	.437
27.5	.015	.017	.016	.612	.629	.640
32.5	.004	.006	.006	.638	.740	.751
37.5	0.	.002	.002	.817	.856	.851
42.5	0.	0.	.001	1.	.962	.932

Raphson solution was attempted but was found to be unstable for some values of interest. Also, the computational time required for each step of the Newton-Raphson solution was prohibitive. An alternate derivation enabled iterative solution of the problem by the method of successive approximations (22) which provided the speed and accuracy required. Details are given in Appendices A and B.

The comparison of experimental and analytical results for series A is presented in Figures 25 and 26 and in Table XIV. Note that the separation efficiency seems to have been influenced by adsorption in the smaller particle sizes just as it was in series C. An optimization routine, GOLD 1, was used to demonstrate that the expected value of CH = .348, yields the best fit of the experimental data while the expected value of the particle shape factor was held at CP = .439. If the effects of the surface forces are indeed more prominent than those of measurement errors, then the majority of the deviation is due to other modes of separation than sieving.

Some General Comments on the Results

While the captured particles can be observed on the surface of a sieve mesh, their microscopic sizing is much more difficult than on a membrane filter. The main reasons are due to light reflected from the sieve and lack of contrast between the particles and the background. Therefore, comparison between experiment and simulated pore size distributions remaining after filtration was not attempted. The simulated post-filtration pore size distributions are listed in Table VX.

The one sample Kolmogorov-Smirnov test, as given by Miller and Freund (20), on page 222, was used to test the null hypothesis that the

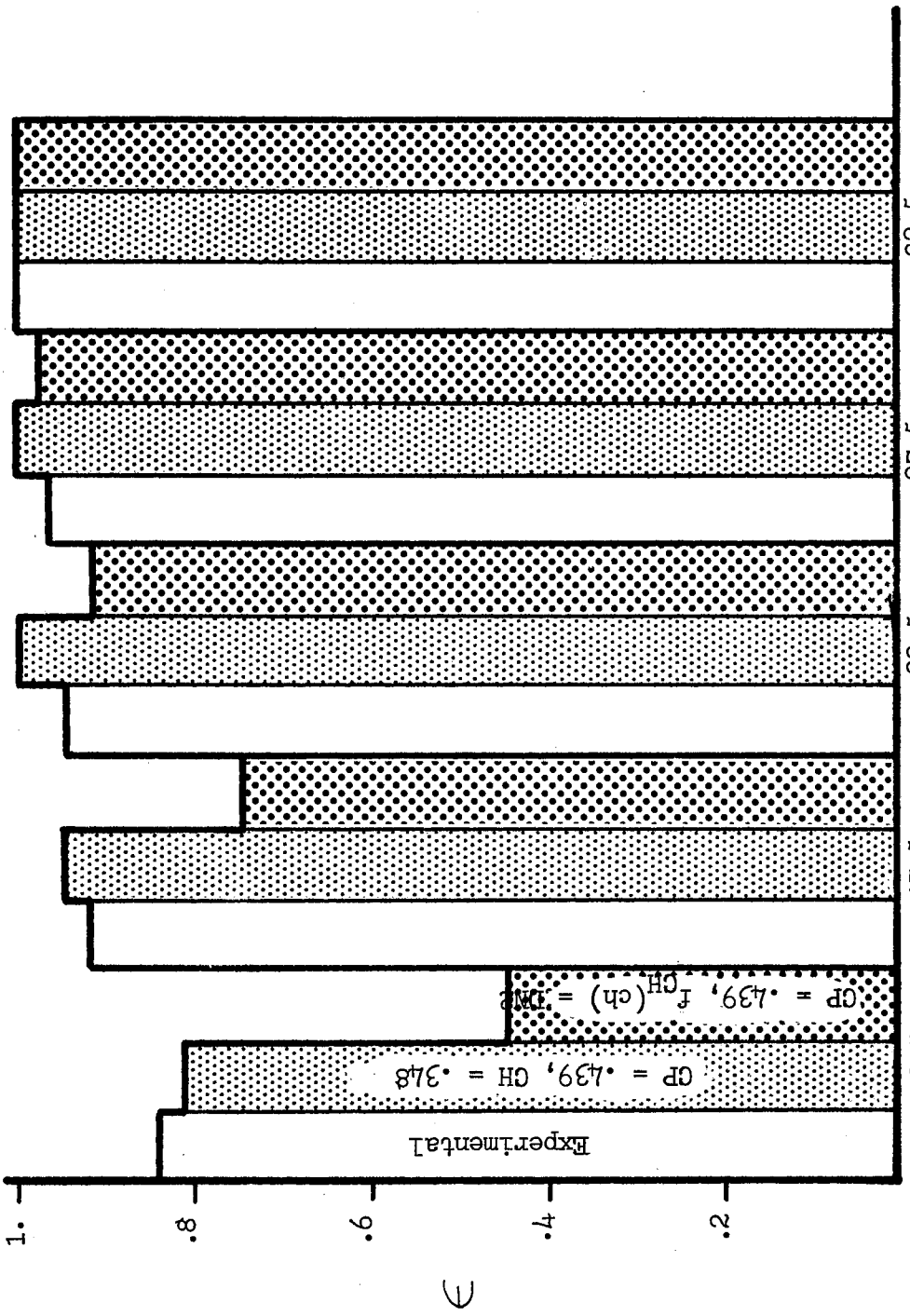

Figure 25. Separation Efficiency vs. Particle Size - Series A

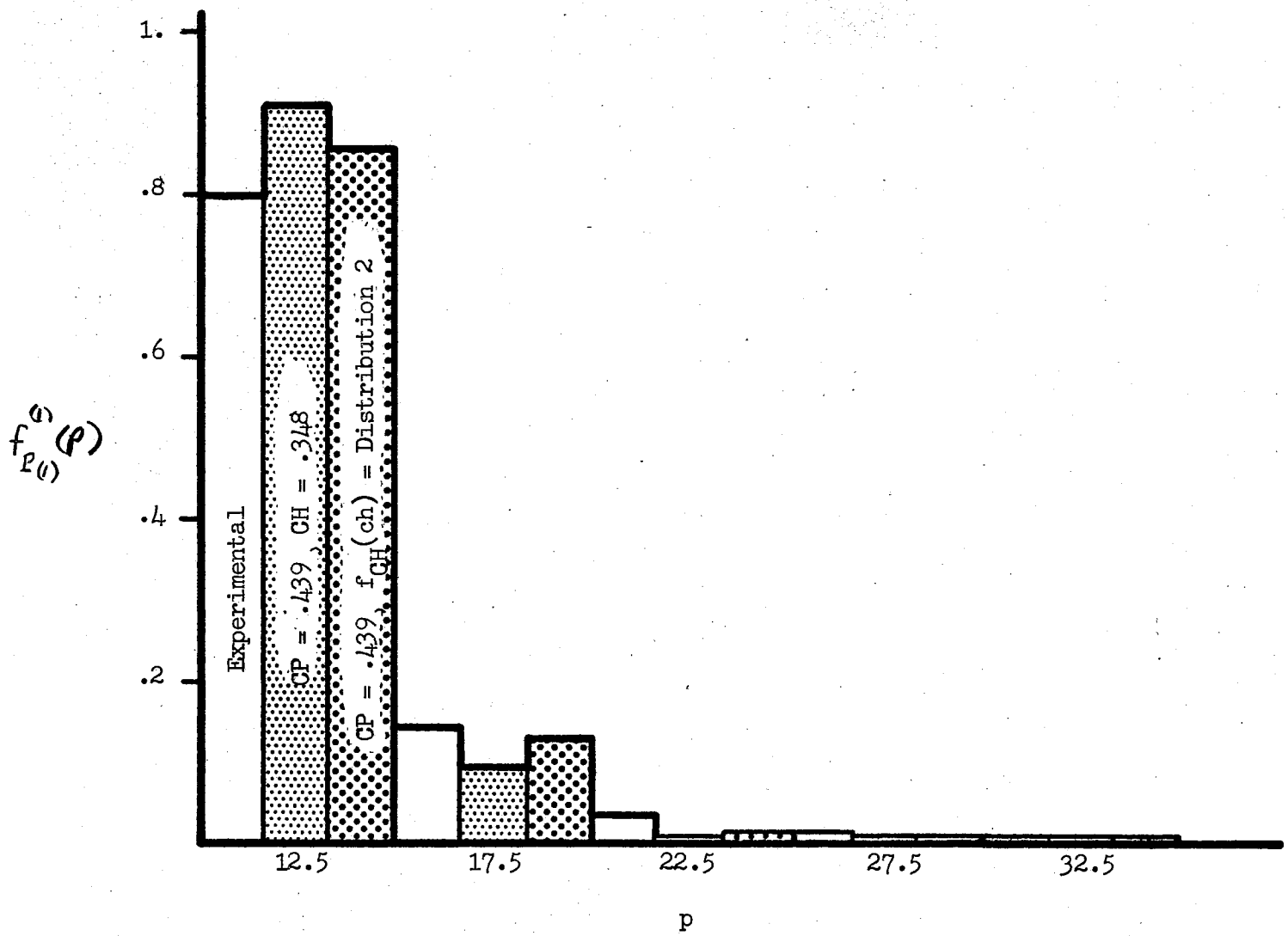

Figure 26. Downstream Particulate Density vs. Particle Size - Series A

TABLE XIV

SERIES A NUMERICAL RESULTS

Particle Size, Micrometers	Downstream Particle Density			Separation Efficiency		
	Experimental	CP = .439 CH = .348	CP = .439 $f_{CH}(ch)$ = Distrib. 2	Experimental	CP = .439 CH = .348	CP = .439 $f_{CH}(ch)$ = Distrib. 2
12.5	.800	.910	.850	.843	.812	.447
17.5	.141	.086	.130	.918	.947	.748
22.5	.037	.004	.017	.946	.994	.916
27.5	.015	0.	.002	.965	1.	.976
32.5	.009	0.	0.	1.	1.	.995

empirically measured separation efficiencies and downstream particulate densities were distributed according to the simulated model. In all of the examples for series A through series E the null hypothesis could not be rejected for a level of significance = .1, on the difference between experimental and simulated results.

TABLE XV

PORE SIZE DISTRIBUTIONS AFTER FILTRATION
- SIMULATION DATA

Square Pore Media

Pore Size, Micrometers	Series B CP = .439	Series C
16.5	.041	.013
17.5	.285	.229
18.5	.328	.265
19.5	.335	.477
20.5	.011	.016

Elliptic Pore Media

Pore Size, Micrometers	Series A $f_{CH}(ch) = DN\ 2$ CP = .439	Series C $f_{CH}(ch) = DN\ 2$	Series E 2d Layer $f_{CH}(ch) = DN\ 2$
7.	.032	0.	0.
9.	.156	.093	.115
11.	.422	.456	.483
13.	.247	.280	.260
15.	.142	.172	.142

A considerable number of parametric values were used in simulations over the course of the present study. It appears that simulated values of separation efficiency are generally more sensitive to change in parameters such as $f_{CH}(ch)$ and $f_{CP}(cp)$ than are the downstream particulate densities. This conclusion would lose significance, however, in the case of downstream particulate densities which are severely skewed toward one end of the independent variable interval.

Since the type of simulation employed is inherently laborious, a word about the computational effort involved is in order. The largest single simulation performed treated six input parameters as random variables and performed an iterative solution of the critical capture angle at appropriate intervals. By use of the relationships developed in Chapter V an estimated $3X10^7$ major sets of calculations were required. The computation required one minute and 56 seconds execution time on an IBM 360/65 computer using fast core. While that computation was reasonably economical, it is easy to see that multiple layer problems or problems in which identification of more than one parameter is required could become prohibitively expensive.

In the next chapter some of the implications for extension of the techniques reported herein will be discussed.

CHAPTER VIII

RELEVANCE OF THE SIEVING PROCESS AND EXTENSIONS OF THE INVESTIGATION

In this chapter an additional feature of the methods already introduced is discussed. An example of filtration of multiple populations of particles with partial pore blockage is given. Some of the many problems in hydraulic filtration mechanics and contamination control which can be treated with the same general approach will be mentioned. It would appear that the input data for a number of interesting extensions of the present study will be available in the near future.

While application of single layer sieve mesh is infrequent in real hydraulic filtration applications, the extension of the models of this study is believed to be of considerable practical value. The use of wire cloth filters is a closely related application which could be modeled by the techniques derived herein. At least one manufacturer has proposed the use of a nontortuous sieve mesh for specialized filtration applications. One apparent advantage of the material would be the availability of an accurate sieving model.

Multiple Population of Particles Example Problem

The digital computer algorithm which is presented in Appendix B to implement the weighted simulation technique is versatile and user

oriented. Some of its features were not demonstrated in the preceding chapter and at least one more is worthy of mention.

Consider a sieve mesh made up of elliptic pores and a spherical contaminant as was the case in series C. As before, the partial blockage relationship is,

$$H_{new} = (H - P)/2CH.$$

Two new pores will be formed for each pore blockage. For this example the effect of multiple populations of particles on the separation efficiency of a single mesh layer will be demonstrated. The initial particle and pore size distributions for the problem are shown in Figure 27. The value of CH will be held at, CH = .5.

Quite obviously, the efficiency of the first population of particles will be a unit step function at p = 5, since all particles below that size will penetrate and all particles above that size will be retained. The pores formed due to partial blockage of the first population will change the pore size distribution so that a non-zero efficiency will be seen at smaller particle sizes. For subsequent populations a more efficient filtration would be expected. The separation efficiency of the problem simulation for individual populations is shown in Figure 28a. Figure 28b shows the total separation efficiency for the populations on a cumulative basis.

Note that the individual layer efficiency reaches a final value more quickly than does the total efficiency simply because the total efficiency includes the early populations of lower efficiency. The practical interpretation is only valid so long as sieving is the predominant mode of capture. In Figure 28a and 28b the regions

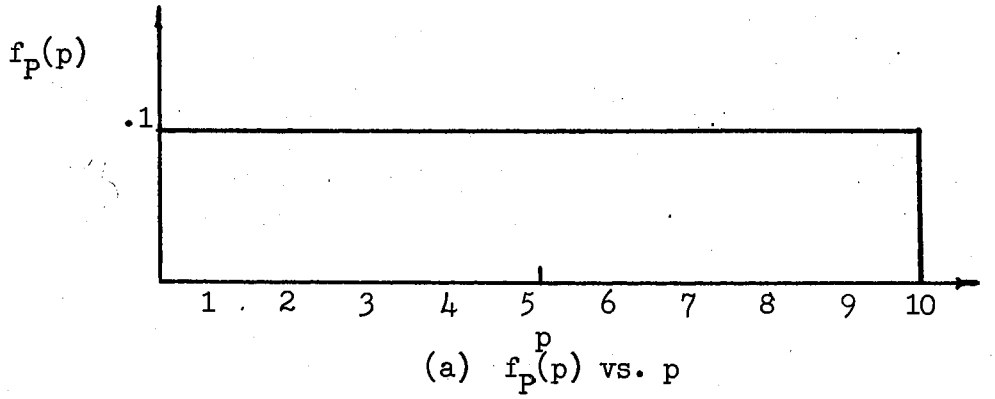

(a) $f_P(p)$ vs. p

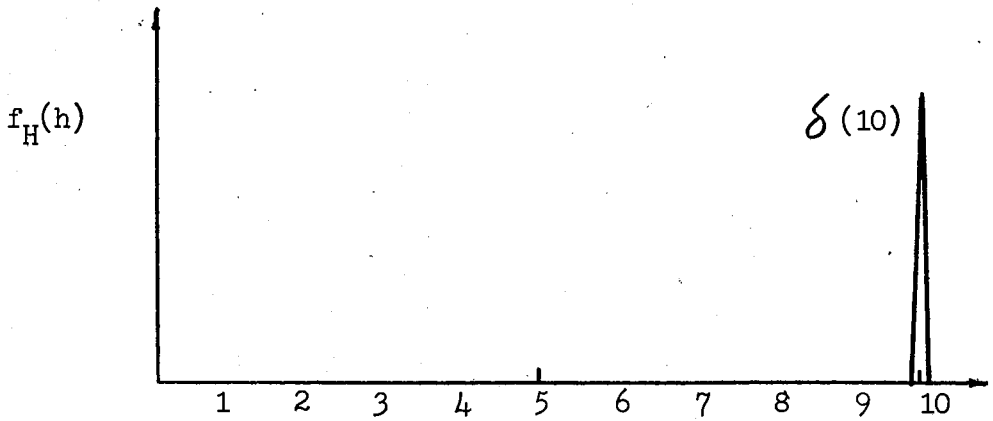

(b) $f_H(h)$ vs. h

Figure 27. Input Random Variables for Multiple Population of Particles Example Problem

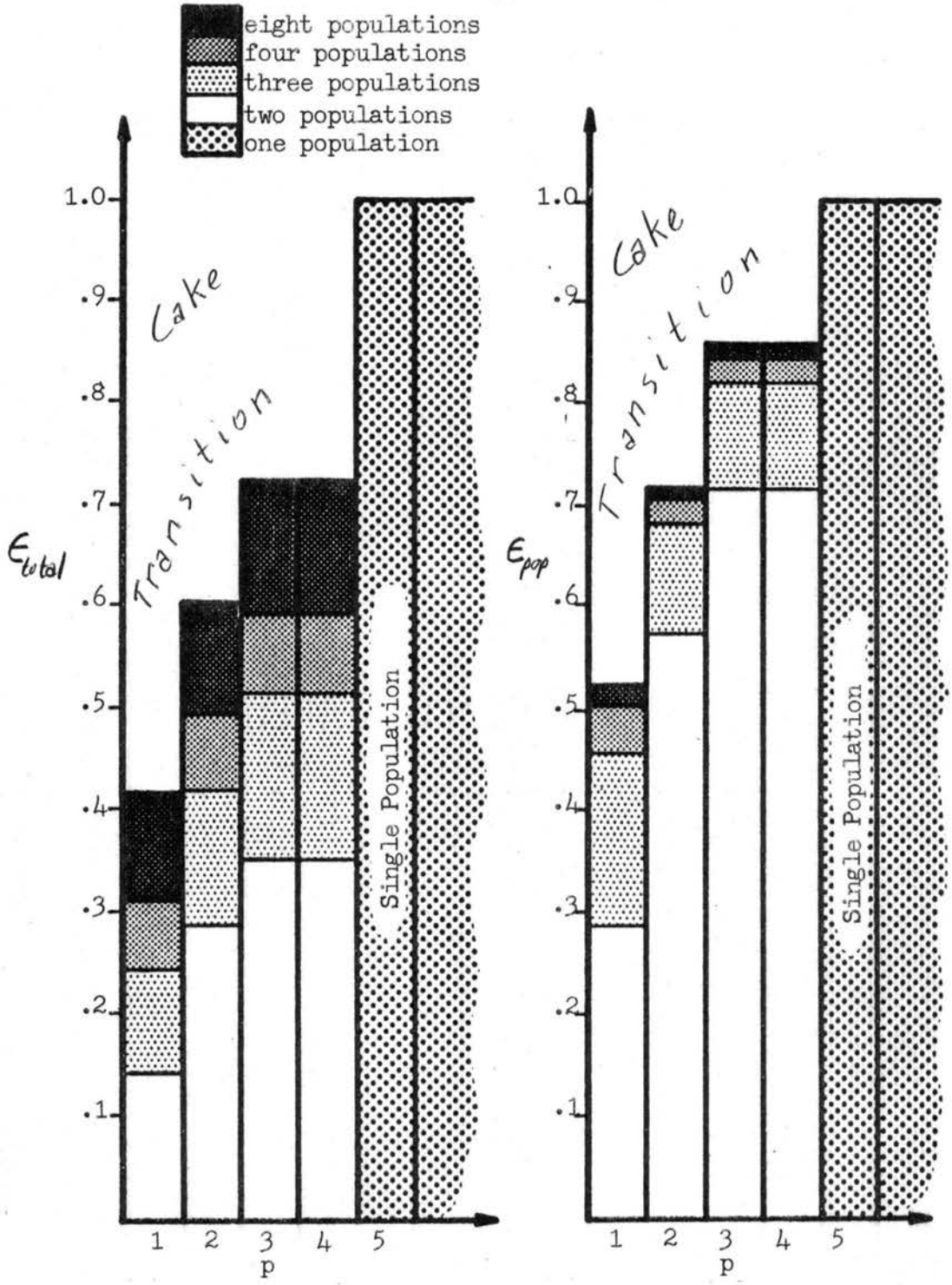

(a) Total Efficiency (b) Incremental Efficiency

Figure 28. Multiple Population of Particles Example Problem

in which one might expect a transition to cake mode filtration are marked.

Extensions of the Present Study

Several direct extensions and a countless number of indirect extensions to the present study exist. In this chapter only topics which pertain to filtration and contamination control will be discussed.

One worthwhile general extension would be to modify the analysis to consider finite input distributions. The extension of the weighted simulation technique to treat a single finite input distribution would be straightforward.

The most obvious extension of the study would be the modeling of depth medium filtration. Since the sieving mechanism has been reasonably modeled for a single layer, and the simulation technique has been developed for multiple layers, extension to the depth medium case requires only an accurate pore geometry model of the depth medium. If the pore geometry model is in terms of geometrically measurable random variables, then direct compensation to change the separation properties of the filter by alteration of its constituent geometry would be possible. The pore size models mentioned in References 4, 5 and 10 are pioneering steps toward such a model.

With a reliable simulated sieving model experimental data gathered from depth media filtration would provide the basis of comparison to identify other retention mechanisms which are active in the process. That is, by deductive reasoning separation not accounted for by the sieving simulation must be attributed to other mechanisms. As was mentioned earlier, the fundamental question that this rationale is

proposed to answer is, at present, unresolved among hydraulic filtration experts.

The broader applications of the techniques utilized in this study include areas of filtration other than the sieving mechanism. In fact, any process in which random variables can be modeled, even as data sets, and deterministic processes described algebraically, can be treated in an analogous way. In all of the possibilities mentioned below, the input random variables include particle geometry, particle position, medium geometry, and fluid velocity field. For practical purposes the velocity field needs to be described in terms of medium geometry. A deterministic problem which is pertinent is discussed in Reference 6.

First, consider unstable sieving. In this mode a particle might be held against an element of the filter medium by viscous shear forces. If the fluid velocity changes significantly the viscous shear experienced by the particle will change and the particle may be removed from its former position. Or, under the new force balance, body forces may overcome viscous forces and the particle be carried away from its former location.

To model the unstable sieving process it would be necessary to supply a deterministic model for drag forces on a particle in terms of particle geometry and the fluid velocity field. The additional complexity introduced by modeling of the velocity field renders the problem significantly more difficult than the ones described in the preceding chapters. Output relationships would ideally describe particles ultimately retained and the remaining pore size distribution.

If the fluid velocity field could, indeed, be modeled as a random variable, then all of the classic deterministic transport mechanism

models summarized in Chapter II could be treated stochastically. The rationale would be to model the spacial concentration of particles at some arbitrary initial condition. The deterministic models then describe the trajectory of a single particle. The methods described herein could be used to describe a concentration which has been modified by the velocity field.

In a similar manner the technique can be applied to a problem for which experimental data is becoming available. The case of particle capture by viscous shear forces was defined by Bensch (31). In this mode it is theorized that a particle may be carried into regions of low fluid velocity by inertial forces. The viscous shear on the particle surface then serves as a retention mechanism.

If the force balance on the particle and the velocity distribution of the fluid can be modeled, this phenomenon can be investigated. The most tractable form of the analysis would treat the nontransient case.

The experimental data which is becoming available treats a semitransient problem in which the medium is used to gather contaminant and the filtrate collected after a fixed period of depressurization. The model to fit such a case would need to simulate unstable sieving and capture due to viscous shear forces as a minimum.

One further attractive filtration problem should be mentioned. The modeling of retention due to surface forces is important in aerosol filtration and, as has been demonstrated, can be significant in hydraulic filtration. Models of attractive forces such as those proposed by Zimon (10) could be coupled with hydrodynamic models such as those of Speilman and Goren (32) to form the necessary deterministic relationships. The techniques treated herein could then be applied to

determine the density of particles actually retained by some idealized medium geometry. In this instance identification of random variables such as particle charge or medium surface roughness might be performed from experimental data.

Many worthwhile extensions of methods presented in this study fall outside the context of filtration mechanics. One example would be the prediction of wear in hydraulic components. If a model of the damage done by a single contaminant particle as it is crushed between two moving surfaces were available, stochastic techniques could be used to introduce such random variables as particle size, particle hardness and component surface properties. Again, identification techniques could be used with experimental data to determine numerical values for random variables for which measurements cannot be obtained.

The above mentioned problems point out the versatility of the approach employed. Limiting factors generally include: the availability of appropriate deterministic models, the measurability of pertinent random variables, and the computational effort required for complicated problems. As has been mentioned previously, closed form solutions have been obtained for only the most simple problems.

CHAPTER IX

SUMMARY AND CONCLUSIONS

Summary

The problem considered in this thesis is the modeling of the sieving mechanism in hydraulic filtration. The overall objective of the study is to develop such a model and demonstrate its use for the case of a nontortuous sieve mesh.

The analytical model is derived in terms of the following geometrically measurable random variables: particle size, particle shape, pore size, pore shape, particle attitude and angular displacement between particle and pore. Generalized integral expressions are developed for separation efficiency, downstream particulate size density, and pore size density after filtration of a population of particles through a sieve mesh. The expressions are extended to consider filtration of multiple populations of particles by a series of combination of sieve mesh layers.

Numerical solution methods for the general problem have been mechanized for digital computer implementation. Five empirically studied example problems, as well as one hypothetical case, are simulated numerically.

In the experimental analysis, five test series were performed under carefully controlled conditions so that the surface of the sieve mesh was microscopically observable. Thus, it was possible to verify

that caking and flocculation did not occur to a significant extent on the surface of the medium. Microscopic analysis provided data for calculation of separation efficiencies and particulate size density after filtration.

Since the simulation of the sieving process is geometric in nature, the deviation of experimental from analytical results can only be due to measurement error or the presence of factors not within the context of the derivation assumptions. The conclusions drawn from the study are summarized in the next section.

Conclusions

From the research described in the preceding chapters, a number of evaluations have been made. The following list summarizes the major conclusions:

1. A rigorous modeling procedure for the sieving mechanism in hydraulic filtration has been developed based on geometrically measurable random variables.

2. Only the most simple input functions allow the closed form solution of the resulting integral expressions. Therefore, numerical techniques must be employed to obtain quantitative results.

3. A weighted simulation technique has been developed to obtain numerical approximations of the post-filtration random variables. That algorithm required less computational effort to achieve a comparable accuracy as that achieved by the Monte Carlo simulation or direct numerical integration of the full integral expressions.

4. Qualitative microscopic observation of the sieving process is possible on the upstream surface of a flat sieve mesh.

5. Simulated output data approximated experimental data in shape and magnitude when geometrically measured and logically assumed input random variables were used. Deviations could be attributed to measurement errors or the effects of surface forces.

6. Random variables can be identified as parameters to force simulated data to more closely approximate experimental data.

7. The general methods developed herein should prove to be a useful tool for further research in filtration mechanics and contamination control.

A SELECTED BIBLIOGRAPHY

(1) Military Specification, MIL-F-25682A. Filter and Filter Elements, Fluid Pressure, Hydraulic, Absolute, 25 Micron (7 August 1963).

(2) Freshwater, D. C. "Some Current Problems in Filtration." Filtration and Separation (1969), 142-49.

(3) Fitch, E. C. Jr. The Compatibility of Hydraulic Power Components with Contaminated Fluid Environments. Oil Hydraulics and Pneumatics Conference, Hannover, Germany (April 26, 1971).

(4) Clarenburg, L. A., and J. F. Van Der Waal. "Influence of Filter Composition on Aerosol Penetration through Glass Fiber Filters." I. and E. C. Process Design and Development, V (April, 1966), 110-17.

(5) Corte, H. K., and E. H. Lloyd. "Fluid Flow Through Paper and Sheet Structure." Transactions of the Cambridge Symposium (1965), 981-1009.

(6) Stuntz, R. M., and L. E. Bensch. Filtration Physics. Basic Fluid Power Research Program Series, Oklahoma State University, No. 70- 2, Stillwater, Oklahoma (1970).

(7) Ives, K. J. "Depth Filtration of Liquids." Filtration and Separation. (December, 1970), 700-04.

(8) Herzig, J. P., D. M. Leclerc, and P. LeGoff. "Flow of Suspensions through Porous Media - Application to Deep Filtration." Industrial and Engineering Chemistry, LXII (May, 1970), 8-35.

(9) Chen, C. Y. "Filtration of Aerosols by Fibrous Media." Chemical Reviews, LV (1955), 595-623.

(10) Zimon, A. D. Adhesion of Dust and Powder. New York: Plenum Press, 1969.

(11) Miles, R. E. "Random Polygons Determined by Random Lines in a Plane." Proceedings of the National Academy of Science, LII (1964), 901-07.

(12) Pickaar, H. W., and L. A. Clarenburg. "Aerosol Filters - Pore Size Distribution in Fibrous Filters." Chemical Engineering Science, XXII (1967), 1399-408.

(13) Pickaar, H. W., and L. A. Clarenburg. "Aerosol Filters—the Tortuosity Factor in Fibrous Filters." Chemical Engineering Science, XXII (1967), 1817-827.

(14) Herdan, G. Small Particle Statistics. London: Butterworths, 1960.

(15) Banacki, W. J., and R. L. Bowers, "Pore Size Testing of Filter Papers." Tappi, XLV (October, 1962), 805-07.

(16) Fitch, E. C., R. E. Reed, and D. E. Long. "Study of Filtration Mechanics and Sampling Techniques." NASA Contract NAS 811009 Annual Report, Oklahoma State University, 1968.

(17) Tucker, R. H. "The Development and Verification of Theoretical Models for the Performance of Wire Cloth Filter Media." (Unpub. Ph.D. dissertation, Oklahoma State University, 1966).

(18) Breipohl, A. M. Probabilistic Systems Analysis. New York: John Wiley & Sons, 1970.

(19) Batchelor, G. K. An Introduction to Fluid Dynamics. Cambridge: Cambridge University Press, 1967.

(20) Happle, John, and Howard Brenner. Low Reynolds Number Hydrodynamics. Englewood Cliffs: Prentice Hall, 1965.

(21) Lamb, Sir Horace. Hydrodynamics, 6th ed. New York: Dover, 1932.

(22) McCracken, D. D., and W. S. Dorn. Numerical Methods and Fortran Programming. New York: John Wiley & Sons, 1964.

(23) System/360 Scientific Subroutine Package (360A - CM - 03X) Version III Programmer's Manual. International Business Machines, White Plains, New York, 1968.

(24) Hahn, G. J., and S. S. Shapiro. Statistical Models in Engineering. New York: John Wiley & Sons, 1967.

(25) Staff of the Computation Laboratory. Table of Cumulative Binomal Probability Distribution. National Bureau of Standards Applied Math Series, No. 6. Washington, D. C.: U. S. Government Printing Office, 1950.

(26) Aerospace Recommended Practice ARP - 598 - A. "Procedure for Determination of Particulate Contamination of Hydraulic Fluids by the Particle Count Method." Revision A (August 1, 1969).

(27) Fairs, G. L. "Developments in the Technique of Particle Size Analysis by Microscopical Examination." Journal Royal Microscope Society, LXXI (1951), 209-20.

(28) McCrone, W. C., R. G. Draftz, and J. G. Delly. The Particle Atlas. Ann Arbor: Ann Arbor Science Publishers, 1967.

(29) Miller, I., and J. E. Freund. Probability and Statistics for Engineers. Englewood Cliffs: Prentice Hall, 1965.

(30) Mischke, C. R. An Introduction to Computer - Aided Design. Englewood Cliffs: Prentice Hall, 1968.

(31) Bensch, L. E. The Hydrodynamic Retention Mechanism in Hydraulic Filtration. (Unpub. Academic Report, Oklahoma State University, 1970).

(32) Speilman, L. A., and S. L. Goren. "Capture of Small Particles by London Forces from Low-Speed Liquid Flows." Environmental Science & Technology, IV (February, 1970), 135-40.

APPENDIX A

GEOMETRIC RELATIONSHIPS

The solution of example problems given in Chapter VII requires geometric relationships derived in this appendix. Expressions are derived for partial pore blockage in series A through E. Since the particle and pore shapes are idealized representations of irregular shapes occurring in nature, some compromise between computational effort and rigorous shape description must be considered.

Before treating of each series geometry individually it will be convenient to derive an expression for the projection of an ellipse. Consider the ellipse of Figure 29 with the major axis p and the minor axis cp·p, which has been rotated through the angle θ. It is desired to find p*.

Define z, x, y, and α as shown so that by definition,

$$z^2 = x^2 + y^2 \tag{A-1}$$

$$cp^2x^2 + y^2 = p^2cp^2/4 \tag{A-2}$$

$$p^*/2 = z \cdot \sin(\alpha + \theta) \tag{A-3}$$

$$\tan\alpha = y/x. \tag{A-4}$$

Substitution of Equations A-1, A-2, and A-4, into Equation A-3, yields

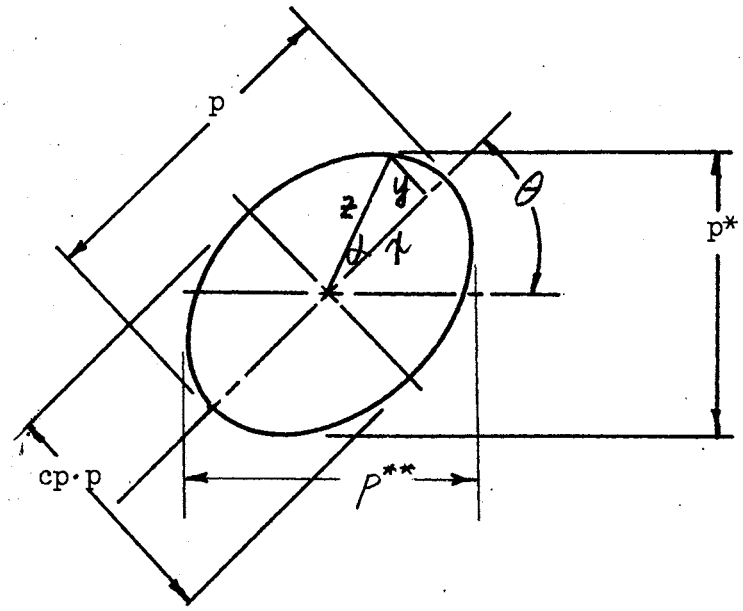

Figure 29. Projection of Ellipse

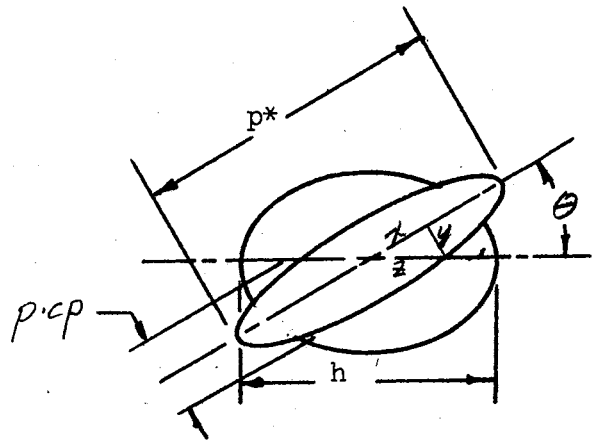

Figure 30. Partial Blockage
Series A

$$p^* = 2\left(cp\sqrt{p^2/4 - x^2}\cos\theta + x\sin\theta\right). \quad \text{(A-5)}$$

To find the maximum value of p* for an arbitrary value of θ with respect of x, set,

$$\frac{\partial p^*}{\partial x} = 0,$$

to find,

$$x(p^* = \text{maximum}) = \frac{p}{2}\frac{\sin\theta}{\sqrt{cp^2\cos^2\theta + \sin^2\theta}}. \quad \text{(A-6)}$$

Combination of Equation A-6 and A-5, yields the desired result,

$$p^* = p\sqrt{cp^2\cos^2\theta + \sin^2\theta}. \quad \text{(A-7)}$$

To find p** consider the same problem with the ellipse tipped through $\pi/2 - \theta$, so that,

$$p^{**} = p\sqrt{cp^2\sin^2\theta + \cos^2\theta}. \quad \text{(A-8)}$$

Now the problem geometries of each series will be considered.

Series A

In this series particles are ellipsoids of revolution and pores are elliptic. A two dimensional analysis can be achieved by comparison of the particle projection and pore shape. The particle projection is an ellipse with major axis p and minor axis cp·p.

Partial blockage can be modeled with the aid of Figure 30, and by definition,

$$cp^2x^2 + y^2 = p^2cp^2 \quad \text{(A-9)}$$

$$x^2 + y^2 = z^2 \quad \text{(A-10)}$$

$$y/x = \tan\theta. \tag{A-11}$$

Combining Equations A-9 through A-11 yields,

$$z^2 = p^2 cp^2 (1 + \tan^2\theta)/(cp^2 + \tan^2\theta). \tag{A-12}$$

Then the desired value of the new pore size is,

$$h_{new} = (h/2 - z)/ch. \tag{A-13}$$

The critical angle, θ, must be found as the limiting case for escape if the condition

$$ch \cdot h < p < h/cp$$

is met. Using the nomenclature of Figure 31 the following general relationships can be obtained:

$$ch^2 x^2 + y^2 = ch^2 h^2/4 \tag{A-14}$$

$$cp^2 x'^2 + y'^2 = cp^2 p^2/4 \tag{A-15}$$

$$\alpha = \tan^{-1} y/x \tag{A-16}$$

$$\beta = \tan^{-1} y'/x' \tag{A-17}$$

$$\beta = \alpha - \theta. \tag{A-18}$$

Now if tangency is assumed

$$y \approx \frac{p}{2}\sqrt{\sin^2\theta + cp^2\cos^2\theta} \tag{A-19}$$

and

$$x^2 + y^2 = x'^2 + y'^2. \tag{A-20}$$

Equations A-14 through A-20 are seven independent nonlinear algebraic equations in seven unknowns $(x, x', y, y', \alpha, \beta, \theta)$. This set is of a form which can be manipulated into the relationship,

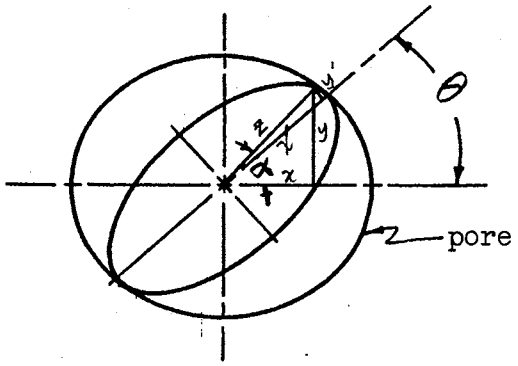

Figure 31. Critical Escape Angle - Series A

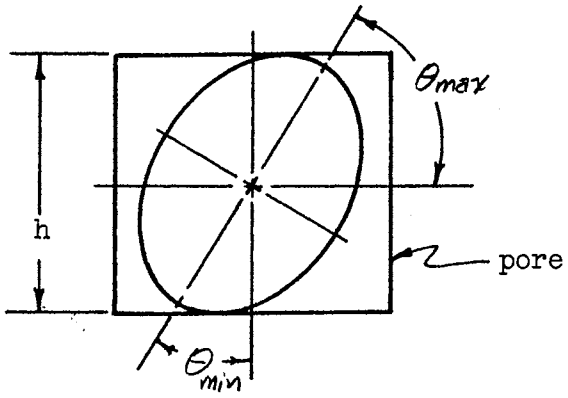

Figure 32. Problem Geometry - Series B

$$\theta = g(\theta),$$

which will converge iteratively from an initial guess of θ. A subroutine, THETCP, was programmed to carry out the iterations. Details are presented in Appendix B.

Another set of eight nonlinear equations in eight unknowns was derived. However, it required a Newton-Raphson solution which was prohibitively slow.

Series B

The geometry of series B consisted of square pores and ellipsoidal particles. The two dimensional projection of the problem is shown in Figure 32. By use of the conventional nomenclature and Equation A-7, the limiting relationship is written as,

$$h = p\sqrt{\sin^2\theta + cp^2\cos^2\theta}. \qquad \text{(A-21)}$$

Equation A-21 can be solved for $\theta(h,p)$ by defining

$$\sin\theta = y/(x^2+y^2)^{1/2}$$

The result is the desired limiting value,

$$\theta_{max} = \tan^{-1}\sqrt{\frac{cp^2p^2 - h^2}{h^2 - p^2}}. \qquad \text{(A-22)}$$

Also from Figure 32 it can be observed that,

$$\theta_{min} = \pi/2 - \theta_{max}. \qquad \text{(A-23)}$$

Since the size of the pores formed due to partial blockage is more sensitive to p, and h than to θ, the new pore formed is modeled on the basis of $E(\theta) = \pi/4$. The resulting expression is,

$$h_{new} = (\sqrt{2}\,h - cp \cdot p)/2. \qquad \text{(A-24)}$$

Series C and E

This model consists of elliptic pores and spherical particles. Symmetry of the particles precludes any angular dependence. The assumption of concentric blockage yields the relationship,

$$h_{new} = (h - p)/2 \cdot ch. \qquad \text{(A-25)}$$

Note that the pore in Figure 33 is not exactly the shape of the pore actually formed, but is an ellipse of the same shape as the original pore and has the correct smallest dimension. Equation A-25 is valid so long as the new interval formed on the pore major axis is shorter than the other dimension of the new pore. The limiting relationship is,

$$ch \cdot h \leq h(1 - ch)/2$$

or

$$ch \geq 1/3.$$

That condition is satisfied in all the problems considered.

Series D

In series D pores were modeled as squares and particles were modeled as spheres. Again, no angular dependency exists. In this case partial blockage is considered in three dimensions as shown in Figure 34. From the right triangle formed in the front view the new pore size formed is seen to be,

$$h_{new} = \frac{\sqrt{p^2 + h^2} - p}{2\sqrt{2}}. \qquad \text{(A-26)}$$

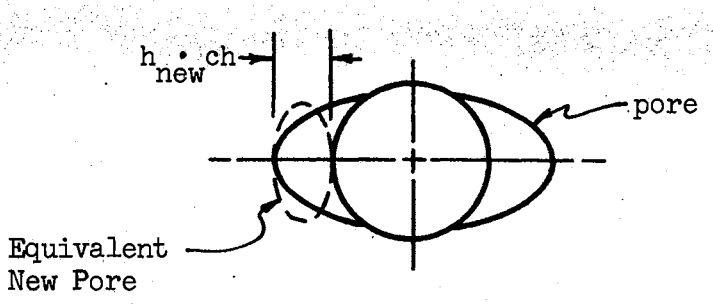

Figure 33. Partial Blockage - Series C & E

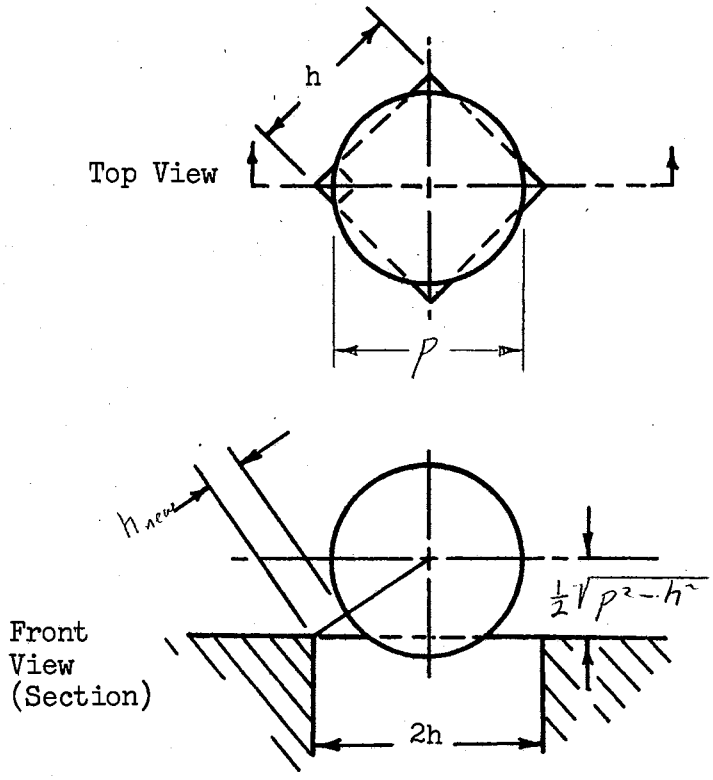

Figure 34. Partial Blockage - Series D

APPENDIX B

NUMERICAL TECHNIQUES

In this appendix the weighted simulation technique will be documented. Also, the subroutine for calculation of the critical angle formed by one ellipse turning concentrically within a second ellipse will be discussed.

In the present study, the weighted simulation technique is used to describe the filtration of a dilute solution of particles through a sieve mesh. Capture conditions and partial pore blockage can be modeled geometrically. The assumption is made that the following input random variables are independent with known density functions:

pore size, H, $f_H(h)$

pore shape, CH, $f_{CH}(ch)$

particle size, P, $f_P(p)$

particle shape, CP, $f_{CP}(cp)$

particle attitude ϕ, $f_\phi(\phi)$

particle/pore angular displacement, θ, $f_\theta(\theta)$.

If input density functions are given in data form they are characterized by the density function value at each interval midpoint. From independence, the joint probability of occurrence of any combination of discrete independent variable values is,

$$f_{H,CH,P,CP,\theta,\phi}(h,ch,p,cp,\theta,\phi) = f_H(h)\cdot f_{CH}(ch)\cdot f_P(p)\cdot f_{CP}(cp)\cdot f_\theta(\theta)\cdot f_\phi(\phi). \quad \text{(B-1)}$$

If every permutation of the independent random variables is considered and the associated deterministic problem describing capture is solved, the resultant downstream particle size density, $f^{(1)}_{P_{(1)}}(p)$, and remaining pore size density, $f^{(1)}_{H_{(1)}}(h)$, can be determined. Partial blockage is weighted according to the number of new pores formed by each capture. The resulting raw density functions are normalized so that their integral summation will have a value of unity.

Accuracy of the method is essentially that of square law integration. The intervals on the independent random variables can be made arbitrarily small to improve accuracy at the expense of increased computational effort.

Separation efficiencies can be calculated by the definition:

$$\epsilon(p) = 1 - \left[Pr\{escape\} \cdot f^{(1)}_{P_{(1)}}(p)\right] / f_P(p), \quad \text{(B-2)}$$

$$\epsilon(p) = \frac{\text{No. Upstream (p)} - \text{No. Downstream (p)}}{\text{No. Upstream (p)}}$$

In terms of the algorithm, Pr $\{escape\}$ is the summation of all joint density expressions (Equation B-1) for which escape is calculated over the entire permutation of the independent random variables.

Extension of Equation B-2 to describe the overall separation efficiency of a population of particles through n sieve layers yields,

$$\epsilon^{T(1)}_{(n)}(p) = 1 - \prod_{i=1}^{n} \frac{\left[Pr_i\{escape\}\right]}{f_P(p)} f^{(1)}_{P_{(n)}}(p). \quad \text{(B-3)}$$

To further extend the model to m initially identical populations of particles the summation of particles escaping must be made. Thus, the expression for the overall efficiency of m populations of particles passing through n sieve mesh layers is,

$$\epsilon_{(n)}^{T(m)}(p) = 1 - \sum_{j=1}^{m} \frac{\left[\prod_{i=1}^{n} \left(Pr_i\{escape\}\right) f_{p_{(n)}}^{(j)}(p)\right]}{m f_p(p)}. \qquad \text{(B-4)}$$

The algorithm which has been developed is user oriented and reasonably versatile. Definitions of program variables are found in the program listing given at the end of this appendix. The flow charts in Figures 35 through 38 summarize the logic of the program. Subroutine SIMSIV iterates through all possible permutations of the independent random variable intervals. SIMSIV calls a function subroutine when calculation of a critical angle of rotation is needed. In the case of series A that function calls subroutine THETCP. Subroutine SIMSIV also calls subroutine CAPTUR. CAPTUR evaluates whether capture or escape occurs for the current values of the independent random variables and calls function PARBLK if a partial blockage must be calculated. This subroutine also increments the new particle and pore density functions. Separation efficiencies are calculated in subroutine SIMSIV.

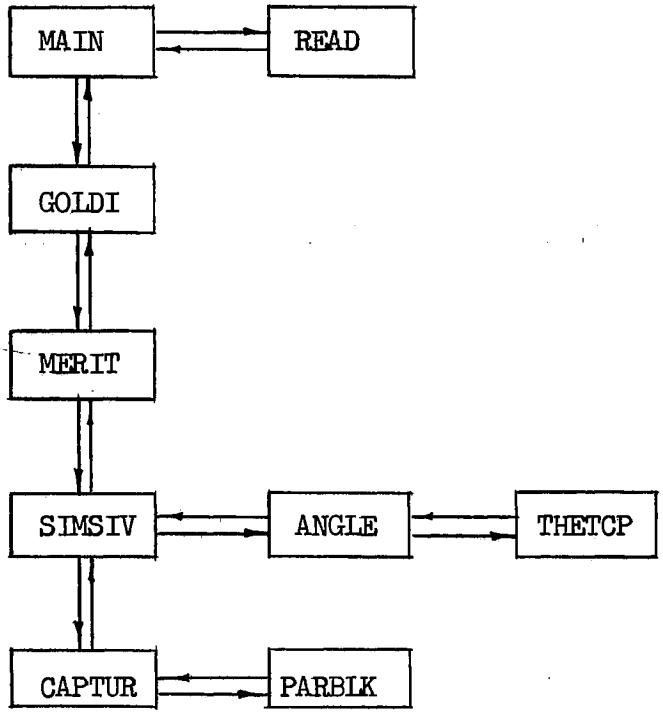

Figure 35. Example of Calling Program Logic for Series A

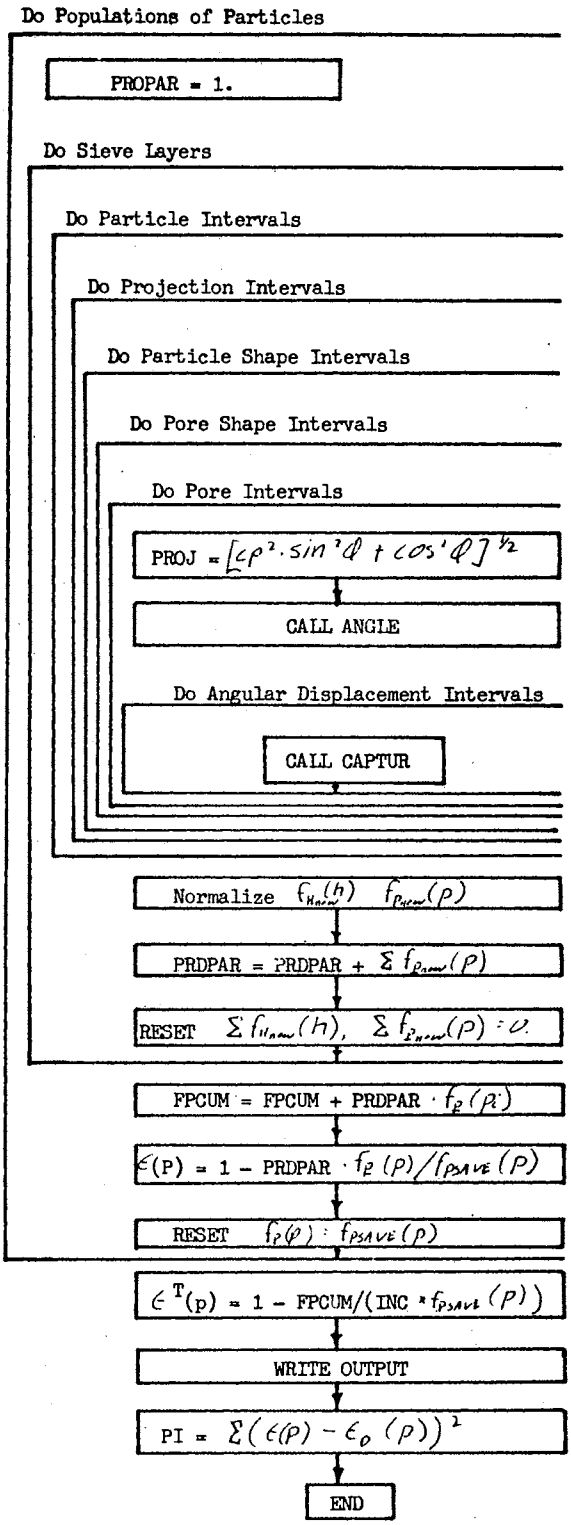

Figure 36. Flow Chart for Subroutine SIMSIV

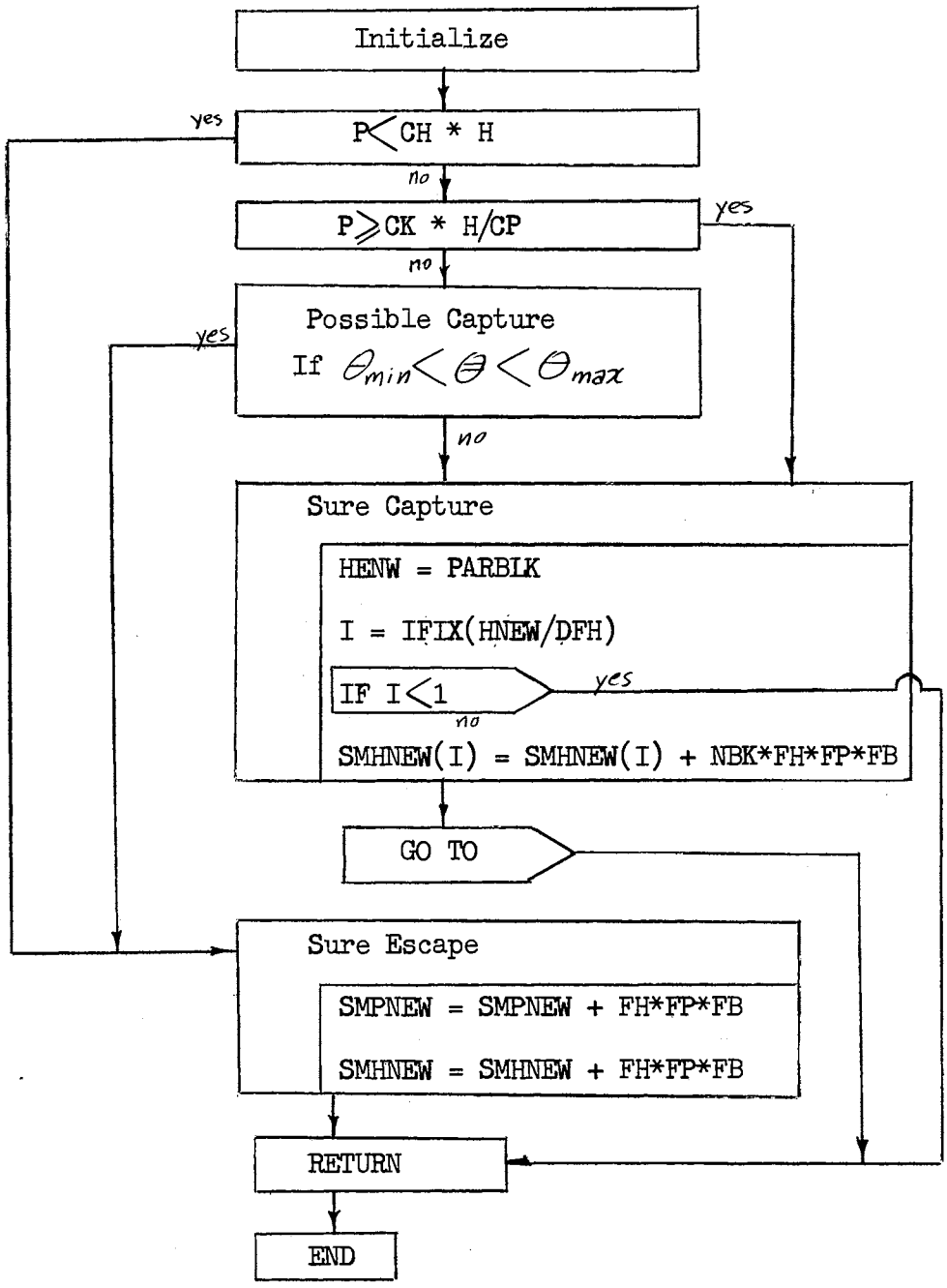

Figure 37. Flow Chart for Subroutine CAPTUR

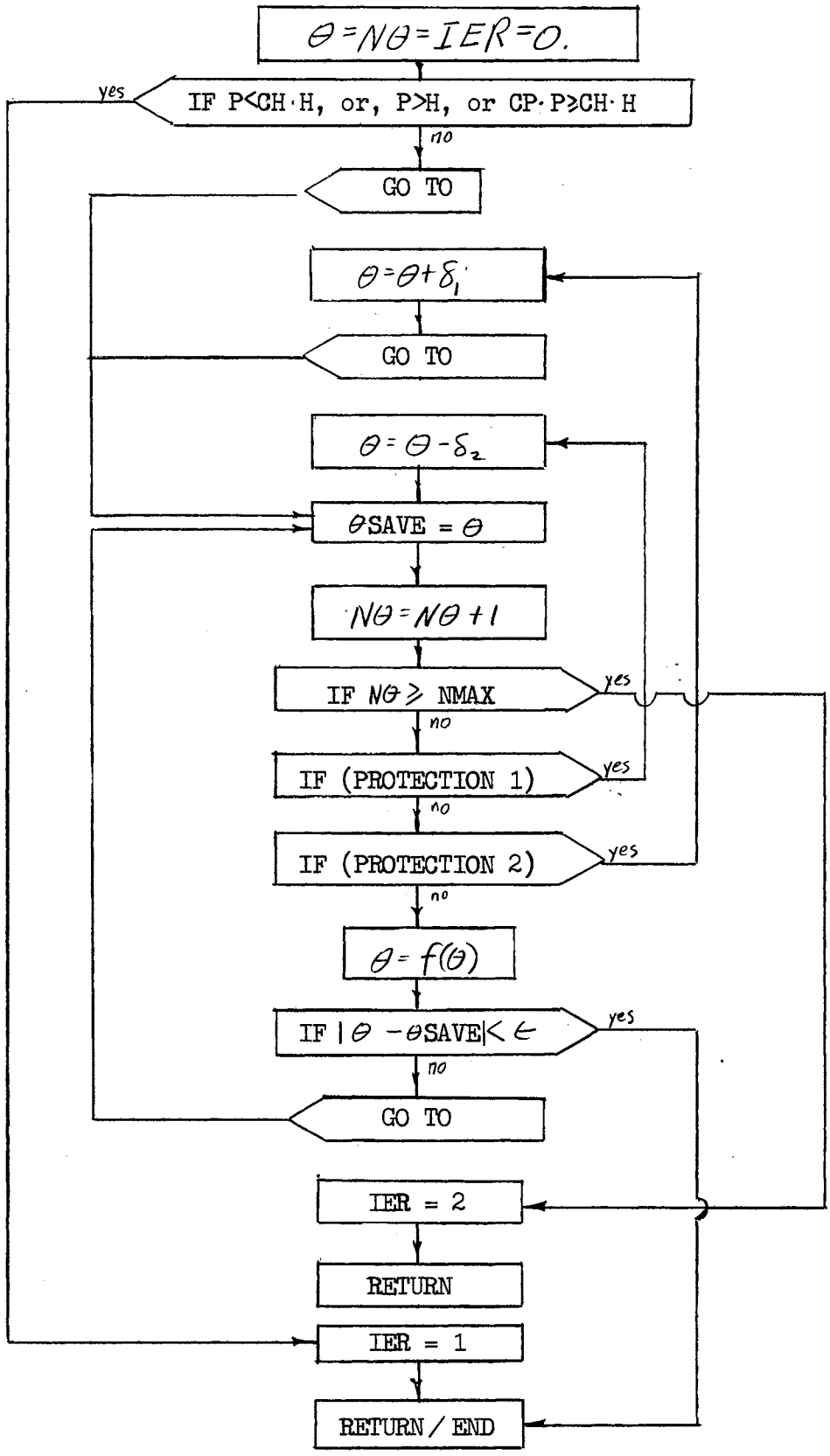

Figure 38. Flow Chart for Subroutine THETCP

```
C     THIS IS THE MAIN CALLING PROGRAM
C
C     SERIES A ..... ACF WITH CHS, CP=.439,CH=DISTRIBUTION 2
      COMMON/DATA1/FH(100,5),H(100),FP(100),P(100),FPSAVE(100),
     1 FHSAVE(100),PROJ(100),FB(100),B(100),FPCUM(100),SMHNEW(100),
     2SMPNEW(100),FPROJ(100)
      COMMON/DATA2/INC,LAY,IPART,IPORE,IBETA,IPROJ,      DFP,DFH,DFB
      COMMON/DATA3/IPA,IPO,IA,IPR,LA,I
      COMMON/DATA4/PPRO,THETA
      COMMON/DATA5/CP(10),FCP(10),CH(10),FCH(10),ICP,ICH,ICPN,ICHN
      COMMON/DATA6/ECOMP(20),HBK,NECOMP
      CALL READ
      CALL       SIMSIV(Y)
      CALL EXIT
      END

      SUBROUTINE READ
C     THIS SUBROUTINE PROVIDES INITIAL VALUES FOR THE COMPUTATION
      COMMON/DATA1/FH(100,5),H(100),FP(100),P(100),FPSAVE(100),
     1 FHSAVE(100),PROJ(100),FB(100),B(100),FPCUM(100),SMHNEW(100),
     2SMPNEW(100),FPROJ(100)
      COMMON/DATA2/INC,LAY,IPART,IPORE,IBETA,IPROJ,      DFP,DFH,DFB
      COMMON/DATA3/IPA,IPO,IA,IPR,LA,I
      COMMON/DATA4/PPRO,THETA
      COMMON/DATA5/CP(10),FCP(10),CH(10),FCH(10),ICP,ICH,ICPN,ICHN
      COMMON/DATA6/ECOMP(20),HBK,NECOMP
C
  101 FORMAT(1H1,'INCREMENTS.....',I3,/,
     1' LAYERS.....',I3,/,
     2' DIVISIONS ON PARTICLE HISTOGRAM.....',I3,/,
     3' DIVISIONS ON PORE HISTOGRAM.....',I3,/,
     4' DIVISIONS ON ANGULAR HISTOGRAM.....',I3,/,
     5' DIVISIONS ON PROJECTION HISTOGRAM.....',I3,/)
  102 FORMAT(1X,'SIZE OF DIVISION OF PARTICLE HISTOGRAM...',F10.5,/,
     3' SIZE OF DIVISION OF PORE HISTOGRAM.....',F10.5,/,
     4' SIZE OF DIVISION ON ANGLUAR HISTOGRAM....',F10.5,/)
  103 FORMAT(1X,'INTERVAL  PORE SIZE     DENSITY        LAYER = ',I3,/)
  104 FORMAT(1X,110,2F14.6)
  105 FORMAT(1X,'INTERVAL  PARTICLE SIZE DENSITY        LAYER = ',I3,/)
  106 FORMAT(1X,'INTERVAL  ANGLE SIZE    DENSITY',/)
  107 FORMAT(1HO,'INTERVAL  SUM PART PDF  EFFICIENCY, AFTER PASSAGE OF',
     I13,' INCREMENTS THROUGH',I3,' LAYERS')
  108 FORMAT(1X,' PROJECTION   ANGLE SIZE    DENSITY ',/)
  109 FORMAT(1X,'ICPN=',I3,' ICHN=',I3)
  110 FORMAT(1X,'INTERVAL  PART. SHAPE F  DENSITY',/)
  111 FORMAT(1X,'INTERVAL  PORE SHAPE F   DENSITY',/)
  112 FORMAT(1X,'ECOMP(',12,')=',F10.5)
  201 FORMAT(8I10)
  202 FORMAT(8F10.5)
  203 FORMAT(2F10.5)
  204 FORMAT(F10.5,I10)
      READ(5,201)INC,LAY,IPART,IPORE,IBETA ,NFHFUN,NFPFUN,IPROJ
      WRITE(6,101)INC,LAY,IPART,IPORE,IBETA,IPROJ
      READ(5,202)DFP,DFH,DFB
      WRITE(6,102)DFP,DFH,DFB
      READ(5,201)  ICPN,ICHN
      WRITE(6,109) ICPN,ICHN
      IF(NFHFUN.EQ.1)CALL CALFH
      IF(NFHFUN.EQ.0)READ(5,203)(H(I),FH(I,1),I=1,IPORE)
      K=0
      WRITE (6,103)K
      WRITE (6,104)(I,H(I),FH(I,1),I=1,IPORE)
      IF(NFPFUN.EQ.1) CALL CALFP
      IF(NFPFUN.EQ.0) READ(5,203)(P(I),FP(I)  ,I=1,IPART)
      WRITE (6,105)K
      WRITE(6,104)(I,P(I),FP(I),I=1,IPART)
      CALL CALFB
      WRITE(6,106)
      WRITE(6,104)(I,B(I),FB(I),I=1,IBETA)
      SUMBTA=0.
      WRITE(6,106)
      DO 5 I=1,IBETA
    5 SUMBTA=SUMBTA+FB(I)
      DO 10 I=1,IBETA
      FB(I)=FB(I)/SUMBTA
   10 WRITE(6,104)I,B(I),FB(I)
   20 CONTINUE
      SMHNEW(1)=DFH
      SPORE=FH(1,1)*SMHNEW(1)
      DO 25 I=2,IPORE
      SMHNEW(I)=2.*(H(I)-H(I-1)-SMHNEW(I-1)/2.)
      SPORE=SPORE+FH(I,1)*SMHNEW(I)
   25 CONTINUE
      WRITE(6,103)K
      DO 30 I=1,IPORE
      FH(I,1)=FH(I,1)*SMHNEW(I)/SPORE
      SMHNEW(I)=0.
      FHSAVE(I)=FH(I,1)
   30 WRITE(6,104)I,H(I),FH(I,1)
      DO 32 I=1,IPORE
      DO 32 J=1,LAY
   32 FH(I,J)=FH(I,1)
      SMPNEW(1)=DFP
      SPART=FP(1)*SMPNEW(1)
      DO 35 I=2,IPART
      SMPNEW(I)=2.*(P(I)-P(I-1)-SMPNEW(I-1)/2.)
      SPART=SPART+FP(I)*SMPNEW(I)
   35 CONTINUE
      WRITE(6,105)K
      DO 40 I=1,IPART
      FP(I)=FP(I)*SMPNEW(I)/SPART
      FPSAVE(I)=FP(I)
      SMPNEW(I)=0.
      FPCUM(I)=0.
   40 WRITE (6,104)I,P(I),FP(I)
      CALL CALPRO
      WRITE (6,108)
      WRITE(6,104)(I,PROJ(I),FPROJ(I),I=1,IPROJ)
      SUMBTA=0.
      WRITE(6,108)
      DO 50 I=1,IPROJ
   50 SUMBTA=SUMBTA+FPROJ(I)
      DO 60 I=1,IPROJ
      FPROJ(I)=FPROJ(I)/SUMBTA
```

```
60 WRITE(6,104)I,PROJ(I),FPROJ(I)
   CALL CALFCP
   WRITE(6,110)
   WRITE(6,104)(I,CP(I),FCP(I),I=1,ICPN)
   SUMBTA=0.
   WRITE(6,110)
   DO 70 I=1,ICPN
70 SUMBTA=SUMBTA+FCP(I)
   DO 75 I=1,ICPN
   FCP(I)=FCP(I)/SUMBTA
75 WRITE(6,104)I,CP(I),FCP(I)
   CALL CALFCH
   WRITE(6,111)
   WRITE(6,104)(I,CH(I),FCH(I),I=1,ICHN)
   SUMBTA=0.
   WRITE(6,111)
   DO 80 I=1,ICHN
80 SUMBTA=SUMBTA+FCH(I)
   DO 85 I=1,ICHN
    FCH(I)=FCH(I)/SUMBTA
85 WRITE(6,104)I,CH(I),FCH(I)
   READ(5,2C4)HBK,NECCMP
   IF(NECCMP.EQ.0) GO TO 90
   READ(5,2C1)(ECCMP(I),I=1,IPART)
   WRITE (6,112)(I,ECOMP(I),I=1,IPART)
90 CONTINUE
   RETURN
   END



   SUBROUTINE CALFP
   COMMON/DATA1/FH(1CC,5),F(100),FP(100),P(100),FPSAVE(100),
  1 FHSAVE(100),PROJ(100),FB(100),B(10C),FPCUM(100),SMHNEW(100),
  2SMFNEW(100),FPROJ(10C)
   COMMON/DATA2/INC,LAY,IPART,IPORE,IBETA,IPROJ,      DFP,DFH,DFB
   DO 10 I=1,IPART
   P(I)=(I-1)*DFP
   FP(I)=1./IPART
10 CONTINUE
   RETURN
   END



   SUBROUTINE CALFH
   COMMON/DATA1/FH(1CC,5),F(10C),FP(100),P(10C),FPSAVE(100),
  1 FHSAVE(1CC),PROJ(1CC),FB(100),B(100),FPCUM(10C),SMHNEW(100),
  2SMFNEW(100),FPROJ(10C)
   COMMON/DATA2/INC,LAY,IPART,IPORE,IBETA,IPROJ,      DFP,DFH,DFB
   DO 10 I=1,IPORE
   H(I)=(I-1)*DFH
   FH(I,1)=1./IPORE
10 CONTINUE
   RETURN
   END
```

```
   SUBROUTINE CALFB
   COMMON/DATA1/FH(1CC,5),F(100),FP(100),P(100),FPSAVE(100),
  1 FHSAVE(100),PROJ(10C),FB(100),B(100),FPCUM(100),SMHNEW(100),
  2SMFNEW(100),FPROJ(100)
   COMMON/DATA2/INC,LAY,IPART,IPORE,IBETA,IPROJ,      DFP,DFH,DFB
   RIBETA=FLOAT(IBETA)
   PID28=3.1416/(4.*RIBETA)
   DO 10 I=1,IBETA
   FB(I)=.636
   FI=FLOAT(I)
   B(I)=PID28*(2.*FI-1.)
10 CONTINUE
   RETURN
   END

   SUBROUTINE CALFCP
   COMMON/DATA5/CP(10),FCP(10),CH(10),FCH(10),ICP,ICH,ICPN,ICHN
   CP(1)=.439
   FCP(1)=1.
   RETURN
   END

   SUBROUTINE CALFCH
   COMMON/DATA5/CP(10),FCP(10),CH(10),FCH(10),ICP,ICH,ICPN,ICHN
   DO 10 I=1,ICHN
   FI=FLOAT(I)
   CH(1)=.35+FI/10.
10 CONTINUE
   FCH(1)=6.
   FCH(2)=17.
   FCH(3)=17.
   FCH(4)=17.
   FCH(5)=17.
   FCH(6)=6.
   RETURN
   END



   SUBROUTINE CALPRO
   COMMON/DATA1/FH(100,5),F(100),FP(100),P(100),FPSAVE(100),
  1 FHSAVE(100),PROJ(100),FB(100),B(100),FPCUM(100),SMHNEW(100),
  2SMFNEW(100),FPROJ(100)
   COMMON/DATA2/INC,LAY,IPART,IPORE,IBETA,IPROJ,      DFP,DFH,DFB
   RIPRC=FLOAT(IPROJ)
   PID2=      3.1416/(4.*RIPRO)
   DO 10 I=1,IPROJ
   FPROJ(I)=.636
   FI=FLOAT(I)
   PROJ(I)=PID2*(2.*FI-1.)
10 CONTINUE
   RETURN
   END
```

```
      SUBROUTINE SIMSIV(Y)
C
C
C
C     THIS PROGRAM CALCULATES SEPARATION EFFICIENCY BY A WEIGHTED
C     SIMULATION TECHNIQUE
C
C     F.M. STUNTZ, SCHOOL MAE
C
C     DEFINITIONS
C
C     IBETA = NUMBER INCREMENTS IN ANGULAR RELATIONSHIP
C     IPART = NUMBER INCREMENTS IN PARTICLE SIZE DISTRIBUTION
C     IPORE = NUMBER INCREMENTS IN PORE     SIZE DISTRIBUTION
C     LAY = NUMBER SIEVE LAYERS
C     INC = NUMBER PARTICULATE INCREMENTS
C     NFHFUN=1 MEANS FH IS SUPPLIED IN FUNCTIONAL FORM
C     NFHFUN=0 MEANS FH IS SUPPLIED IN DATA FORM.
C     NFPFUN = 1 MEANS FP IS SUPPLIED IN FUNCTIONAL FORM
C     NFPFUN = 0 MEANS FP IS SUPPLIED IN DATA FORM
C     FH= PROBABILITY DISTRIBUTION FUNCTION OF ORIGINAL PORES
C     FP= PROBABILITY DISTRIBUTION FUNCTION OF ORIGINAL PARTICLES
C
C     FUNCTIONS AND SUBROUTINES REQUIRED:  USER SUPPLIES EITHER FUNCTIONAL
C     FORMS IN CALFH, CALFP AND CALFB, IF DATA IS NOT READ.  FUNCTION
C     PAREA MUST BE SUPPLIED FOR PARTIAL BLOCKAGE.  IF NO PARTIAL BLOCK-
C     AGE EXISTS SET NHPRBK=0.  FUNCTION ANGLE MUST BE SUPPLIED TO DEFINE
C     THE CRITICAL ANGLE OF CAPTURE.  IF NO ANGULAR RELATIONSHIP EXISTS
C     SET IANGLE=1 IN MAIN, SET B(I)=0. AND FB(I)=1. IN CALFB.
C     ANG ANGLE=0. IN FUNCTION ANGLE
C     CH = PORE SHAPE FACTOR

      COMMON/DATA1/FH(100,5),H(100),FP(100),P(100),FPSAVE(100),
     1 FHSAVE(100),PROJ(100),FB(100),B(100),FPCUM(100),SMHNEW(100),
     2SMPNEW(100),FPROJ(100)
      COMMON/DATA2/INC,LAY,IPART,IPORE,IBETA,IPROJ,      DFP,DFH,DFB
      COMMON/DATA3/IPA,IPO,IA,IPR,LA,I
      COMMON/DATA4/PPRC,THETA
      COMMON/DATA5/CP(10),FCP(10),CH(10),FCH(10),ICP,ICH,ICPN,ICHN
      COMMON/DATA6/ECOMP(20),HBK,NECOMP
      Y=0.
  103 FORMAT(1X,'INTERVAL  PORE SIZE     DENSITY       LAYER = ',I3,/)
  104 FORMAT(1X,I10,2F14.6)
  105 FORMAT(1X,'INTERVAL  PARTICLE SIZE DENSITY       LAYER = ',I3,/)
  107 FORMAT(1HC,'INTERVAL  SUM PART PDF  EFFICIENCY, AFTER PASSAGE OF',
     1I3,' INCREMENTS THROUGH',I3,' LAYERS')
  301 FORMAT (1X,7I3,6E14.6)
C     ITERATE THROUGH ALL COMBINATIONS OF INTERCEPTION AND ESCAPE.
      DO 500 IN=1,INC
      PROPAR=1.
      DO 400 LA=1,LAY
      DO 300 IPA=1,IPART
      DO 250 IPR=1,IPROJ
      DO 225 ICP=1,ICPN
      DO 215 ICH=1,ICHN
      DO 200 IPC=1,IPORE
      PPRC=P(IPA)*SQRT((CP(ICP)*SIN(PROJ(IPR)))**2+COS(PROJ(IPR))**2)
      THETA=ANGLE(PPRC,H(IPC),CH(ICH),CP(ICP))
      DO 100 IA=1,IBETA
      I=1
      CALL       CAPTUR
  100 CONTINUE
  200 CONTINUE
  215 CONTINUE
  225 CONTINUE
  250 CONTINUE
  300 CONTINUE
C      NORMALIZE AND STORE PARTICLE AND PORE DISTRIBUTIONS.
      SPORE=0.
      DO 310 I=1,IPORE
  310 SPORE=SPORE+SMHNEW(I)
      WRITE(6,103)LA
      DO 320 I=1,IPORE
      FH(I,LA)=SMHNEW(I)/SPORE
      SMHNEW(I)=0.
  320 WRITE(6,104) I,H(I),FH(I,LA)
      SPART=0.
      DO 330 I=1,IPART
  330 SPART=SPART+SMPNEW(I)
      PROPAR=PROPAR*SPART
      WRITE(6,105)LA
      DO 340 I=1,IPART
      FP(I)=SMPNEW(I)/SPART
      SMPNEW(I)=0.
  340 WRITE(6,104)I,P(I),FP(I)
  400 CONTINUE
C      RESET PARTICULATE INCREMENT FOR NEXT TRIP THROUGH THE LAYERS
      LAM1=LA-1
      WRITE(6,107)IN  ,LAM1
      DO 410 I=1,IPART
      FPCUM(I)=FPCUM(I)+PROPAR*FP(I)
C     CALCULATE INCREMENT EFFICIENCIES FOR THE INTH INCREMENT
      EFF=1.-PROPAR*FP( I)/FPSAVE(I)
      IF(NECOMP.EQ.0) GO TO 405
      Y=Y+(EFF-ECOMP(I))**2
  405 CONTINUE
      WRITE(6,104)I,FP(I),EFF
  410 FP(I)=FPSAVE(I)
  500 CONTINUE
      INM1=IN-1
      WRITE(6,107)INM1,LAM1
      DO 600 I=1,IPART
      EFF=1.-FPCUM(I)/(INC*FPSAVE(I))
  600 WRITE(6,104)I,FPCUM(I),EFF
      Y=-Y
      RETURN
      END
```

```
      SUBROUTINE CAPTUR
      COMMON/DATA1/FH(100,5),H(100),FP(100),P(100),FPSAVE(100),
     1 FHSAVE(100),PROJ(100),FB(100),B(100),FPCUM(100),SMHNEW(100),
     2SMPNEW(100),FPROJ(100)
      COMMON/DATA2/INC,LAY,IPART,IPORE,IBETA,IPROJ,      DFP,DFH,DFB
      COMMON/DATA3/IPA,IPO,IA,IPR,LA,I
      COMMON/DATA4/PPRO,THETA
      COMMON/DATA5/CP(10),FCP(10),CH(10),FCH(10),ICP,ICH,ICPN,ICHN
      COMMON/DATA6/ECCMP(20),HBK,NECOMP
C      SEE COMMENT CARDS IN OTHER DECK
      PID4=3.1416/4.
      IF(PPRO.LT.CH(ICH)*H(IPO)) GO TO 100
      IF(PPRO.GT.HBK*H(IPO)/CP(ICP)) GO TO 50
C     P IS LT H AND GT CH*H. CALCULATE LIMITING VALUES OF THETA
      IF((B(IA).GT.PID4-THETA).AND.(B(IA).LT.THETA+PID4)) GO TO 100
C     CAPTURE
   50 CONTINUE
C     RESET PARAMETERS BECAUSE OF CAPTURE
      HNEW=PARBLK(PPRO,H(IPO),B(IA),NHPRBK,CH(ICH),CP(ICP))
C     SIZE HNEW
      IF(HNEW.LT. H(1    )) GO TO 140
      I=0
   60 I=I+1
      IF(HNEW.LE. H(I    )) GO TO 70
      GO TO 60
   70 CONTINUE
      SMHNEW(I)=SMHNEW(I)+NHPRBK*FP(IPA)*FH(IPO,LA)*FB(IA)*FPROJ(IPR)
     1*FCP(ICP)*FCH(ICH)
      GO TO 150
  100 CONTINUE
C      RESET PARAMETERS BECAUSE OF ESCAPE
      SMPNEW(IPA)=SMPNEW(IPA)+FH(IPO,LA)*FP(IPA)*FB(IA)*FPROJ(IPR)
     1*FCP(ICP)*FCH(ICH)
      SMHNEW(IPO)=SMHNEW(IPO)+FP(IPA)*FH(IPO,LA)*FB(IA)*FPROJ(IPR)
     1*FCP(ICP)*FCH(ICH)
      GO TO 150
  140 I=1
  150 CONTINUE
      RETURN
      END
```

```
      SUBROUTINE THETCP(P,H,CH,CP,IER,EPS,NTHETA,NMAX,THETA)
C
C      THIS SUBROUTINE COMPUTES THE MAXIMUM ANGLE OF ROTATION OF ONE
C     ELIPSE WITHIN A SECOND ELIPSE.
C
C     ERRORS:  IER=0  --  NO ERROR
C                 =1 --  PROBLEM GEOMETRY UNACCEPTABLE
C                 =2  --  CANNOT OBTAIN ACCURACY DEMANDED BY IER WITH
C
      P2=P*P/4.
      THETA=0.
      NTHETA=0
      IER=0
      IF((P.LE.CH*H).OR.(P.GE.H).OR.(CP*P.GE.CH*H)) GO TO 100
      CP2=CP*CP
      GO TO 10
    5 THETA=THETA+.01
      GO TO 10
    7 THETA=THETA-.034
   10 THESTO=THETA
      NTHETA=NTHETA+1
      IF(NTHETA.GT.NMAX) GO TO 90
      Y2=P2*(SIN(THETA)*SIN(THETA)+CP2*COS(THETA)*COS(THETA))
      X2=(H*H/4.)-Y2/(CH*CH)
      XP2=(X2+Y2-CP2*P2)/(1.-CP2)
      YP2=CP2*(P2-XP2)
      IF((Y2 .LE.0.).OR.(YP2.LE.0.))GO TO 5
      IF((X2.LE.0.).OR.(XP2.LE.0.))GO TO 7
      THMIN=THETA
      Y2DX2=Y2/X2
      YPDXP1=YP2/XP2
      YDX=SQRT(Y2DX2)
      YPDXP=SQRT(YPDXP1)
      THETA=ATAN(YDX)-ATAN(YPDXP)
      IF(ABS(THETA-THESTO).LT.EPS) GO TO 110
      GO TO 10
   90 IER=2
      THETA=THMIN
      GO TO 110
  100 IER=1
  110 RETURN
      END
```

```
      FUNCTION ANGLE(P,H,CH,CP)
C      SERIES A ..... CHS MEDIA AND ACF TEST DUST
      EPS=.005
      NMAX=160
      CALL       THETCP(P,H,CH,CP,IER,EPS,NTHETA,NMAX,THETA)
      ANGLE=THETA
      RETURN
      END


      FUNCTION PARBLK(P,H,BETA,NHPRBK,CH,CP)
      NHPRBK=2
      PARBLK=(H/2.-CP*P*SQRT((1.+TAN(BETA)**2)/(CP*CP+TAN(BETA)**2)))/CH
      RETURN
      END
```

```
INCREMENTS.....  1
LAYERS.....  1
DIVISIONS ON PARTICLE HISTOGRAM.....  9
DIVISIONS ON PORE HISTOGRAM.....  5
DIVISIONS ON ANGULAR HISTOGRAM.....  9
DIVISIONS ON PROJECTION HISTOGRAM.....  9

SIZE OF DIVISION OF PARTICLE HISTOGRAM...   5.00000
SIZE OF DIVISION OF PORE HISTOGRAM.....   2.00000
SIZE OF DIVISION ON ANGULAR HISTOGRAM....   0.07840

ICPN=  1 ICHN=  6
INTERVAL  PORE SIZE     DENSITY       LAYER =   0

        1      7.000000      11.000000
        2      9.000000      21.000000
        3     11.000000      36.000000
        4     13.000000      14.000000
        5     15.000000       7.000000
INTERVAL  PARTICLE SIZE DENSITY       LAYER =   0

        1     12.500000       0.616200
        2     17.500000       0.206700
        3     22.500000       0.085000
        4     27.500000       0.040000
        5     32.500000       0.020700
        6     37.500000       0.011500
        7     42.500000       0.006800
        8     47.500000       0.004200
        9     52.500000       0.002700
INTERVAL  ANGLE SIZE    DENSITY

        1      0.087267       0.636000
        2      0.261800       0.636000
        3      0.436333       0.636000
        4      0.610866       0.636000
        5      0.785400       0.636000
        6      0.959933       0.636000
        7      1.134465       0.636000
        8      1.308999       0.636000
        9      1.483532       0.636000
INTERVAL  ANGLE SIZE    DENSITY

        1      0.087267       0.111111
        2      0.261800       0.111111
        3      0.436333       0.111111
        4      0.610866       0.111111
        5      0.785400       0.111111
        6      0.959933       0.111111
        7      1.134465       0.111111
        8      1.308999       0.111111
        9      1.483532       0.111111
INTERVAL  PORE SIZE     DENSITY       LAYER =   0

        1      7.000000       0.123595
        2      9.000000       0.235955
        3     11.000000       0.404494
        4     13.000000       0.157303
        5     15.000000       0.078652
INTERVAL  PARTICLE SIZE DENSITY       LAYER =   0

        1     12.500000       0.620045
        2     17.500000       0.207990
        3     22.500000       0.085530
        4     27.500000       0.040250
        5     32.500000       0.020829
        6     37.500000       0.011572
        7     42.500000       0.006842
        8     47.500000       0.004226
        9     52.500000       0.002717
PROJECTION   ANGLE SIZE    DENSITY

        1      0.087267       0.636000
        2      0.261800       0.636000
        3      0.436333       0.636000
        4      0.610866       0.636000
        5      0.785400       0.636000
        6      0.959933       0.636000
        7      1.134465       0.636000
        8      1.308999       0.636000
        9      1.483532       0.636000
PROJECTION   ANGLE SIZE    DENSITY

        1      0.087267       0.111111
        2      0.261800       0.111111
        3      0.436333       0.111111
        4      0.610866       0.111111
        5      0.785400       0.111111
        6      0.959933       0.111111
        7      1.134465       0.111111
        8      1.308999       0.111111
        9      1.483532       0.111111
INTERVAL  PART. SHAPE F  DENSITY

        1      0.439000       1.000000
```

```
INTERVAL  PART. SHAPE F  DENSITY
        1      0.439000      1.000000
INTERVAL  PORE SHAPE F   DENSITY
        1      0.450000      6.000000
        2      0.550000     17.000000
        3      0.650000     17.000000
        4      0.750000     17.000000
        5      0.850000     17.000000
        6      0.950000      6.000000
INTERVAL  PORE SHAPE F   DENSITY
        1      0.450000      0.075000
        2      0.550000      0.212500
        3      0.650000      0.212500
        4      0.750000      0.212500
        5      0.850000      0.212500
        6      0.950000      0.075000
INTERVAL  PORE SIZE     DENSITY       LAYER =   1
        1      7.000000      0.022116
        2      9.000000      0.156605
        3     11.000000      0.422114
        4     13.000000      0.246738
        5     15.000000      0.142426
INTERVAL  PARTICLE SIZE DENSITY       LAYER =   1
        1     12.500000      0.849960
        2     17.500000      0.129657
        3     22.500000      0.017713
        4     27.500000      0.002419
        5     32.500000      0.000251
        6     37.500000      0.0
        7     42.500000      0.0
        8     47.500000      0.0
        9     52.500000      0.0

INTERVAL  SUM PART PDF  EFFICIENCY, AFTER PASSAGE OF  1 INCREMENTS THROUGH  0 LAYERS
        1      0.849960      0.446907
        2      0.129657      0.748477
        3      0.017713      0.916440
        4      0.002419      0.975749
        5      0.000251      0.995145
        6      0.0           1.000000
        7      0.0           1.000000
        8      0.0           1.000000
        9      0.0           1.000000

INTERVAL  SUM PART PDF  EFFICIENCY, AFTER PASSAGE OF  0 INCREMENTS THROUGH  0 LAYERS
        1      0.342942      0.446907
        2      0.052314      0.748477
        3      0.007147      0.916440
        4      0.000976      0.975749
        5      0.000101      0.995145
        6      0.0           1.000000
        7      0.0           1.000000
        8      0.0           1.000000
        9      0.0           1.000000
```

APPENDIX C

PROCEDURE TO TEST THE SINGLE-PASS FILTRATION PERFORMANCE OF A FLAT RECLEANABLE HYDRAULIC FILTER MEDIUM

1. Purpose: To evaluate the filtration performance of a flat, recleanable hydraulic filter medium as exposed to a specific contaminant.

2. Scope: The test shall measure the filtration performance of a flat recleanable filter medium for a specified contaminant under single pass conditions for the sieving mode or for the sieving and the cake mode.

3. Definitions:

   3.1 Sieving Mode: Separation due to mechanical capture of a particle by the filter medium or the filter medium and other particles.

   3.2 Cake Mode: Separation due to mechanical capture entirely by other particles.

   3.3 Adsorption Mode: Separation of a particle smaller than the pore upon which it impinges due to surface forces.

4. Equipment and Supplies:

   4.1 Vacuum source.

   4.2 Wide mouth vacuum flask. See Figure 13.

   4.3 Filter mounting funnel (and appropriate gaskets if necessary), Millipore XX1504700 or equivalent.

4.4 Cleaning equipment (as necessary for particular medium).

4.5 Particle counting facilities (must be able to count largest dimension regardless of distribution).

4.6 Microscope.

4.7 Filter medium.

4.8 Liquid vehicle (particle free).

4.10 Analytic balance.

4.11 Dessicator.

4.12 Sample bottles (particle free).

5. Test Procedure:

5.1 Clean filter medium.

5.1.1 Microscopic inspection should reveal no particles.

5.1.2 Pass clean test fluid at twice test flow rate through medium. Downstream count must be less than one particle/10 ml. in filtrate.

5.2 Determine proper dilution.

5.2.1 With apparatus set up as shown in Figure 13 determine the concentration required to give the desired mode of filtration in three-fourths the volume of the collection bottle.

5.2.1.1 Sieving mode: More than 50 percent of the pores shall be blocked, but less than five percent of the observed particles may be captured solely by other particles.

5.2.1.2 Cake Mode: Flow stops at vacuum of 14.0 psid.

5.2.2 The concentration desired = (weight contaminant determined in 5.2.1)/(.75 volume collection bottle).

5.3 Disperse the proper amount of contaminant in the test liquid.

5.4 Determine uniformity of dispersion with counting and measuring apparatus.

5.5 Remove an appropriate quantity of the contaminated solution and count the particle size distribution (upstream count).

5.6 Filter the remaining quantity of contaminated fluid through the filter medium at the flow rate recommended by the manufacturer. Under no circumstances allow flow to cyclone in the filtration funnel. The filter medium should be grounded at all times.

5.7 Microscopically examine the filter medium to observe pore blockage and verify mode of capture.

5.8 Count particles collected in the downstream sample.

6. Interpretation: Separation efficiency will be calculated for particles size, p, as,

$$\epsilon(p) = \frac{N_u(p) - N_D(p)}{N_u(p)}$$

where,

$N_u(p)$ = number particles/ml. of the largest dimension, d, upstream,

$$p - \delta/2 < d \leq p + \delta/2 .$$

$N_D(p)$ = number particles/ml. of the same size range in the downstream sample.

δ = interval size.

VITA

Ross Maxwell Stuntz

Candidate for the Degree of

Doctor of Philosophy

Thesis: THE SIEVING MECHANISM IN HYDRAULIC FILTRATION

Major Field: Engineering

Biographical:

Personal Data: Born in Tulsa, Oklahoma, January 4, 1941, the son of Mr. and Mrs. Ross M. Stuntz, Jr.

Education: Graduated from Central High School, Tulsa, Oklahoma, in May, 1959; received Bachelor of Science degree from Oklahoma State University, Stillwater, Oklahoma, in June, 1964; received Master of Science degree from Oklahoma State University in June, 1965; completed the requirements for the Doctor of Philosophy degree in July, 1971.

Professional Experience: Employed by Humble Oil Company, Summer of 1963; graduate assistant, Oklahoma State University, January, 1964-May, 1965; research engineer, Deere and Company, June, 1965-January, 1966; field maintenance officer and R and D coordinator, U. S. Army, January, 1966-December, 1967; project engineer, Oklahoma State University, January, 1968-present.

Professional Organizations: Society of Automotive Engineers, Phi Kappa Phi, Pi Tau Sigma.